Max-Planck-Institut für Kolloid und Grenzflächenforschung

Development of Detector for Analytical Ultracentrifuge

Dissertation
zur Erlangung des akademischen Grades
"doctor rerum naturalium"
(Dr. rer. nat.)
in der Wissenschaftsdisziplin „Kolloidchemie“

eingereicht an der
Mathematisch-Naturwissenschaftlichen Fakultät
der Universität Potsdam

von
Saroj Kumar Bhattacharyya
Aus Guwahati, Indien

Potsdam, den 18 April 2006
Korrigiert eingereicht 14 August 2006

In memory of late beloved “Aai” (my grandmother)

Table of contents: **Page No.**

Chapter 1

1.1 Analytical Techniques in Science[1,2]

The role of analytical science is well realized today. With the importance of understanding the constitution of matter or studying their transformations under various circumstances remaining the prime motivation for various applications in science, analytical science has seen spectacular growth in the last four decades. From the development of routine methods to determine concentration of pollutants in atmosphere on ppm or in ppb level to designing the protein databank, this field has undergone huge growth. A large proportion of contributions towards this astounding development and popularity stems from the progress in the field of analytical techniques, in particular in separation science. Advent of analytical techniques and their continued importance contrary to classical analysis methods has apparently brought to an end to what has been called "hole-in-the-wall analysis" where samples were passed through a hole in the lab wall for an isolated and impartial assay. Development in this field has always remained quite interdisciplinary: developments in the field of electronics and instrumentation as well as developments in laboratory computers which could revolutionize the data handling and data analysis. Both of these improvements could gradually introduce total system automation of analytical instruments, with the advantage of high throughput sampling (HTS)[3], as well as giving birth to new fields[4,5]. The impact of analytical instrumentation and their automation can be felt when one looks at the advances it has created in the fields of Chromatography[6] and their hyphenated techniques like: GC/MS[7], LC-MS[8]; Spectroscopy[9-16], Process Chemometrics[17], Informatics[18] etc. Automated sample processing has been widely applied in pharmaceutical research, particularly in the early drug discovery and drug development processes of analytics and screening technology for profiling absorption, distribution, metabolism, excretion, and physicochemical properties. Although the drivers for using these technologies are common, they often use different approaches[19].

The importance of analytical science rose to its current level largely as a result of contemporary development contemporary in the separation techniques. The extensive use of chromatographic instruments (like HPLC or GC) in industry and other laboratories is indicative of this. It is well known that the detection system in any separation technique plays a crucial role and continuous efforts are made to improve upon these systems in order to enhance its applicability of the techniques. The detection systems like visible and UV spectrometers as non destructive methods or Iodine and Ammonia vapours to enhance sensitivity to organic acids for detection on a TLC plate were used in former times. With the advent of new technologies, separation techniques have been coupled with new systems (optical detection as well as other hyphenated techniques) for the obvious reason that this approach enriches the available analyte information. The ever increasing popularity of orthogonal chromatography[20] in combination with its multidimensional[20,21] application leads to the realization of applicability of Multidetection systems in fractionation techniques. Application of such strategies can give a better insight into a complex analyte mixture under investigation by supplying information of the analyte behaviour[22] and allowing the determination of specific physicochemical parameters that are characteristic of the technique. Recently, detection systems employing spectroscopic techniques like Raman, FTIR and MS have come into picture. Other examples include possible ESR detection for understanding aging process in living tissues[23], and the use of tandem TLC-HPTLC-MS contrary to their solo technique nowadays.

However, the development of new detection systems to separation techniques usually focuses on chromatographic methods, and such application to other techniques have so far been overlooked. Analytical Ultracentrifugation (AUC) is a powerful fractionation technique that has supplied valuable information to biochemists and biophysicists. With its implementation in the last century by Thé Svedberg[24,25], this technique has seen some spectacular development in instrumentation along with the inception of new optical detection systems, such as absorbance, interference or Schlieren optics. However, other detection systems can also be implemented to AUC. Such detection systems include multiwavelength detection which can provide valuable information for interacting macromolecular systems[26] or information about the wavelength dependency of

particle size, a light scattering detector which can be used for online molar mass detection. Also, it may also be mentioned that for the AUC detection systems, the inceptions of the contemporary development in electronics or other related fields have not been so common. It is clear in the history of developments of AUC that improvements in the detector hardware have been neglected, in comparison to development of the data evaluation software[27-30]. In the present work, effort has been made to fill this gap by introducing adoptable developments from other area of science, towards improved detection capabilities in AUC experiments.

1.2 Analytical Ultracentrifugation (AUC)-A brief introduction

An Analytical Ultracentrifuge (AUC) is a centrifuge that allows to spin a rotor at accurately controlled speed and temperature, whilst allowing for the recording of the concentration distribution of the sample at known times. In order to achieve rapid sedimentation and to minimize diffusion, high angular velocities may be necessary. The rotor of an analytical ultracentrifuge is typically capable at speeds up to 60,000 rpm. In order to minimize frictional heating, and to minimize aerodynamic turbulence, the rotor is usually spun in an evacuated chamber. It is also necessary for the instrumentation of an AUC that the rotor be free of wobble and precession.

The power of the technique of AUC lies in the fact that the separation of solute components can be achieved in the centrifugal field. The separation is based on molar mass, density, shape and charge. This endows unique characteristics to this technique that unlike in other fractionation techniques, the solute components do not interact with the solvent in another phase. During an AUC experiment, it is necessary to monitor the concentration gradient of sedimenting molecules, and this must be achieved using optics[31] as physical contact with the sample is not possible. Thus, there remains the requirement of designing ways to shine a beam of light through the sample in an AUC cell and use some optical property of the solute to determine its distribution in the ultracentrifuge cell. The optical properties of the solute currently exploited in existing common AUC detectors are

concentration dependent variation in Absorption and Refractive Index of the sample. A schematic representation of the optics in AUC is shown in fig. 1

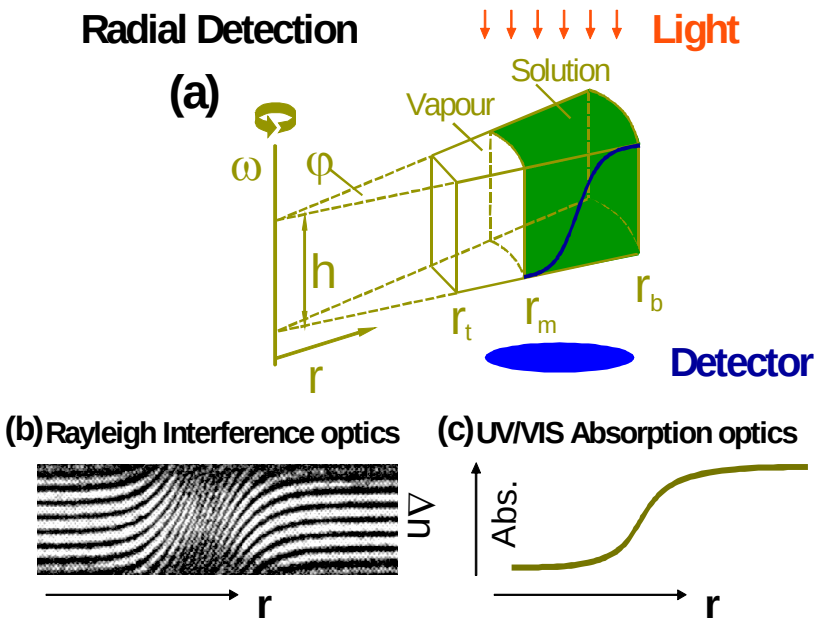

Fig. 1 Schematic representation of AUC detector optics. (a) Diagram of the cell sector (b) and (c) display of online data from commercial Rayleigh and UV/Vis optics.

1.3 Theory of Analytical Ultracentrifugation(AUC)

When a solute particle is suspended in a solvent and subjected to a gravitational field, three forces act on the particle (Figure 2).

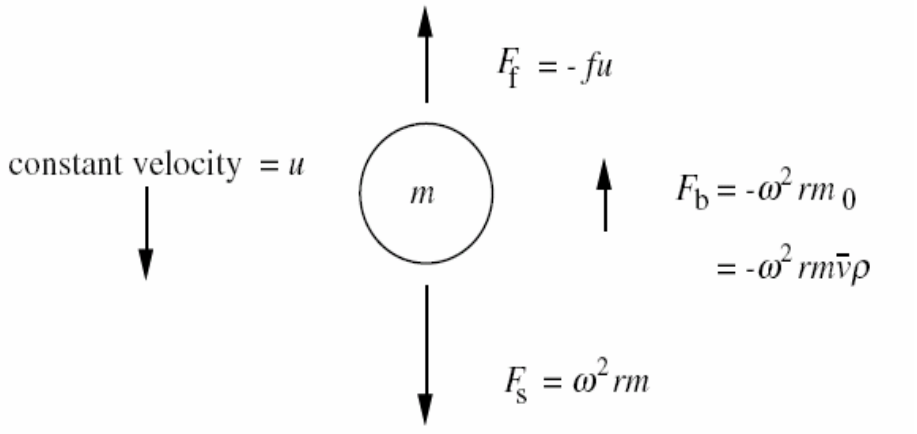

Fig. 2 The forces acting on a solute particle in a gravitational field: Gravitational force, F_s; Buoyant force, F_b; Frictional force, F_f (see text).

First, there is a sedimenting, or gravitational force, F_s, proportional to the mass of the particle and the acceleration. In a spinning rotor, the acceleration is determined by the distance of the particle from the axis of rotation, *r*, and the square of the angular velocity, ω (in radians per second).

$$F_s = m\,\omega^2 r = (M/N)\,\omega^2 r \qquad (1)$$

Here, *m* is the mass in grams of a single particle, *M* is the molar mass of the solute in g/mol and *N* is Avogadro's number. Second, there is a buoyant force, F_b, that, from Archimedes' principle, is proportional to the weight of fluid displaced:

$$F_b = -m_0\omega^2 r \qquad (2)$$

where, m_0 is the mass of fluid that can be displaced by the particle. Thus we can have

$$m_0 = m\,\bar{v}\,\rho = (M/N)\,\bar{v}\,\rho \qquad (3)$$

Here, $\bar{v}$ is the partial specific volume in mL/g (the increase in volume if one gram of the solute is added to an infinite amount of solvent) and ρ is the density of the solvent (g/mL). Provided that the density of the particle is greater than that of the solvent, the particle will begin to sediment. Since particles moving through a viscous fluid experience a frictional drag that is proportional to the velocity, the particle will experience a frictional force:

$$F_f = -fu \qquad (4)$$

where *f* is the frictional coefficient, which depends on the shape and size of the particle and u is the velocity of the sedimenting particle. Bulky or elongated particles experience more frictional drag than compact, smooth spherical ones. The negative signs in equations (2) and (4) indicate that these two forces act in the opposite direction to sedimentation. Within a very short time (usually less than 10^{-6} s) the three forces come into balance:

$$F_s + F_b + F_f = 0 \qquad (5)$$

$$(M/N)\,\omega^2 r - (M/N)\,\bar{v}\,\omega^2 r - fu = 0 \qquad (6)$$

Rearranging:

$$M/N(1-\bar{v}\,\rho)\,\omega^2 r - fu = 0 \qquad (7)$$

Collecting the terms that relate to the particle on one side, and those terms that relate to the experimental conditions on the other, we can write:

$$M(1-\bar{v}\rho)/Nf = u/\omega^2 r \equiv s \qquad (8)$$

The term $u/\omega^2 r$, the velocity of the particle per unit gravitational acceleration, is called the sedimentation coefficient, and can be seen to depend on the properties of the particle. In particular, it is proportional to the buoyant effective molar weight of the particle (the molar weight corrected for the effects of buoyancy), is inversely proportional to the frictional coefficient, and is independent of the operating conditions. Molecules with different molecular weights, or different shapes and sizes and densities, will, in general, move with different velocities in a given centrifugal field; *i.e.,* they will have different sedimentation coefficients. The sedimentation coefficient has dimensions of *seconds*. The Svedberg unit (S) is defined as 10^{-13} seconds, in honor of Thé Svedberg. As soon as a concentration gradient is formed by sedimentation the process of diffusion opposes that of sedimentation. If the rotation speed is chosen low enough to prevent complete sedimentation, after an appropriate period of time the two opposing processes approach equilibrium in all parts of the solution column and, for a single, ideal solute component, the concentration of the solute increases exponentially towards the cell bottom. At sedimentation equilibrium, the processes of sedimentation and diffusion are balanced; the concentration distribution from the top of the cell to the bottom no longer changes with time, and is a function of molecular weight. As indicated above, the process of sedimentation depends on the effective molar weight, corrected for the buoyancy: $M(1 - \bar{v}\rho)$. If the density of the solute is larger than that of the solvent, the solutes will sediment towards the cell bottom. However, if the density of the solute is less than that of the solvent, the solute will float towards the meniscus at the top of the solution. This is the situation for many lipoproteins and lipids in aqueous solutions. The analysis of such situations is similar, except that the direction of movement is reversed. When the densities of the solute and solvent are equal, $(1 - \bar{v}\rho) = 0$, there will be no tendency to move in either direction. Use can be made of this to determine the density of a macromolecule in density gradient sedimentation. A gradient of density can be made, for example by

generating a gradient of concentration of an added solute such as sucrose or cesium chloride from high concentrations at the cell bottom to lower values at the top. The macromolecule will sediment if it is in a region of solution where the density is less than its own. But macromolecules that find themselves in a region of higher density will begin to float. Eventually, the macromolecules will form a layer at that region of the cell where the solvent density is equal to their own: the buoyant density.

1.4 Experiments in Analytical Ultracentrifugation

The basic equation for ultracentrifugation experiments is the Lamm equation (equation 9), which describes the local concentration variations of the sample in the ultracentrifugal field with time due to the sedimentation and diffusion transport processes[32].

$$\frac{\partial c}{\partial t} = \frac{1}{r}\frac{d}{dr}\left(\underbrace{r D \frac{dc}{dr}}_{\text{Diffusion term}} - \underbrace{s \omega^2 r^2 c}_{\text{Sedimentation term}} \right) \qquad (9)$$

Based on the Lamm equation, there are four basic experiments that can be performed with an Analytical Ultracentrifuge. Each of them can deliver its own range of physicochemical information about the sample.

i) Sedimentation velocity experiment: A sedimentation velocity experiment is carried out in a centrifugal field which should be high enough for the molecules or particles to be sedimented. Under such conditions, a separation of mixture components takes place and one can detect a step-like concentration profile in the AUC cell usually exhibiting an upper and a lower plateau.

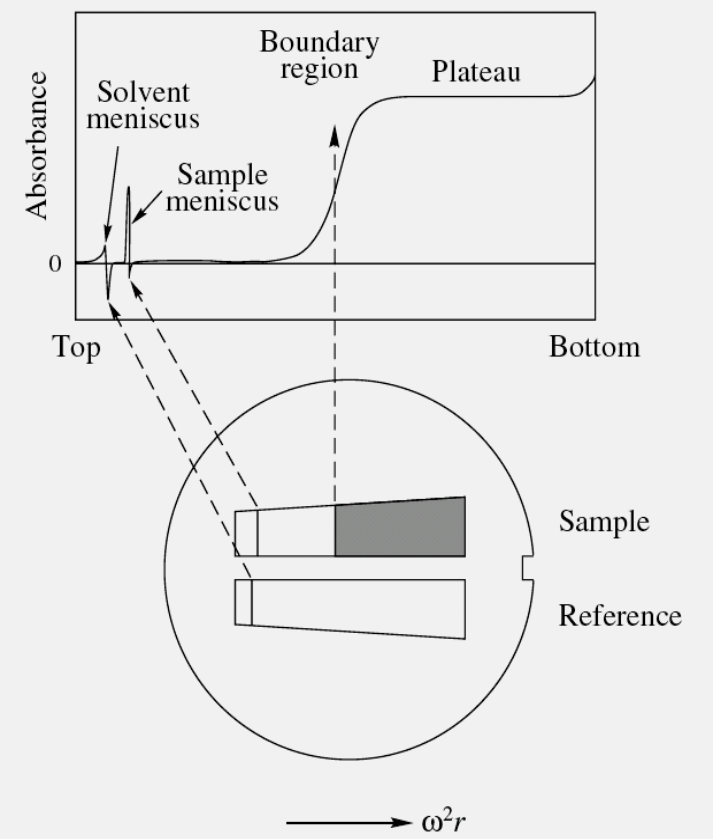

Fig3. A radial scan from a sedimentation velocity experiment with its different characteristics. The corresponding boundary region in the graph represents a pattern with diffusion (reproduced with permission from ref. 33).

If one detects the radial concentration gradient in certain time intervals, the sedimentation of the molecules can be monitored. From the velocity of the sedimenting boundary, one can determine the sedimentation coefficient *s* according to the following relation:

$$s=\ln(r/r_m)/\ \omega^2 t \qquad (10)$$

where, r is the position of the midpoint or second moment point of the moving boundary, r_m the radial distance of the meniscus, t the time and ω the angular velocity of the rotor. A plot of $\ln(r/r_m)$ vs $\omega^2 t$ is a line with the slope *s*= sedimentation coefficient. If the diffusion coefficient is known from other experiments such as light scattering, one can calculate the molar mass of the sample according to the Svedberg equation:

$$M=sRT/D(1-\bar{v}\,\rho_0) \qquad (11)$$

where, R is the gas constant, T the absolute temperature, and ρ_0 the solvent density. The partial specific volume is a critical value, but it can be determined with good precision in a

density oscillation tube if enough sample material is available. In biochemistry, often only a very small amount of sample is available so that this measurement can present a problem, however different workarounds are also available, such as the calculation of $\bar{v}$ from the amino acid composition.

In general, sedimentation velocity experiments offer a good possibility for the rapid determination of molar mass but also of equilibrium constants of interacting systems which is especially advantageous for unstable systems which can not be subjected to sedimentation equilibrium experiments due to the danger of sample degradation during the experiment[34]. There are many procedures to determine the sedimentation coefficient from sedimentation velocity data. Of these, the Moving Boundary method[35] or Van Holde-Weischet method[36,37] are the best known. The moving boundary method allows evaluation of the diffusion coefficient from the spreading of the boundary during the experiment, allowing calculation of M[38]. In the Van Holde-Weischet method the diffusion broadening of boundaries is eliminated by selecting a fixed number of data points from one experimental scan that are evenly spaced between the baseline and the plateau. This is followed by calculation of an apparent sedimentation coefficient s^* for each of the data points, which when plotted versus the inverse root of the runtime, yielding the typical van Holde-Weischet plot. Another method for the evaluation of s from the sedimentation data is the Time derivative method[39,40,41] that determines the time derivative of the radial scans acquired at different times. This method serves better for treatment of data for multimodal distribution of solutes, which is a general case for polymers, and works by determining the differential form of G(s) the g(s).

ii) Sedimentation equilibrium experiments: In contrast to the sedimentation velocity experiments, a sedimentation equilibrium experiment is carried out at a centrifugal field so that the solute under interest does not sediment completely. Here, the sedimentation of the sample is balanced by back diffusion according to Fick`s law caused by the established concentration gradient. After the equilibrium between these two transport processes is achieved, an exponential concentration gradient is formed in the ultracentrifuge cell. Therefore, the sedimentation equilibrium analysis is based on solid

thermodynamics. The time of equilibrium attainment considerably depends on the column height of the solution[42] so that short column techniques, with solution columns of about 1mm, can be employed wherever a rapid equilibrium (within 1-2 hours or less) is desired[43]. The concentration gradient contains information about the molar mass of the sample, the second osmotic virial coefficient, or interaction constants in case of interacting systems independently of the shape of the molecule. An advantage is that the detection of the concentration gradient is possible without disturbing the chemical equilibrium even of weak interactions. Various procedures exist for the evaluation of sedimentation equilibrium data. The classical approach for the evaluation of sedimentation equilibrium concentration gradients is to plot ln c vs. r^2 to obtain the weight average molar mass M_w from the slope according to equation:

$$M_{w,app.} = \frac{2RT}{(1-\bar{\nu}\rho)\omega^2}\frac{d(\ln c)}{dr^2} \qquad (12)$$

It must be noted that these M_w-values have apparent character because they are calculated for finite sample concentrations. Consequently, they are named $M_{w,app.}$. The true M_w can be obtained by an extrapolation of a concentration series to infinite dilution. The evaluation according to equation (12) works well for monodisperse ideal samples because in such cases, the ln (c) vs. r^2 plot is linear. However, in most cases in colloid analysis, this plot is curved due to multiple effects (aggregation, polydispersity, non-ideality), which normally yield erroneous $M_{w,app.}$-values from linear regression. There have been efforts to introduce factors so as to end up with better conclusions from sedimentation equilibrium data.

iii) Density gradient experiment: The second principal possibility of separation in an analytical ultracentrifuge is the separation due to the chemical structure expressed in different solute densities in a density gradient. To generate a continuous density gradient in the ultracentrifuge cell, either a high density salt (CsCl etc.) or substances like sucrose are dissolved in water or a mixture of two organic solvents with very different density is applied. Under the action of the centrifugal field, the salt or the more dense solvent sediments towards the cell bottom and thus changes the density of the solution continuously toward the cell bottom. If a sample is placed into the density gradient, it will

sediment /float to a position where its density matches that of the gradient. In case of a mixture, this leads to a banding of the components due to their chemical structure/density. As this experiment was not of main concern in the work carried out, the detail of this method will not be discussed. More information about this can be found in literature[44].

iv) Synthetic Boundary experiment: In a synthetic boundary experiment, changes of a boundary between solution and solvent with time are observed at low centrifugal fields where no sedimentation of the sample occurs. Such experiments require special cells where the solvent is layered upon the solution column under the action of a certain centrifugal field. This is achieved by capillaries which connect the solvent compartment of the cell with the solution compartment and which allow a flow at a certain hydrostatic pressure. The details of these experiments are also available in literature[45].

An alternative approach of ***zone or band sedimentation*** approach was developed by Vinograd et al[46]. In this method, macromolecules are transferred, on the initiation of centrifugation, through a channel from a small well in the centrifuge cell to the sample sector solution which contains a solution of greater density than the macromolecular solution. A self-generated density gradient caused by the diffusion of small molecules between the macromolecular lamella and the main liquid column prevents convection, thereby stabilizing the macromolecules in a sedimenting band or zone. Band centrifugation was applied successfully for characterization of DNA and RNA with CsCl, NaCl, D_2O as the primary small solute for generating the self-diffusion density gradients for nucleic acids and band stabilization[47]. It has the potential advantage of working with low sample quantity (1/20 th of that conventional sedimentation velocity experiment uses) and distinct separation of the sedimenting species. Software has also been developed to work out the sedimentation coefficients from the band data[48].

1.5 Optical Detection systems in Analytical Ultracentrifugation

As already discussed, the present detection systems in AUC rely on absorption or Refractive Index variation of the sample with solute concentration. All existing detection systems for AUC have a similar setup, where light from a source is guided through the cell

sector containing the sample for measurement, and the light of interest is detected by a photosensor. However, an improved detection system can always be designed to meet the demand of increasing potential of AUC. An overview of existing detection system in AUC is discussed here.

i) ***UV/Vis Absorption Optics:*** This detection system of AUC is quite simple. The commercial version of this system, the Beckman Optima XL-A instrument[49], uses a UV-enhanced xenon flashlamp as the light source, which is projected from a 1mm circular aperture which makes the light to impinge on a holographically generated, toroidally curved diffraction grating especially designed for this application. This grating is aberration-corrected so that the system has a nominal 2 nm band pass between 200 nm and 800 nm with very low stray light. The grating is rotated by a precision gear train to select or scan a wavelength in this range. This diffraction grating is additionally blazed by ion bombardment to intensify the first-order light efficiency in the UV range, which also decreases chromatic stray light. Light which is not passing out of the exit aperture of the monochromator is absorbed by a series of semi-reflective and non-reflective absorbing filters to prevent this light at the exit of the monochromator. Stray light levels at 210nm are typically 0.1%. Light leaving the diffraction grating then impinges on an 8% reflector that reflects this light back to a solid-state detector, mounted at the virtual focal point of the monochromator system. Thus the detector monitors the intensity of light incident on the sample in the cell assembly. This intensity value, in conjunction with the transmitted intensity value measured by the PM tube at the detection end of the system, is used to normalize the pulse-to-pulse variation in the light intensity emitted from the flashlamp. This is necessary as the reference and the sample sectors in the cell are measured separately. The exit aperture of the monochromator prevents illumination of the sector not being measured. This eliminates spectral stray light and the resulting non-linearity in absorption measurement. Light passing through the mid-plane of the sector being measured is then refocused by the camera lens assembly into the plane of a slit above the PM tube. This slit and lens assembly is moved so that they undergo motion directly proportional to the image size of the cell. The active area of the PM tube is larger than this

distance and, therefore, remains stationary. A schematic description of this optical system is shown in the figure below:

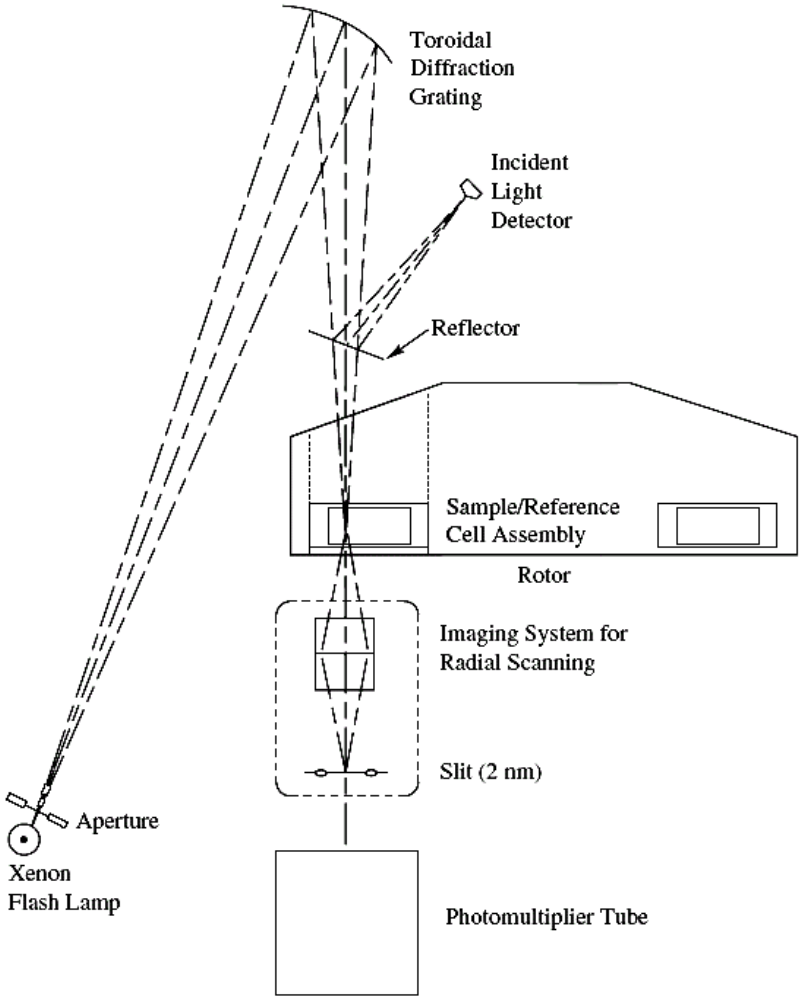

Fig. 4 Absorbance Optics system in commercial Beckmann Optima XL-A (with permission from ref.33)

There have been quite a few contributions from various researchers for the instrumentation of the absorption optics. In the oldest version of this detection system, photographic plates were used. In some modifications with photographic plates as detectors, efforts were made in several ways to illuminate the cell and to grab photographs of sedimenting analyte[50]. This was followed by the use of photoelectric scanner, although in their simplest form these do little more than replace the photographic plate by a photoelectric detector (e.g a PMT), the most highly developed of which was introduced by Lamers, Putney, Steinberg and Schachman (1963)[31]. In later developments, researchers

used a scanner based on a video camera[50]. In one significant development introduced by Flossdorf[51] with the introduction of parabolic mirror based collimator optics in the absorbance optical system exhibited a pronounced enhancement of detected UV/Vis intensity.

ii) Interference Optics: The fundamental principle of this detection system relies on the fact that the velocity of light passing through a region of higher refractive index is decreased. The optical setup consists of monochromatic light that passes through two fine parallel slits, one above each sector of a double-sector cell containing, respectively, a sample of solution and a sample of solvent in dialysis equilibrium. Light waves emerging from the entrance slits and passing through the two sectors undergo interference when combined by a focusing lens and yield a band of alternating light and dark "fringes." When the refractive index in the sample compartment is higher than in the reference, the sample wave is retarded relative to the reference wave. This causes the positions of the fringes to shift vertically in proportion to the concentration difference relative to that of some reference point which is usually the meniscus air/solution. If the concentration of the reference point, c_{rF}, is known, the concentration at any other point can be obtained:

$$c_r = c_{rF} + a\Delta j \qquad (13)$$

where Δj is the vertical fringe shift, and a is a constant relating concentration to fringe shift. In interference optics, the Rayleigh interferometer in the analytical ultracentrifuge produces a cell image in which the concentration at each radial position is presented as the vertical displacement of a set of equally-spaced horizontal fringes. A schematic depiction of the optics as adopted for a commercial Ultracentrifuge is shown below:

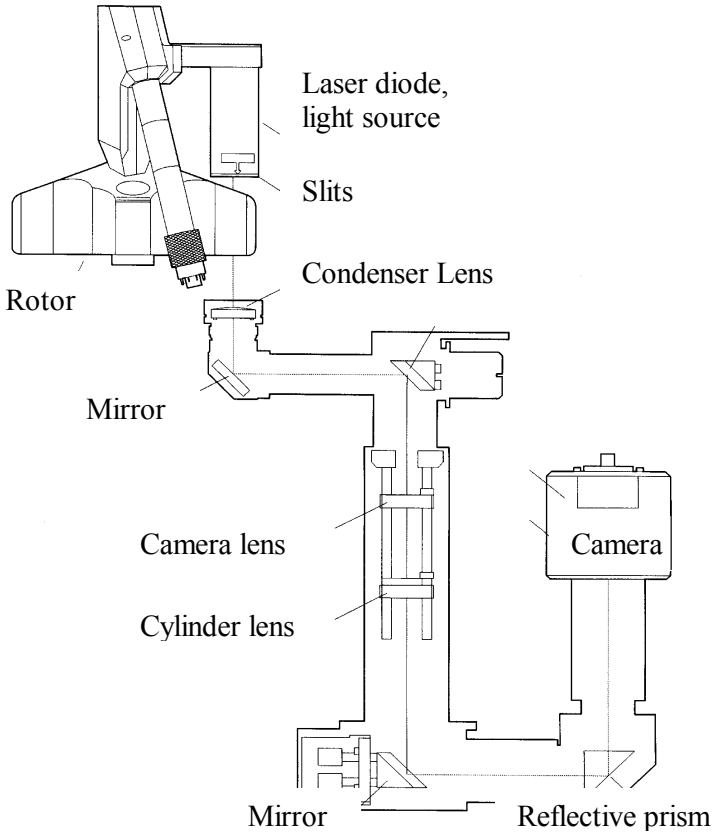

Fig.5 The Interference optics in commercial Beckman XL series instruments with the various parts.

There has been some developmental work with significant contributions from several researchers to reach the state of today's interference optics. The development of an on-line interferometer[52] and finally its adaptation to the Beckman Model E analytical ultracentrifuge[53] platform is one of the pronounced works. This also covers the use of synchronized light source and first use of television camera and finally inception of CCD based cameras with the data evaluation with on-line software. The implementation of automatic interpretation[54,55] of fringe shift patterns may also be mentioned as developmental aspect for this optics. A considerable enhancement in the quality of the Rayleigh interference patterns was achieved with a pulsed laser[54,56]. Also the introduction of two families of interferometric optical schemes demonstrated great sensitivity that exceeded the sensitivity of refractometric Schlieren systems by an order of magnitude[57]. The schemes with Jamen and Rayleigh interference optics belong to the first family and

those with Lebedev, Bringdahl, and Beutelspacher belong to second family[58]. The path of light beam in these two shift interferometric patterns is shown below:

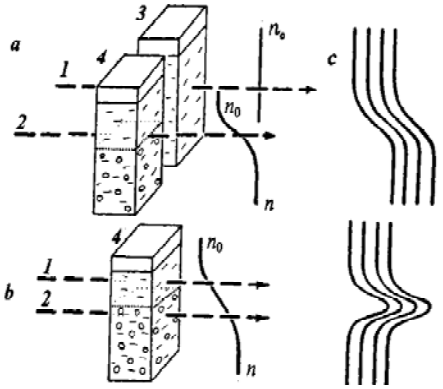

Fig.6 Schematic path of beams in the shift interferometers of the two families of interferometric optics. 'a' and 'b' refers to the first and second families as mentioned in the text. 'c' presents the resulting interference patterns. 1 and 2 are two systems of light beams shifted from one another; 3 is the reference cell sector with a solvent, and 4 is the sample cell; n and n_0 are refractive indexes of the solution and the solvent respectively (reproduced with permission from ref. 58)

All this experience has been combined in the present commercial interferometric optics with Rayleigh interferometer. Apart from the commercial one, the Lebedev interferometric[59] optics is used by some researchers. This is a polarizing interferometer with three main advantages (that can provide the user with a better image of the process within the cell): 1) high sensitivity 2) absence of optical error for high speed experiments 3) the system is free of astigmatic optical elements. It has been constructed for use on a MOM AUC platform. The optical scheme (ref. Fig, 7) consists of a mercury lamp (1) as the light source which passes through a monochromatizing device, and is focused by a lens (2) on the point diaphragm (3). With the aid of another lens (4) it travels further as a parallel beam. The beam is polarized with a polaroid (6) (with optical axis oriented at an angle of 45° to the radial direction) and separated into two beams by a birefringent plate (7) made, for example from Iceland spar. Consequently, the interacting beams in the cell are mutually shifted from one another by the distance *a* (spar twinning), the direction of the shift being normal to the plane of the solution-solvent interface. After passing a half-wave plate (λ/2) (mica plate rotating the planes of polarization of both beams by 90°) and Polaroid (13), crossed with the first (6), make it possible to observe the interference pattern of the two polarized beams. A telescopic system of lenses (10, 11) transforms one

parallel light beam into another one, varying the optical magnification of the pattern. With the aid of that system, the interference pattern is projected onto a photographic film (14). The system also projects the middle of the cell (8) onto the film 14. The edge of the wedge (12), and the axes of spar the plates (7,9) are mutually oriented in the radial direction.

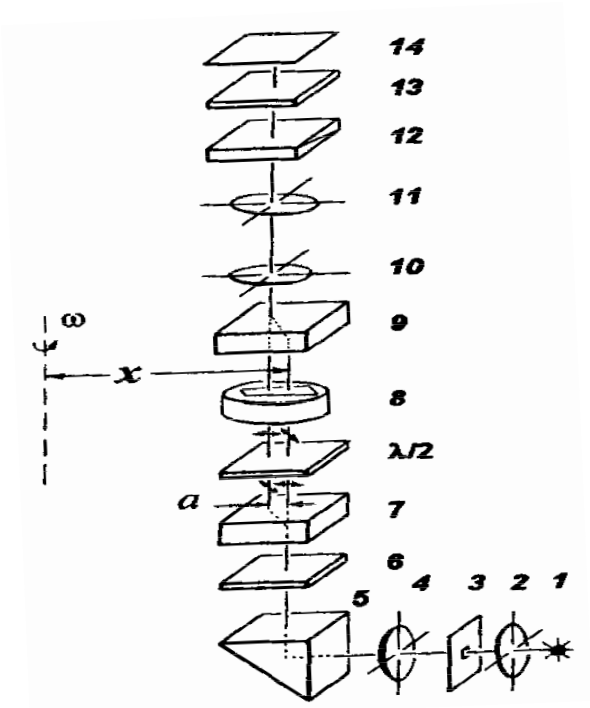

Fig 7. Optics scheme of polarizing interference developed for an AUC of MOM series 3180. x is the coordinate of the point in the cell as counted from the axis of rotation. Light source (1) (mercury lamp); lenses (2, 4, 10, 11); point diagram (3); prism with total internal reflection (5); polaroids (6, 13); spars with a twinning of *a* (7,9); half-wave plate (λ/2); cell (8); wedge (12); photographic film (12).

iii) Schlieren Optics: The Schlieren optical system, not in use in commercial AUCs, was a very popular optical system in AUC earlier models such as the Model E, MOM. This optical system was originally developed by Toepler[60] in 1864 for detecting inhomogenities in the glass used for the manufacture of lenses. The term was coined from the German name *Schlieren*, a phenomenon which occurs due to incomplete mixing resulting in long, thin, streamer-like regions with refractive indices sharply different from the bulk of the material. Since this system detects these Schlieren by the deviations they cause in a beam of light passing through them, the name 'Schlieren' is applied to any optical system which measures changes in refractive index within a transparent medium by means of the deviation of a beam of light quite similar to the Foucault knife-edge test used to detect

aberrations in lenses and mirrors. This optical system has developed slowly from quite simple forms to its present complexity. In the AUC cell, as there is a concentration gradient, the light passing through a region in the cell is deviated radially and the Schlieren optical system converts the radial deviation of light into a vertical displacement of an image at the camera. This displacement is proportional to the concentration gradient. The Schlieren image is thus a measure of the concentration gradient, dc/dr, as a function of radial distance, r. The change in concentration relative to that at some specified point in the cell (e.g. the meniscus) can be determined at any other point by integration of the Schlieren profile. Much of the existing literature on sedimentation, particularly sedimentation velocity, has been obtained with the use of this optical system. The earliest Schlieren system was described by Thovert (1902) and on the basis of his system, various workers developed AUC Schlieren systems (e.g. Tanner[61] 1927). A sample design was reported by Lamm[62] (1937), in which a transparent scale was mounted close to, but not coincident with, the cell, and is photographed through the cell. The image of the scale was distorted by gradients of the refractive index in the cell, and by careful measurement of this distortion it was possible to deduce the variation of dn/dr with r within the cell. A much simpler way of locating the maxima in the gradient curve was described by Tiselius, Pedersen, and Eriksson-Quensel (1937) as described below:

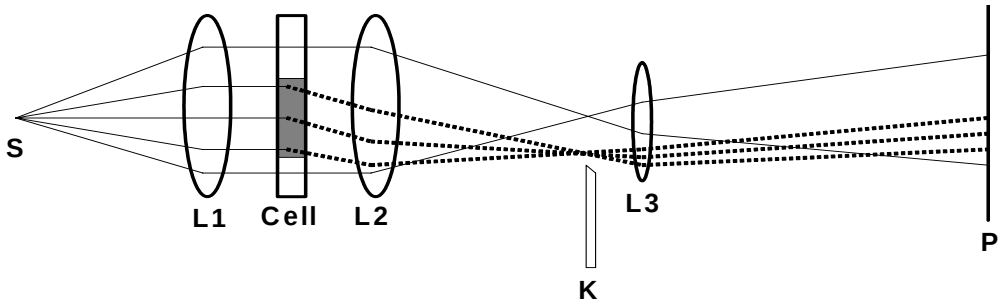

Fig.8 One of the earlier form of the Schlieren optical system (described by Tiselius, Pedersen, and Eriksson-Quensel. The source S is a horizontal slit, K is a knife-edge parallel to S which can be moved from the position towards the optical axis.

The light source was a horizontal slit. The light emerging from this slit was rendered parallel by the collimating lens (L1). The horizontal slit acts as a point in the vertical plane so that in this direction (the only one that matters in the cell) the light passing through the cell is parallel. After passing through the cell, the light passes through the condensing lens

(L2), which forms an image of the light source in its focal plane. Light passing through the parts of the cell with no gradient refractive index forms am image on the optical axis. However, rays of light that are deviated by passing through a concentration gradient in the cell produce an image displaced from the optical axis (shown in dotted line in the figure) The light rays pass through a camera lens L3 which forms an image of the cell on a photographic plate or ground-glass screen P.

The optics have been modified in many ways and adopted in commercial instruments. A representative ray diagram of the optics path as implemented in the commercial instruments[63] is as shown below:

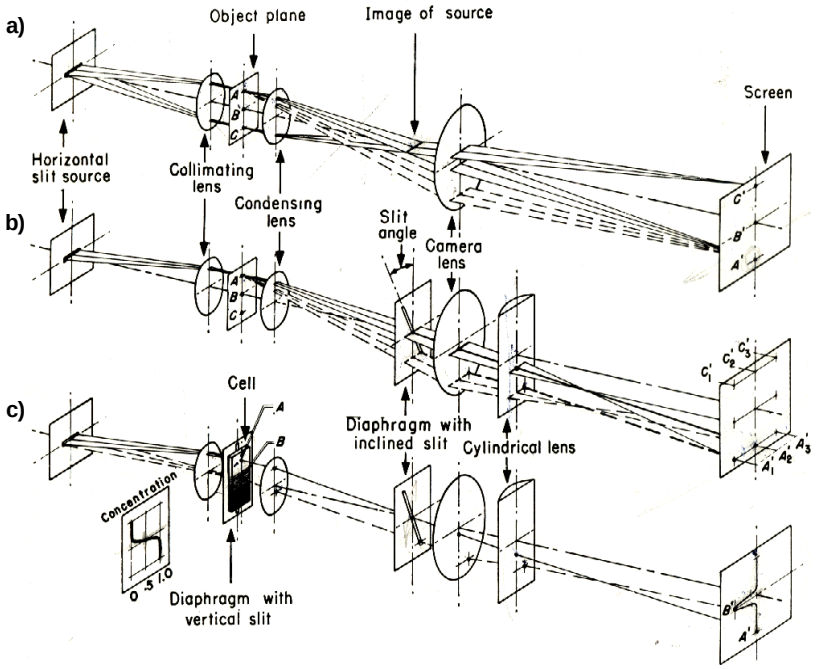

Fig.9 Components describing the Schlieren optical system (with permission from ref.56)

In another development for a Schlieren optical system for the AUC, an ultra sensitive version of this detection system was introduced by Cölfen et al[64] with more flexibility towards working with the phase plate angle. The development was based upon the fact that the existing optics had the limitation that with the decrease in the phase plate angle, the Schlieren curve is broadened causing inaccuracies in the picture evaluation. This was one of the two main factors behind increased sensitivity, the other being the observation of lower sample concentrations than previously possible, due to enhancement

of the y-axis of the Schlieren pattern (fig.10). However, the installation of the optical setup, which was possible for adaptation in bigger version of the instruments like that of Beckman model E or the MSE MKII, cannot be implemented in today's commercially available Ultracentrifuges because of space constraint (unless special modification in the mechanical setup is carried out). The schematic depiction of the optical setup for the ultrasensitive Schlieren optics is shown below with comparison to the commercial optics:

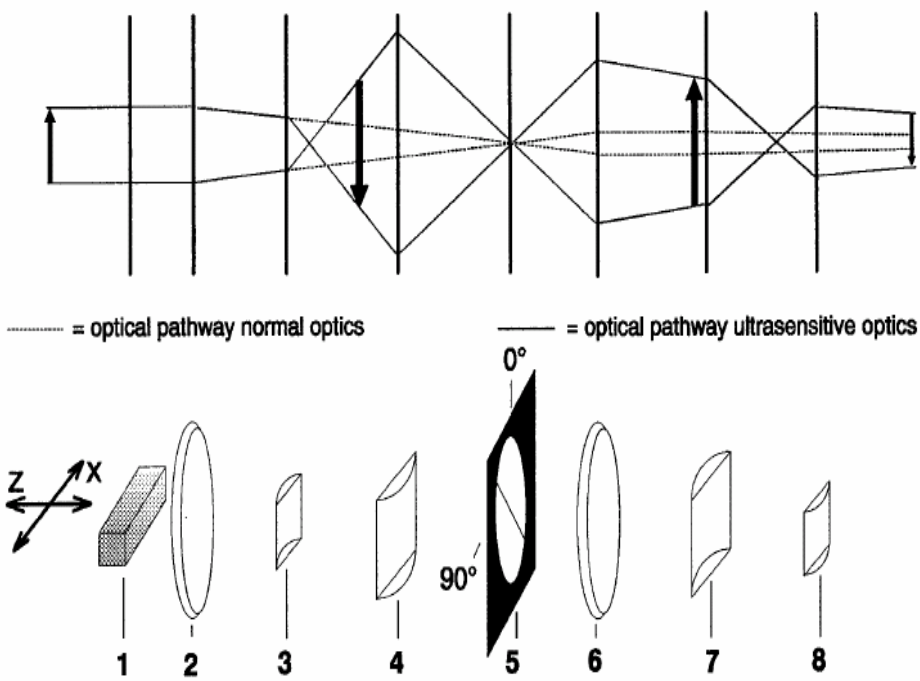

Fig 10. Ultrasensitive Schlieren optics. 1. Sample, 2. condensing lens, 3.cylindrical lens with small focal length, 4. cylindrical lens with larger focal length, 5. phase plate, 6. camera lens, 7. cylindrical lens with relatively large focal length comparable to that of 4, 8. Cylindrical lens with small focal length comparable to 3. (with permission from ref.57)

With a special design of the heat sink and modification of the vacuum chamber, the Schlieren optics has been implemented into an Optima XL ultracentrifuge in BASF, Ludwigshafen, Germany[65]. Workers from the same laboratory also constructed a digital Schlieren optical setup[66,67]. The computer based picture evaluation of the Sclieren patterns enabled fast and efficient evaluation of these records, which previously had to be photographed[68-70]. Also another system built up at the University of Leicester[114] with high rates of data acquisition could greatly improve the usefulness of the detection system.

IV) Fluorescence Detection: Apart from the usual, above described detection systems, Fluorescence detection can also be applied in AUC with a recent and modern version available for the XL-A AUC[71]. The Fluorescence detection system provides the advantage of working with trace quantities of material, down to pM concentration level, a unique feature that is not possible with any other optical system. In the old version of this system, development was performed on the basis of a Spinco Model E[72]. The optical system used a scanning microscope in which only a very small area of the sample is illuminated by an electron beam or a laser beam, and the intensity of the emitted or reflected radiation is recorded under a wide angle of observation. A schematic representation of the fluorescence detection system, as developed and used for the Model E platform, is shown in Fig.11 below:

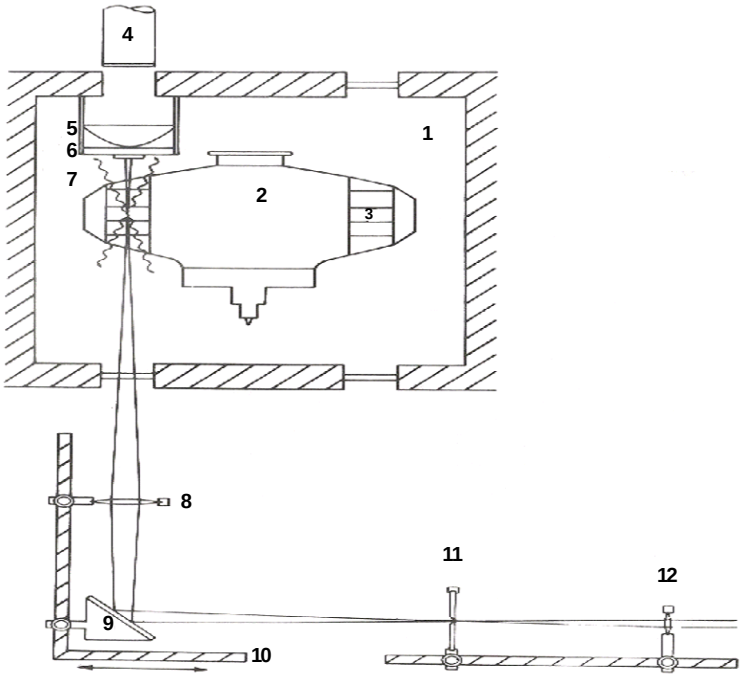

Fig 11. Fluorescence Detection system for the Beckman to Model E. 1. vacuum chamber; 2. rotor; 3. cell; 4. photomultiplier tube; 5. collector lens; 6. set of filters; 7. light trap; 8. projector lens; 9. reflector; 10. positioning table; 11. entrance aperature; 12. collector lens; (reproduced with permission from ref. 65)

In the modern version[72] compatible with the XL series of Beckman Ultracentrifuges, the optics uses a co-axial excitation and emission design similar to some confocal fluorescent microscopes. An argon laser provides a continuous 488-nm excitation beam. Radial resolution is achieved by scanning the focused beam along the radial axis.

Detection of the fluorescence signal uses a co-axial, front-face optical configuration to reduce inaccuracies in the concentration caused by inner filter effects. A high-speed data acquisition system allows the fluorescence intensity to be monitored continuously and at a sufficiently high angular resolution that at any radial position the intensities from all the samples may be acquired at each revolution. The fluorescence detector is capable of detecting concentrations as low as 300 pM for fluorescein-like labels.

v) Turbidity detection: Another detection system used in AUC is turbidity optics. This detection system is useful for obtaining the information about the particle size distribution. This system was first introduced by Cantow[73]. The principle of measurement is comparable to that of an absorption detector, but is much simpler, because the turbidity $A=\log(I_0/I)$ is measured only at a fixed radial position. A diagrammatic representation of this detector is described below:

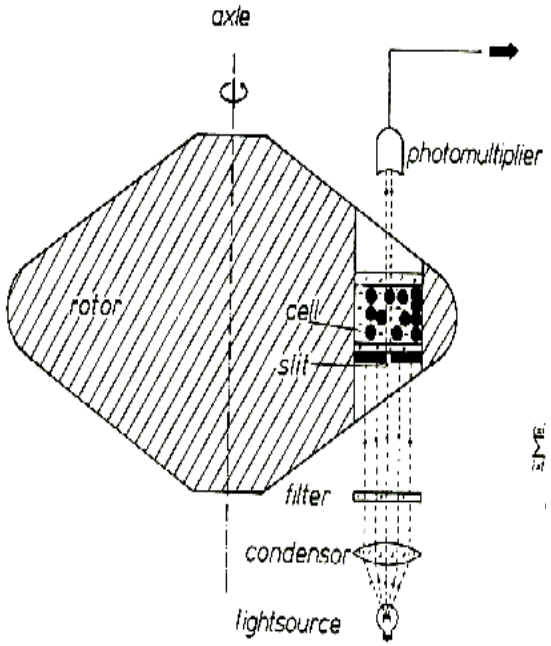

Fig 12. The components describing Turbidity optics

Two types of turbidity detectors[74,75] exist in the user community. The intensity of the incident beam, which is reduced due to light scattering by the analyte inside the measurement cell, is registered by the photomultiplier tube and recorded as a function of the running time t. The registered turbidity has to be corrected for the effects of particle

size and refractive index by application of MIE theory to yield the particle concentration of a particular size. In the newly constructed version in the same laboratory, a narrow continuous beam of a laser diode (λ =670nm) is used as the light source and a fast photodiode is used as light detector[76].

1.6 Analytical Ultracentrifugation (AUC) in Science

Analytical Ultracentrifugation (AUC) has proven to be a valuable tool for the study of macromolecular systems since its invention by Svedberg[77.] Earlier studies by Svedberg were confined to the study of proteins and particle size characterization of gold colloids, however, the importance of the technique could soon be felt in several areas where macromolecular characterization is of prime importance. There are numerous examples of information derived by one of the four basic experiments or combinations thereof using an ultracentrifuge. The impact of AUC is well discussed in many reviews that cover different aspects of the technique[78-84].

i) Application of AUC in analysis of colloids: The application of analytical ultracentrifugation for the determination of particle sizes and their distributions to was already realized by the pioneers of this technique, because sedimentation velocity experiments provide a sensitive fractionation due to particle sizes or molar masses[85-88]. It is relatively straightforward to convert a sedimentation coefficient distribution to a parameter that can be determined from Ultracentrifugation experiments: using the equation $s = \ln(r / r_m) / \omega^2 t$ for every data point (a) r_i (if a radial scan is obtained at a specified time) or (b) t_i (if a concentration detection at a specified radius has been performed as a function of time) to a particle size distribution. Assuming the validity of Stoke's law (e.g. if the sample is spherical), the following derivative of the Svedberg equation is obtained

$$d_i = \sqrt{\frac{18\eta s_i}{\rho_2 - \rho}} \qquad (14)$$

where d_i is the particle diameter corresponding the sed. Coefficient to s_i, ρ_2 is the density of the sedimenting particle (including solvent/polymer etc. adhering to the sample), and

η the solvent viscosity. If the particles are not spherical, only the hydrodynamically equivalent diameter is obtained unless form factors are applied if the axial ratio of the particles is known from other sources like e.g. TEM. The conversion of the sedimentation coefficient distribution to a particle size distribution highly relies on the knowledge of the density of the sedimenting particle. Thus the determination of the particle size from Analytical ultracentrifugation is quite robust and rapid, with comfortable statistical accuracy (since every sedimenting particle is detected) in contrast to transmission electron microscopy (TEM) which delivers information about the particle shape but often suffers from the drawbacks due to drying artifacts. Determination of particle size distribution from TEM images requires counting hundreds or thousands of particles, although this problem has been partly diminished by the advent of commercially available picture evaluation algorithms. A combination of TEM, AUC and X-ray diffraction techniques can provide a complete insight into a colloidal system[89]. AUC in combination with electron microscopy in its various forms can be considered the most powerful characterization approach for the determination of particle size distributions and particle morphologies known to date. There have been many examples that illustrate the fractionation power of the AUC for latex[90,91]and especially for inorganic colloids[92].

ii) Application for Investigating Biological systems: AUC has proven to be a widely used method for the characterization of self-association and heteroassociation of macromolecules in solution. Such interaction was predominantly studied with sedimentation equilibrium experiments which were further supported by the determination by X-ray diffraction crystal structure.

Nowadays, sedimentation velocity is also increasingly applied for the determination of interaction constants. Examples have shown how both sedimentation velocity and the sedimentation equilibrium experiment can be used to investigate in detail the self-association of insulin analogues under formulation conditions[93] for pharmaceuticals. The implications for the pharmacokinetic and pharmacodynamic responses of these insulin analogues were discussed, and it was suggested that

sedimentation analysis can help in developing improved rapid-acting insulin therapies, and furthermore that AUC is one of the few techniques where analysis can be performed on the formulation and result in quantification of the protein interactions under those conditions[94]. An excellent example of the application of sedimentation equilibrium analysis to characterize protein ligand and receptor interactions is mentioned in the work of Philo and his colleagues[95]. Sedimentation equilibrium analysis at varying rotor speeds could reveal the very weak binding constant of receptor and protein. Various studies indicating the study for characterization of receptor protein ligand interactions can also be found[96,97]. There have been reported applications of a wide range of applications of the use of sedimentation equilibrium to characterize protein oligomerization including the dimerization of human growth hormone by zinc[98] or self-association of biglycan[99].

AUC has also found application in the study of biopharmaceutical stability and homogeneity. This step is one of the most important steps in the development of pharmaceuticals; the degradation products of biopharmaceuticals often include aggregates and fragments. One possible way to identify these degradation products is to determine their average molecular weights by using sedimentation equilibrium analysis[26,100]. For highly purified and homogeneous molecules, the average molecular weights for the pure and non-self-associated macromolecules under ideal conditions should be very similar to the monomer molecular weights. On the other hand, for macromolecules that have undergone aggregation or fragmentation, the apparent average molecular weights under ideal conditions will vary from the monomer molecular weights. The purity of biopharmaceuticals can also be determined by the sedimentation velocity analysis. Several sedimentation velocity methods have been developed to determine the distribution of protein species, the most useful one being van Holde and Weischet analysis[101,102]. This approach is well documented to provide a rigorous test of sample homogeneity[103] and has been successfully utilized to study the homogeneity of macromolecules[104,105]. A different method, with the extrapolation based on the time derivative of concentration distribution has also found application in the identification of impurities in macromolecules[106,107]. This method has been used in combination with other methods viz. SDS, polyacrylamide gel

electrophoresis and gel permeation chromatography, to help determine the purity and homogeneity of macromolecules in solution[108].

Another quite useful application area of AUC is the determination of the binding affinity of protein interaction to biopharmaceuticals. This property of proteins is thermodynamically reconcilable and hence the sedimentation equilibrium experiment has proved to be the most rigorous method for its determination[33]. The sedimentation equilibrium method has been successfully and extensively used by many workers to investigate the association constants of interacting systems [27,109,110]. AUC has also been extensively used by biochemists and biophysicists for the study of biopolymers with respect to solution conformation, conformational changes, association behaviour, and homologous and heterologous interactions (including the thermodynamics)[111,112].

Apart from the above mentioned applications AUC has also been prominently used to study other bio macromolecular systems such as polysaccharides[113].

Chapter 2

2.1 Current Trends in Analytical Ultracentrifugation (AUC) Research - The Need for Development of New Detection Systems

Developments in AUC have been of interest to several research groups worldwide. This includes the development of AUC to investigate novel systems, improvement of data evaluation methodologies to solve biophysical questions etc. The least developed, yet most vital component in AUC is the detection system. This is primarily due to the hardware development time necessary for detection systems. Final adaptation of a new system to an existing AUC platform needs design and construction of new mechanical and electronic parts which are often time consuming. However, to meet the experimental demand of sensitive, faster, and increasingly online data generation, the development of new detection system has become essential. Also, the present detection systems for AUC can not supply a satisfactory amount of chemical information. In his visionary paper, Mächtle[114] mentioned about the future requirement of AUC detection systems with the need to implement a light scattering, IR or Raman detection system to generate data enriched with more chemical information. Such optical systems can be developed and designed for simultaneous use with the present absorption and Rayleigh interference optics.

2.2 Components in AUC Optics

AUC optics comprises a light source for illumination of the cell followed by other optical components (e.g lenses, mirrors) and finally a photosensor to collect the light emerging out of the cell. When designing the optics for AUC, an adaptable system is necessary to address the different parameter of various experiments. Unlike the selection of the light source, selection of other components are difficult as they may depend upon various factors such as aberration effects[115] (e.g. spherical aberration, monochromatic off-axis aberration, chromatic aberration etc.). In the selection of the photosensor, there are

also choices available and one can decide on the basis of the need, for enhanced sensitivity, faster response, or a compromise between these two. A photomultiplier tube, for example can well serve for high sensitivity, while a photodiode can result in faster response but less sensitivity. Examples include: photographic plates (in today's context with the use of cameras), vacuum devices like a Photomultiplier tube (PMT), semiconductor devices (a photodiode) or gaseous photodetectors. Light from the source uses illumination optics to make it incident on the cell sector which after emerging from the cell sector is collected by detection optics and finally passed to the photosensor. The primary requirement of the illumination optics design is for light to be drawn into the AUC vacuum chamber as the detector should collect data from a sedimenting sample in ultracentrifugal field in this chamber. In order to achieve this, optical fibers can be used. There are many types of commercially available optical fibers so that one can make a selection on the basis of the required working wavelengths (e.g. if the fiber needs to guide light for UV light, a quartz fiber will have to be used) or enhanced photo flux (e.g. for enhanced intensity a larger cladding/ core diameter fiber can be used). For the design of illumination and detection optics, components like lenses, mirrors or prisms can be used.

In order to maximize the performance of the detector, operation of the lamp and the photosensor needs to be controlled. This requirement arises as synchronization of the light source with the rotor movement is necessary. The desired situation is that light should enter the photosensor only when the sample is in the path of optics. With today's technology, one can implement this synchronization by triggering the detector read out device (the photosensor) along with the light source, when the sample cell comes into this path. Use of suitable multiplexer technology can enable this, and various research based on the development of multiplexers for AUC[116-119] has developed such a system. In the present XL series of AUCs, the multiplexer signal can be input from the XL-I boards directly and can be used for triggering signal of the optics (see Fig.13). These signals come as TTL (Transistor Transistor Logic) signals and can be used by software as information source of rotor movement. However, the XL preparative platform requires conversion of the rotor signal obtained from the XL board to a TTL signal.

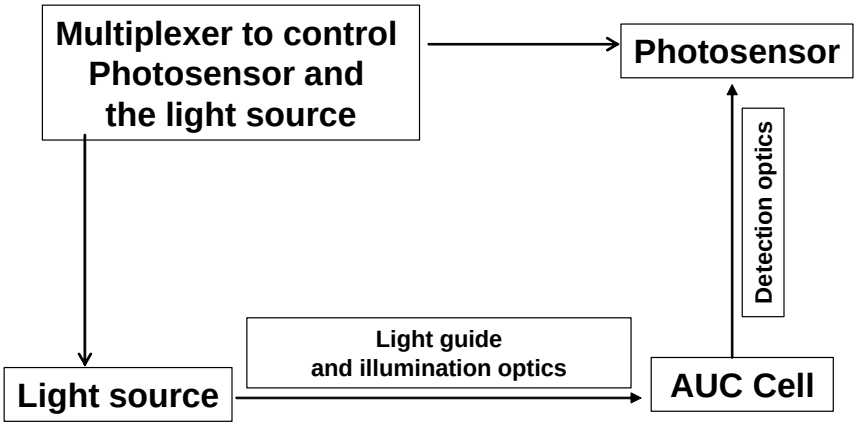

Fig.13 AUC optics scheme

2.3 Alignment of the Optical System

For any optical system to yield an accurate and meaningful result, it is necessary for all the optical components to be aligned on a common optical axis and positioned on the basis of this axis. Once a detection system is designed or developed, it becomes important to find a procedure for such an alignment. The exact procedure necessary to achieve the precise alignment will vary from system to system. In the case of alignment of the optics, the optical axis must be defined from the light source to the cell and then to the detector readout device (the photosensor). Primary trials for this should be performed on an optical bench. Once the optical axis is defined, all the components comprising the optical systems (e.g. lens, mirror etc.) must exactly match this previously defined optical axis. After precise alignment of each component e.g for lens (with its correct focusing/imaging)), mirrors, pinholes and filters (coupling in/out correction), one can make a preliminary check of the alignment of each component by using an optical power meter or a spectrometer (as applicable) to confirm the degree of alignment (in many cases this may be indicated by the fact that the intensity of light is at its maximum). An ultimate goal for defining the optical alignment should be determined with respect to maximum intensity from the optics or image formation.

Chapter 3
A Raman Detector for Analytical Ultracentrifuge

3.1 Introduction

Raman Spectroscopy is a well known technique, often used complementary to infrared spectroscopy, and is capable of providing quantitative analysis and detailed information about molecular structure. The importance of this technique has been well realized for investigating a wide variety of samples ranging from the molecular changes while studying ultra fast reaction dynamics of proteins[120] or protein ligand interactions[121] to polymer studies[122] and inorganic complexes in solution[2]. Unlike IR spectroscopy, Raman spectroscopy provides informations about symmetric molecular vibrations and allows one to obtain spectral information in aqueous solution. This property makes the technique a quite valuable tool for biochemists and also for the analysis of polymers and colloids as different components in a mixture could be chemically characterized. Thus, combination of Raman data for a fractionated sample in a centrifugal field will supply chemists with valuable information from a sample mixture as different components in a mixture could be chemically characterized while simultaneously obtaining the chemical group-dependent concentration information. Although there has been quite an advancement for the Raman instrumentation with new technologies e.g. with CCD detection, the high cost of the instrumental setup is often a constraint. However, one can consider the building of a Raman setup coupled to an Ultracentrifuge by assembling only commercially available components[123], and this was the initial motivation for constructing a Raman detection system.

3.2 Hardware Development

As the first step it was necessary to construct an adoptable Raman optics setup for AUC. Therefore, it was decided to make an overview of commercial products for which possibility for adaptation to AUC would be possible. The following setup considered likely to yield optimum data quality if adapted to AUC was envisaged:

1. **Fiber optics based Raman probe for data sampling in back scattering mode:** Working with a fiber optics based probe allowing light guiding inside the AUCvacuum chamber.
2. **Raman probe of focal length 3cm:** This was decided on the basis of the fact that the Raman probe will have to be kept at a distance away from the sample in the spinning rotor while we can get optimum signal quality.
3. **Application of pulsed laser:** A pulsed laser can well serve the purpose of working with short exposure time for a spinning sample in conjunction with a detector that can be triggered allowing for multi-cell operation.

Samples of polystyrene latex with varying concentrations were sent to manufacturers whose products looked adaptable to an AUC and who were willing to perform test measurements for such an evaluation (Chromex Inc. USA, Kaiser Optical Systems SARL France, Jobin Yvon Horiba, Germany)[124-126]. Satisfactory data was obtained to encourage the assembling of a Raman AUC detection system n the laboratory, the best result being obtained from Chromex Inc, USA (Fig.14 and 15). However, it should be mentioned that the laser was in continuous mode while performing the experiment due to suppliers' operational constraint.

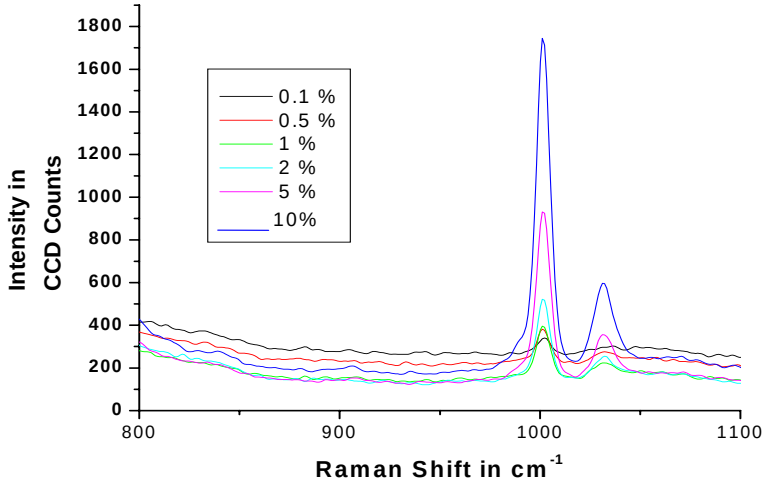

Fig.14 Raman spectra for a polystyrene latex sample with different concentrations and with integration time of 2s. The data collection was performed in back scattering mode with a 785nm laser of power 500mW, detector: CCD 1024×256 pixels.

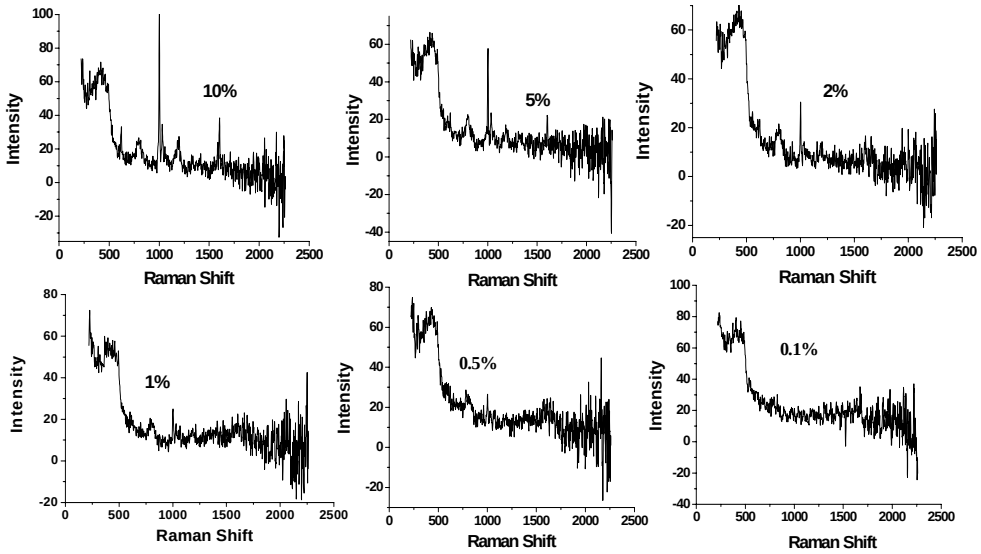

Fig. 15. Raman signal observed for different concentrations of a Polystyrene latex with integration time 0.1s. Similar instrumental configuration as in fig. 13.

The data from the commercial instrument (Chromex Inc) showed linearity in response in the 2s integration time. However, the results looked quite inferior in very low integration time, the 0.1% concentration with 2s integration time was almost at the noise level. For AUC measurements this is not a satisfactory situation as this concentration does not corresponds to the lowest detection limit of AUC. Furthermore, this integration time for AUC experiments is not realistic for which an integration time in the ms range is required. Also the very high cost of the setup ($110,878 in Nov. 2003) looks to be a prime constraint. Thus we decided to try a possible Raman setup for AUC with facilities in hand, to check for the integrity of such an AUC detection system.

3.3 Check of Integrity of a Raman Setup to an Analytical Ultracentrifuge (Front scattering mode)

3.3.1 Construction of Setup for measurements to be performed in AUC

As a first test for a Raman setup to be adaptable to an AUC, it was decided to work with optics in front scattering mode. This was because of the fact that for such a setup hardware components were available which could be constructed on the existing preparative XL-centrifuge platform in hand. The following components were procured to perform a first check on a real AUC setup:

i) Laser: Compass^{TM} 315M (obtained from BASF-AG)

Wavelength: 532nm, Power: ~20mW

Laser Source: Diode Pumped Nd:YAG

The laser was equipped with a Schäfter + Kirchhoff two fiber system that ends with a single mode fiber with polarization maintained on both sides FC-APC (8° angled polish) connectors, mode field diameter 4 μm, NA: 0.11.

ii) Spectrometer: Spectrapro 500i (Acton Research) with software "Scancontrol Spectroscopy Plus". The spectrometer is equipped with a TE cooled CCD camera (Obtained from the Interface department, MPI-Golm).

iii) Optical fibers: 600 micron patch fiber UV/Vis (Ocean optics, The Netherlands)

iv) Other Optical elements: one 90° Prism, Biconvex lens (f=20.6mm, 20mm and 10mm) all from Linos, Göttingen, Germany.

In order to work with the above facility the following setup was applied (fig.16). However, due to hardware constraints, in the preliminary set-up the measurements had to be performed while keeping the centrifuge door open to feed in the fibers. The maximum working speed is 3000 rpm in such a situation.

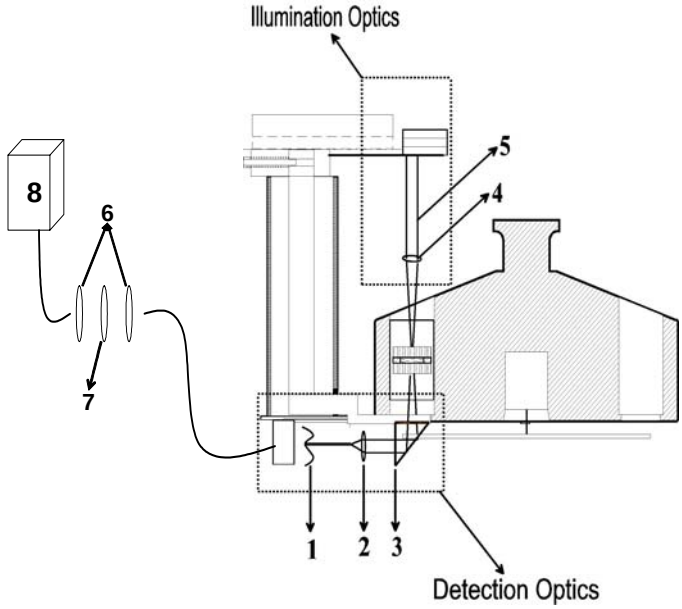

Fig.16 Schematic of the Raman detector setup: (1) 600 micron patch fiber UV/Vis (Ocean optics), (2) The collimating lens system (self built), f= 20.6mm biconvex, (3) 90° Quartz Prism, (4) Converging lens to focus laser to the cell sector f = 20 mm biconvex, (5) Laser (6) Biconvex lens (f=10mm) (7) Edge filter (8) Spectrometer.

3.3.2 Results and discussion:

Gold colloid and polystyrene latex samples were selected to observe the signal quality of the setup. The sample selection was made on the basis of the high intensity of Raman scattering peak of these samples since the rotation of the rotor will diminish the signal intensity to a large extent. However, from a low speed of 1000 rpm no Raman signal could be observed. With a standstill rotor and the sample directly in front of the Laser, very weak Raman signal from the Polystyrene sample (for 5% Polystyrene latex sample, peak position at~1000cm^{-1}) could be observed (fig 17).

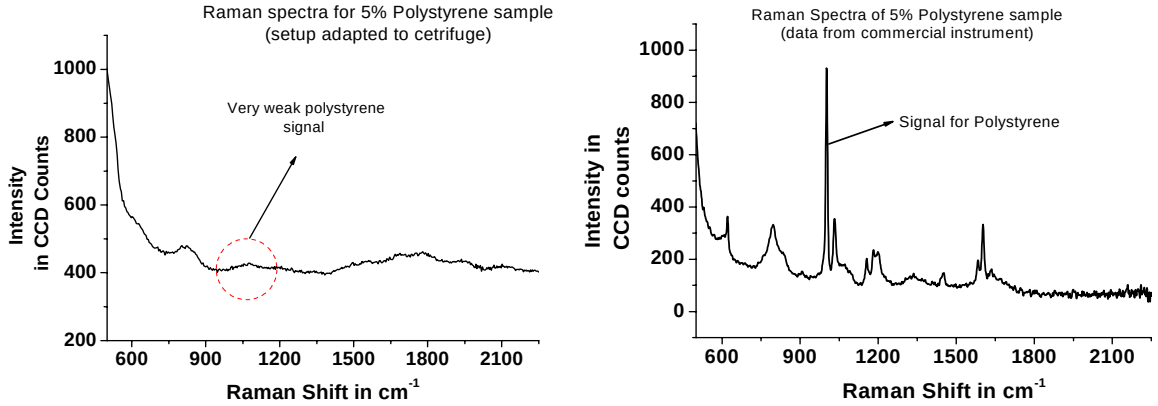

Fig.17. Signal from a Polystyrene latex sample (5%in water) Signal intensity was very weak with the setup adapted to the centrifuge (5s integration time with 3 acquisitions, standstill rotor).

Similar results with very weak Raman signal were also obtained for Gold colloid sample. Raman spectrum recorded with the setup for Gold colloid is shown below:

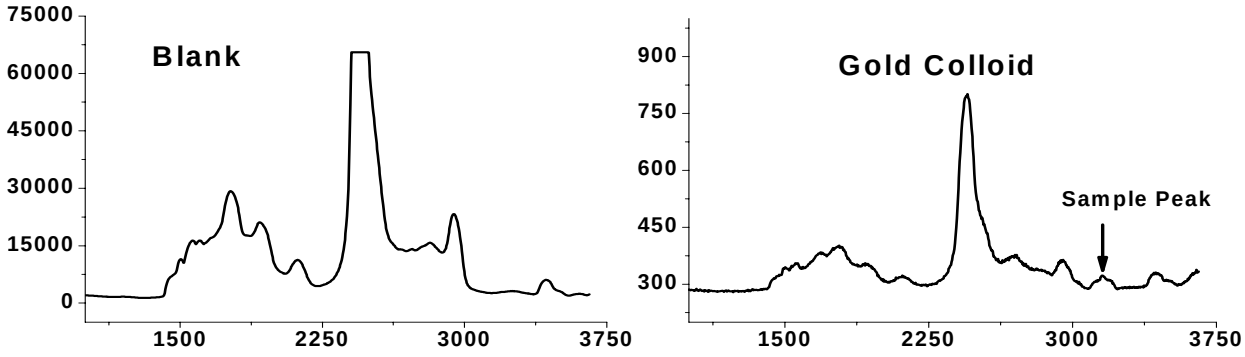

Fig.18 Raman spectrum of Gold colloid sample recorded with the setup (30s integration, 3 acquisitions). The very high background signal (the other peak, aside from the sample which come from the background, air, solvent etc.) shows that front scattering mode should not be a preferred mode. The higher intensity of the background signal in blank is due to lower turbidity of the solution compared to the gold colloid sample. With less turbid sample, more of incident radiation can pass through the sample and finally more intensity arrives at the detector, hence the contribution to background signal is higher.

Even varying the recording parameters, sufficient signal intensity of the spectra could not be observed. Thus it was concluded that the required Raman signal for adoption to AUC would not be possible working with the present setup. Possibly, a 20mW laser may not be sufficiently powerful to generate an observable Raman signal, however, the huge contribution from the background, the signal being ~1/3 of the background in every case, is also quite discouraging.

3.3.3 Requirement for getting a satisfactory Raman signal

Loss of light due to the Optical setup:

One possible reason for the very weak signal intensity from our setup could be that the intensity of light at the detector was not optimal. Many coupling positions exist in the setup where loss of light is inevitable. Thus as a next step, it was decided to check for the loss of light intensity at different positions in the optics where coupling was performed. Figure 19 summarizes the loss of light at these positions. Measurement in loss of intensity was performed with an optical power meter, collecting the light directly from each position with the help of a fiber.

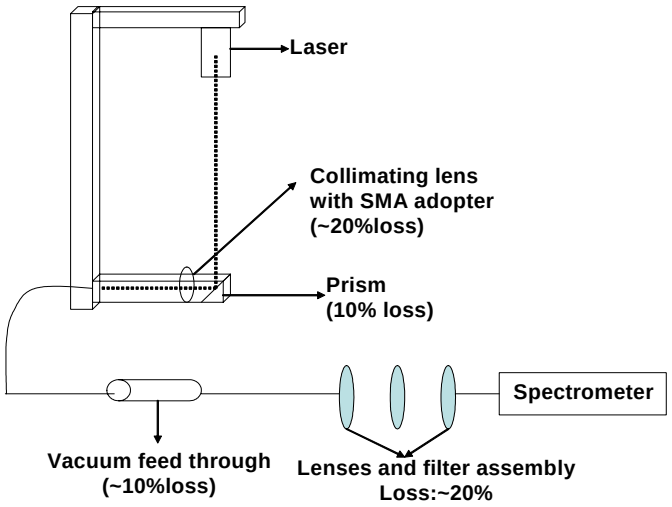

Fig.19 The different coupling points in the optics showing the amount of light intensity lost from light source to each position. A total loss of ~60% incident light intensity was observed.

From the amount of light loss in the above in description, the loss of 10% light due to the vacuum feed through could be regained with the use of penetrating type feed through, instead of receptacle type ones, as this removes the necessity to use an extra fiber

coupling. However, with the present setup the other losses could not be overcome due to the time constraint and necessity of major modifications to the hardware mechanics of the heat sink. Therefore, a ~60% loss of light intensity from the incident light to the point of insertion to the spectrometer was concluded. The loss of ~20% light intensity before and after the filter may not be correct as for measuring this loss, the filter had to be removed.

Calculation of Laser power requirement for working in the current setup:

During the spectra recording while looking for the satisfactory Raman signal a strong peak at ~4400cm^{-1} could be observed (Fig. 20). The intensity of this peak can be regarded as a reference for calculating the necessary laser power for making the Raman setup adaptable to AUC. This peak can be assigned to scattering by the sapphire window.

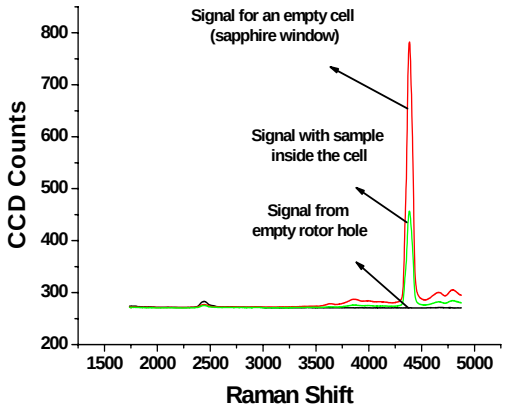

Fig.20 Signal due to sapphire window of an AUC cell. A proof of the fact that the peak at ~4400cm^{-1} was from the sapphire window material.

The peak at ~4400cm^{-1} showed a diminishing of intensity by a factor of 87.5 times (Fig.21, the peak intensity comes down to 2 from 177 after the rotor was rotating at 1000 rpm). With this observation it was concluded that the necessary laser power necessary for a satisfactory Raman signal, with the present setup, was 20 x 87.5 = 1750mW (for a laser of wavelength 532nm and a rotation speed of 1000rpm).

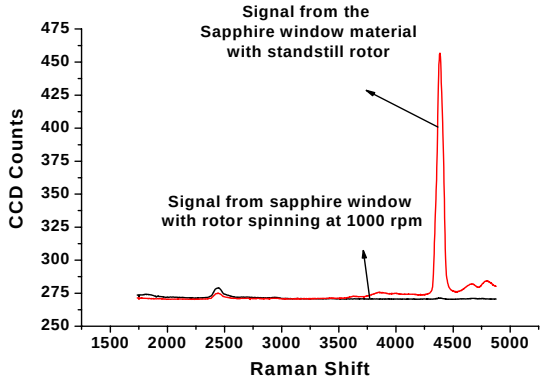

Fig 21. Diminishing signal intensity with spinning rotor

However, with minimizing the loss of intensity at different coupling positions and improvements with the use of a pulsable laser, there is enough potential for gaining in the signal intensity.

3.4. Raman setup in Back scattering mode

A test for back scattering mode was also performed in the existing preparative XL-ultracentrifuge platform. The components used were similar to the earlier, front scattering setup except for the fiber collimator (pigtail style collimator from OZ optics, Canada) for collecting the scattered light. This collimator was fixed in the optics hardware at an angle of 10° with respect to the direction of propagation of the laser (Fig. 22). The other end of the fiber collecting the scattered light was fitted to the lens filter assembly and then to the spectrometer respectively.

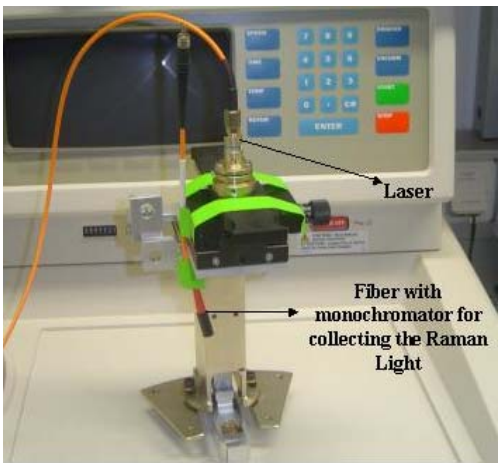

Fig.22: Detector arm fitted with the illuminating laser and fiber optics collimator for collecting the back scattered light.

With this kind of setup, no signal could be observed for a 5% polystyrene latex sample with long integration time and increased acquisition numbers (Fig 23). It should be mentioned that in the detection part of the optics, one extra fiber coupling had to be incorporated in order to achieve the necessary length of the fiber optic cable to the lens filter assembly before the spectrometer. The very low signal for the back scattering Raman setup was expected as for this mode the scattered light intensity is the least.

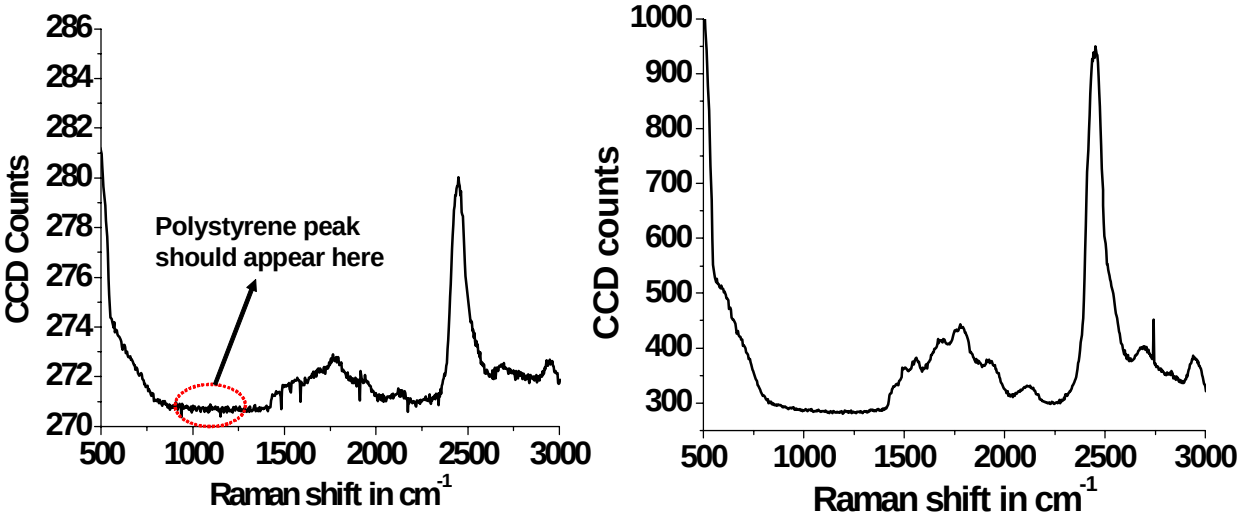

Fig.23 Raman signal observed in back-scattered mode. Left: Raman spectra for a 5% polystyrene latex sample. Right: Background signal for the same sample. (Experimental conditions: 30s integration time, 5 acquisitions, rotor standstill). No Raman signal could be observed in the back scattered mode. The higher background signal may be attributed to the lower turbidity of the blank sample.

3.4.1 Discussion: For Raman spectroscopic measurements, the preferred setup is the back scattering mode, since this mode decreases the possible problems that may be faced for aligning the optics. However, in our case a back scattering angle of 180° was not possible as this would require major modification of the test optics hardware with the incorporation of additional optical elements. However, such a mode is suggested for future trial, with the use of a high power pulsable laser.

Chapter 4

Small Angle Laser Light Scattering Detector for the Analytical Ultracentrifuge

It is well established that the intensity of scattered light is dependent on the molecular weight or the particle size. AUC experiments can also be used to measure these two parameters. With a light scattering detector, one can measure the online molar mass distribution of an ideal sample. AUC measurements have the advantage that, with respect to interference from dust particles and aggregates, which typically cause problems in traditional LS measurements a sample in the ultracentrifuge will be ideal due to the simultaneous fractionation in the centrifugal field. Moreover, with the use of the Svedberg equation, the sedimentation coefficient and molar mass distribution can yield the diffusion coefficient distribution. The relationship (molar mass) $\propto$ (particle size)^3 is the basis for determination of particle size distribution as a function of molar mass. Since scattered light intensity is proportional to the sixth power of particle size, detection of large aggregates would be possible even at very low concentration. The present technique requires very careful and time consuming measurements. As for determination of large aggregates one needs to perform AUC experiments in a special way such that data collection is possible. For studying biomacromolecules, light scattering experiments have proved to be quite informative[127]. Light scattering studies can cover a wide variety of samples and can serve as a general detection system[128] while simultaneously supplying additional information. In this chapter a summary of the development of a light scattering detector for AUC is presented. A part of this work was carried out with Carlo Sarnthein, former PhD student in our group (up to section 4.2.1)

4.1 The Initial measurement

In the first step for developing a static light scattering detector for AUC, one needs analyze the light scattering signal from an AUC cell, to determine the effect of cell component on the signal. To study this effect experiments were performed on an optical bench with a setup as shown in Fig. 24.

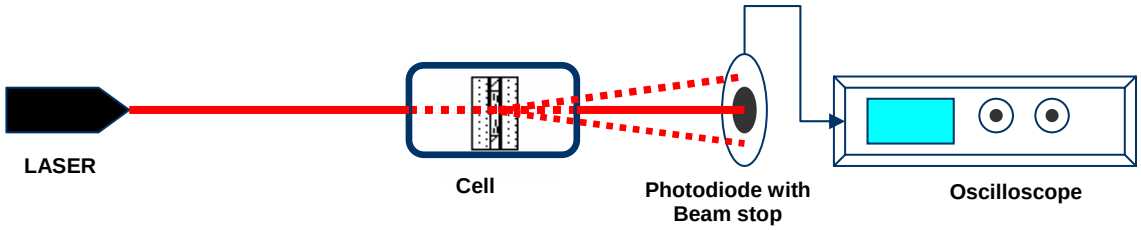

Fig. 24. Schematic of the light scattering setup.

The experiments carried out involve a pulsable 675nm diode laser of power 30mW flashed through the sample contained in an AUC cell. For detecting the scattered light, a large area photodiode (area: 10^{mm}, supplier: AMS Technologies AG, Munich, Germany) was used with a beam stop and the signal intensity of the scattered light was measured by an oscilloscope (TekTronix oscilloscope TDS 724 A). Enhanced signal intensity was obtained for an AUC cell with sample inside it and compared to the corresponding blank as shown in the figure below:

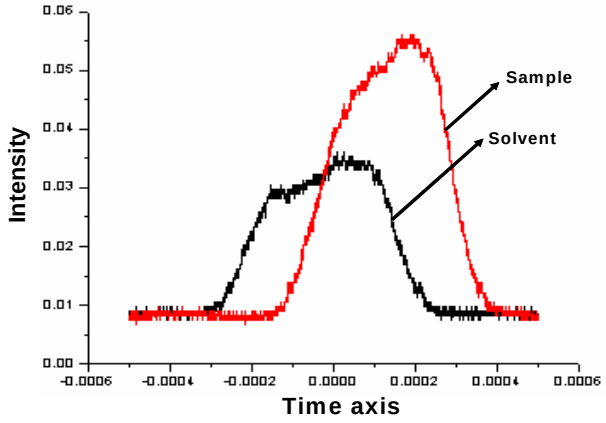

Fig 25. Scattered light signal from an AUC cell with sample inside and the corresponding blank solvent (sample: a 5% polystyrene latex, 200nm). The experiment was performed with a 675nm diode laser of power 30mW in pulsed mode and scattered light was collected in a large area ($10mm^2$) photodiode. The scattered light intensity was measured with an oscilloscope. Shift in the signal position may be attributed to the fact that the cell had to be placed in the path of the optics manually and this resulted in different window position to be illuminated for sample and the blank measurement as discussed in point (iv) in this section later.

The above observation clearly indicates that LS measurement is feasible from an AUC cell. In the next step, the following facts were established from the bench experiment:

i) **For a meaningful measurement of scattered light from an AUC cell, the restricted angle of measurement is restricted to the range of 2° to 5°:** This was established by replacing the photodiode with an optical power meter and varying the position of the power meter along the vertical direction (Fig. 26). Observation for increased power was noted with the variation of the position of the power meter. This can be explained by the fact that as the sample reside inside a sector-shape sample cell, the scattered light can not emerge in all directions. The angle 0-2° can not be reached as the corresponding area in the photosensor is the area for the primary beam (the beam stop) since the detector to sample distance can not be altered.

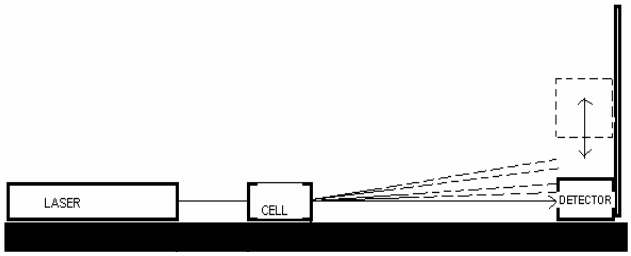

Fig.26 Experiment to establish the minimum and maximum angle of the scattered light from an AUC cell.

ii) **The interference from aggregates is unavoidable in the bench measurements**: This was observed from the fact that increased intensity of light was observed from an AUC cell with polystyrene latex sample. The signal intensity which disappeared once the same sample was placed in the optics path after brief centrifugation.

iii) **Very high background signal due to cell components:** For every experimental observation, the scattered light signal was always accompanied by a huge background signal. A detailed observation of the primary beam at the position of the beam stop showed that the main contribution to this signal was from the sector shaped wall of the cell. As the light propagates through the cell sector, it touches the sector wall and generates the background signal. Also, the cell wall gives rise to a multiple reflection signal.

iv) **Scattered light intensity for blank and the sample should be carried out from the same cell with intact cell window position:** The molar mass of samples was

measured from the scattered light intensity. However, the application of the Zimm formalism resulted in non reproducible and negative molar masses. Alternately, the calculation for molar mass was tried with the application of the following equation:

$$I/Io = kC\overline{M_w} \qquad (15)$$

where, I and Io are the scattered and incident light intensity and the new constant k = (r^2N/VK). This equation was derived from the equation

$$R_\theta = Ir^2/IoV = KC\overline{M_w} \qquad (16)$$

The comparison for the molar mass calculations was performed with the molar mass calculation derived from a sphere volume calculation on the basis of density data according to the following equation:

$$M = mN_A = N_A V \rho = N_A(4/3\pi r^3)\rho_p \quad (17)$$

Where, m is the mass of one molecule of the analyte, V is the volume occupied by it, r is the size of the latex in radius term and ρ_p is the particle density. For applying this equation, the value of 'k' needed to be estimated for every setup (the beam path, cell and the solvent had to be unchanged). It was also observed that by application of this equation, the molar mass calculation was not reproducible if the measurement for the reference solvent intensity is performed using a different cell. Thus for carrying out the measurement, the scattered light intensity for sample and solvent needs to be measured from the same cell. Recording of the scattered light intensity of the sample was done by placing the AUC cell in the optics path. The sample was then sedimented by centrifuging for a time long enough and the scattered light intensity for the reference solvent was recorded. For calculation of the intensities of blank and sample, the data points at the top of the signal were averaged and regarded as the intensity value for that signal. The following result could be obtained for one polystyrene latex sample:

Molar mass calculated with scattered light intensity: 2.3×10^9 gm/mol

Molar mass calculated from density data : 2.9×10^9 gm/mol

In this test setup, the agreement was reasonable.

4.2 *Online Measurement in the Centrifuge*

It was decided to make the online measurement of molar mass for a sedimenting sample in the AUC with adaptation of the above mentioned setup to it. The interference optics path in the XL centrifuge could be used for such experiments to be carried out. The applied setup is shown in Fig. 27.

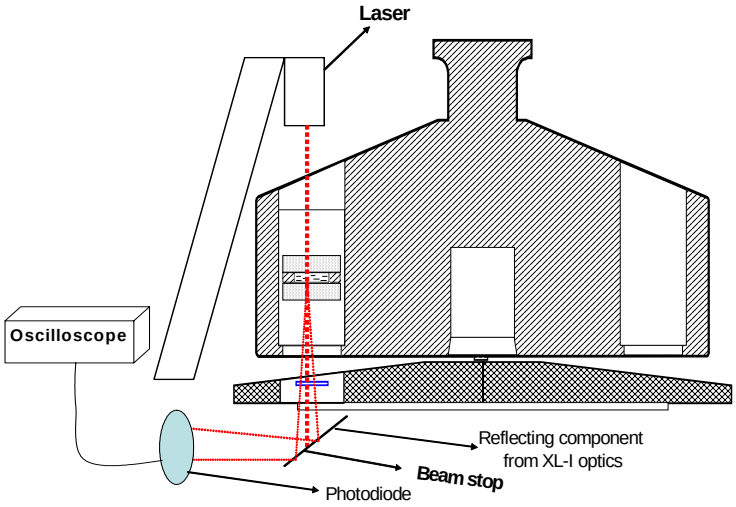

Fig. 27. Light scattering setup for online measurement of scattered light

However, the calculated molar mass did not correspond to the reference value (the label value of the sample). Owing to the very irregular shape of the signal from the scattered light and its very high dissimilarity from an ideal signal shape, such a setup could possibly always lead to an error while selecting the initial and final position of the signal for averaging the data points. It was quite obvious that for such a setup, the ideal signal shape should be a rectangular one. The signal should show its sharp rise when the rotor hole with the sample cell is in front of the laser and this intensity should continue until the sector is in the path of the optics (Fig.28). At position 1 as described in this figure, the cell sector is not in the path, and, no light reaches the photodiode. At position 2 the edge of the cell sector comes in the optics path and light hits the photodiode, giving signal intensity. At position 3, the cell sector is fully in the path and observation of signal intensity continues. At position 4, the opposite end of the cell sector comes in the path and the signal intensity is observed. At position 5, the cell sector leaves the path, no light enters the photodiode and no intensity is observed. With a pulsed laser synchronized with the rotor movement, the possibility of touching the edge of the cell sector is minimized and therefore, a

rectangular signal can be expected. Thus, it was decided to work on improving the signal shape as this will help to select the position in the signal for calculating the respective intensity.

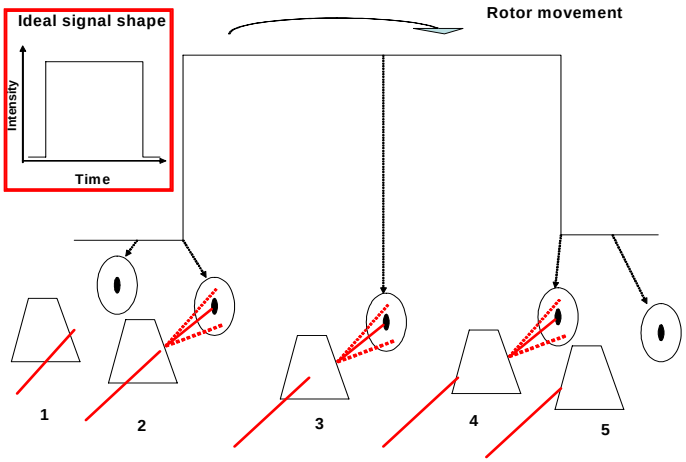

Fig.28. Description of the generation of the ideal signal shape. The red line indicates the laser beam propagation direction. The black spot with a circle is the beam photodiode with beam stop. The trapezium shape is the representative shape of the cell sector. Inset: the desired signal shape for the scattered light intensity with the cell sector as the sample holder.

4.2.1 Signal shape improvement

For measuring the scattered light intensity the XL-I optical path was used. The complex optical components can potentially contribute to the inferior signal shape, as the possibility that distortion occurs when passing through these optics components can not be ruled out. As a trial, signal shape was tested with systematic removal of the "complex" optical components. The figures 29-30 show respectively, a schematic of these components and photograph of the setup.

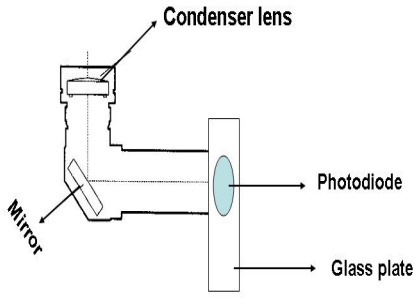

Fig.29 The part in the interference optics system with the photodiode fitted into it. The glass plate , mirror and the condenser lens were removed from the optics path for getting the ideal signal shape. (ref. fig.5 for the complete optics)

Fig.30 Photographs showing the fitting of the photodiode with the beam stop fitted to the optics. The photodiode with the beam stop was fitted in the optics path by gluing it on a glass plate and by removal of the components starting from the prism in XL-I optics(ref. fig. 5)

The results of the trial, presented in Fig. 31 show that the ideal shape could be obtained with removal of the optics components.

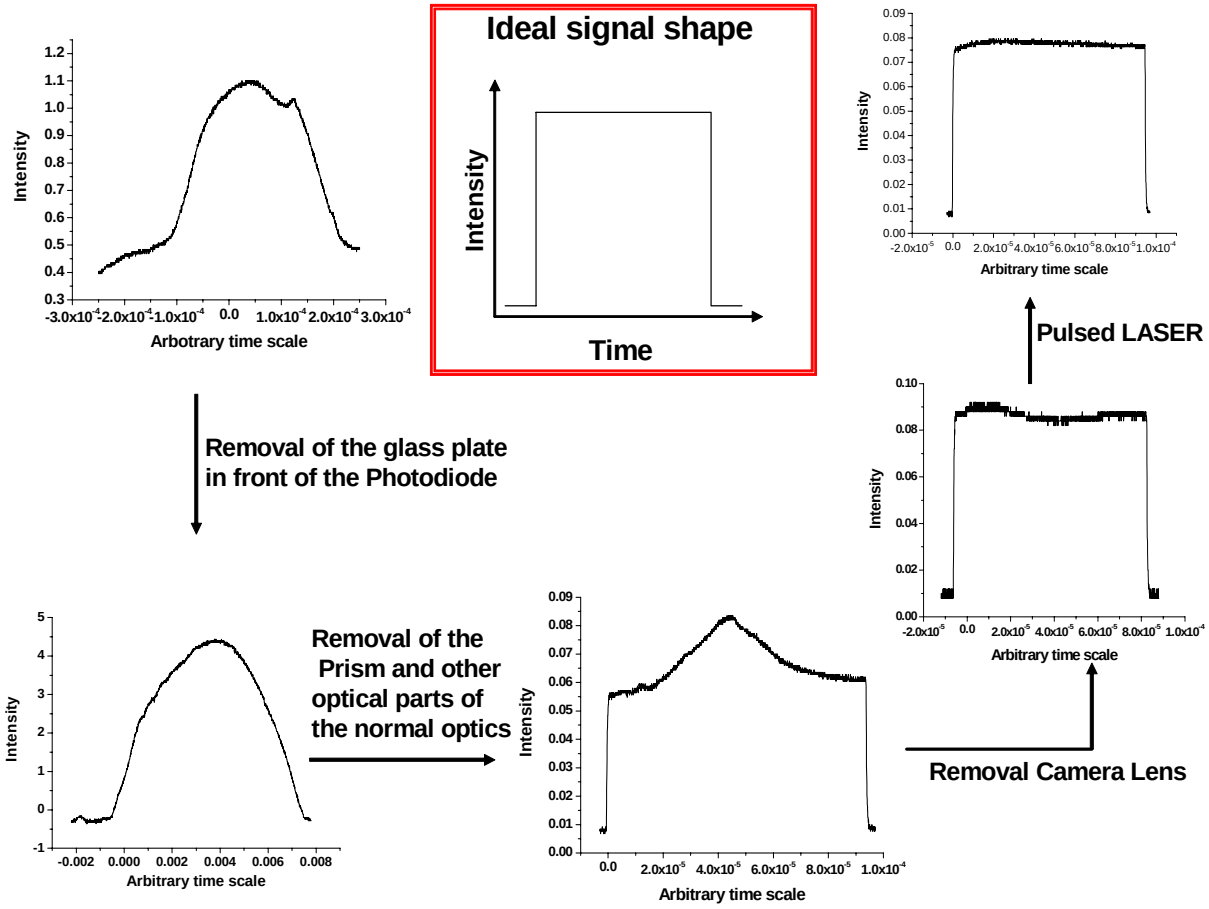

Fig 31. Improvement of signal shape by simplifying the XL-I optics

Thus, with the above results, it was decided to work with the following optics setup (Fig. 32) with simplified optics for recording the scattered light intensity.

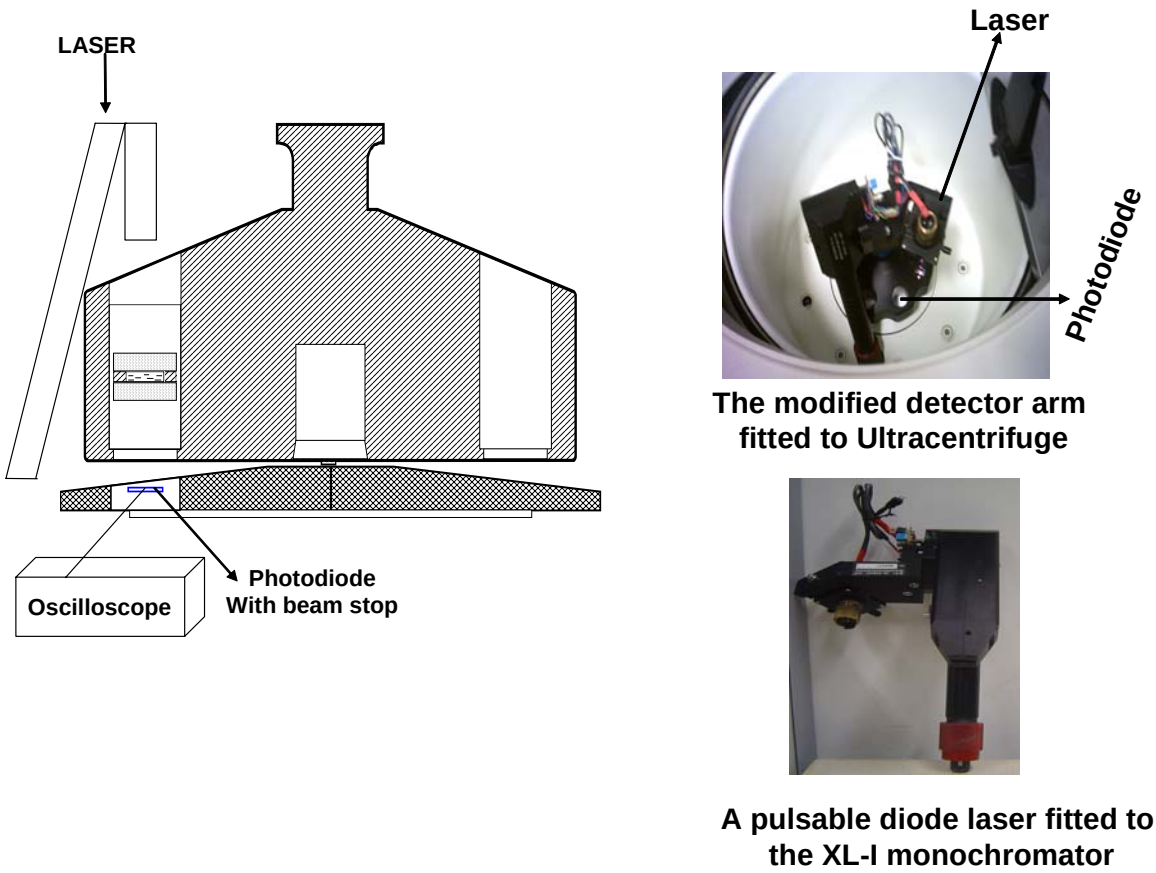

Fig.32 Modified setup for measurement with improved signal shape. Left is a sketch of the setup shown. The photograph in top right shows the setup as fitted in the AUC chamber. The photograph in bottom right shows the diode laser fitted instead of the original laser in XL-I monochromator.

Experimental result:

With the aforementioned setup, experiments for online calculation of molar mass were carried out. The photodiode was fitted in the place of the condenser lens in the AUC. As a result, working with a full vacuum in the centrifuge was not possible. In the test setup, a bigger polystyrene latex (d=185nm) was selected. Signal reading from the oscilloscope was recorded at regular intervals and with higher frequency (~2mins.) at the time of sedimentation of the particles, which was established from a reference experiment in a commercial XL-A. Fig 33 shows the observed sedimentation pattern which resembled the reference experiment, indicating conformity to sedimentation behaviour. It was also observed that the scattered signal showed a sharp decrease in intensity initially which disappeared with filtration of the sample, showing the presence of large aggregates in the sample, information that could not be extracted from the XL experimental data.

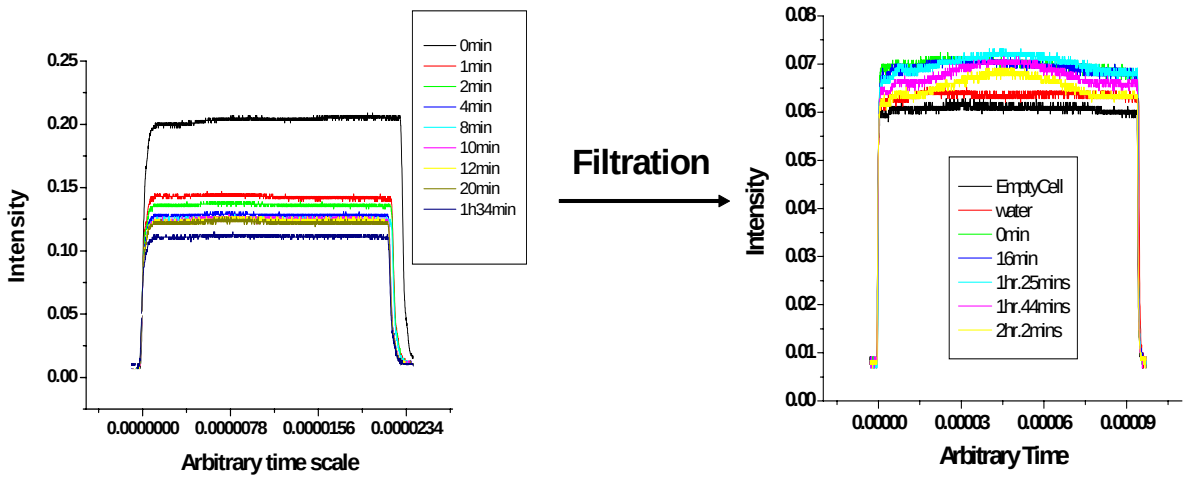

Fig.33. The decreasing intensity of scattered light with sedimentation of the sample. Presence of large aggregates were evident from the fact that the initial sharp increase in signal intensity vanished with filtration of the sample.

The molar mass calculated (using equation 15) for the sample is 3.2×10^9 gm/mol from the use of the scattered light signal. The comparative data generated from the XL-A led to a molar mass of 3.4×10^9 gm/mol (particle size: 185nm) (calculated using equation 17). This experimental result confirms that measurement of scattered light for an online AUC experiment was possible. Fig. 34 shows the XL-A data evaluation for determination of sedimentation coefficient that was used to calculate particle size and finally the molar mass of the sample.

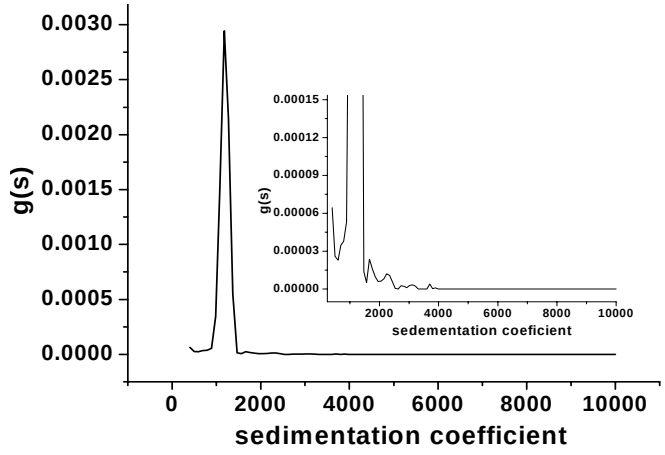

Fig.34 XL-A data evaluation with sedfit for the sample as in fig 33. Inset: zoomed version of the same distribution plot to show that the presence of large aggregate were not indicated.

4.2.2 Minimum molar mass detection limit for measurement

In next step of development, a sample with lower molar mass was measured with our setup. However, since the sensitivity of a PIN photodiode was the limiting factor, the measurements were performed instead with a photomultiplier tube (PMT) in the setup. Scattered light at a position away from the primary beam was collected with the help of a fiber which was coupled to the PMT. This was the only easy way to check incorporation of the PMT. These attempts produced erroneous results, possibly due to the fact that there was large interference from the primary beam with the fiber, which thus collected large amount of background light.

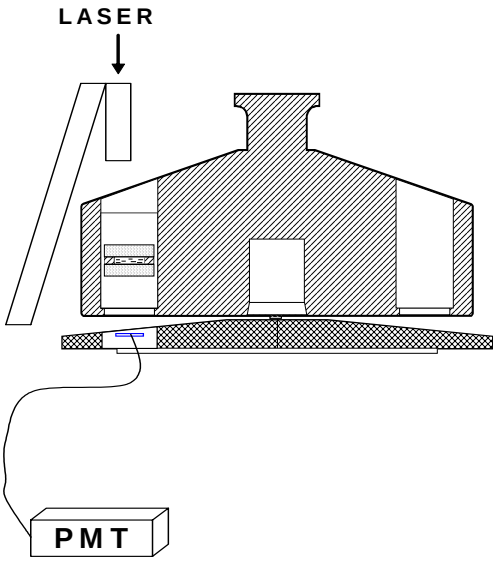

Fig.35 Setup for online measurement with PMT

Alternately, these experiments were performed on an optical bench to position the fibers while keeping the working angle of 2° to 5° intact. This modified setup was designed as follows (Fig. 36):

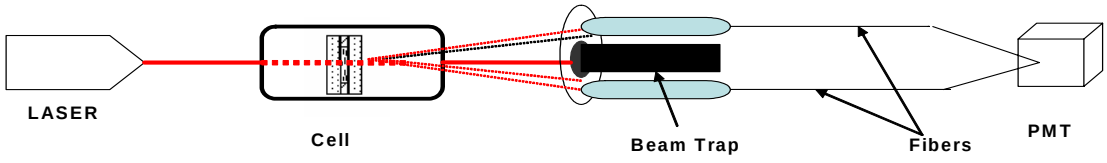

Fig. 36 Optics setup in bench using PMT for detecting scattered light

Experimental observation:

The experimental results showed poor reproducibility from calculation of molar mass. However, recording of scattered light intensity for a sample as dilute as 0.1% BSA

can nevertheless be observed. The molar mass calculation showed a dependency on the selection of the calibration standard for use in equation (15). The following data were obtained using the above mentioned setup with the use of different calibration standard for calculation of 'k' in equation (15).

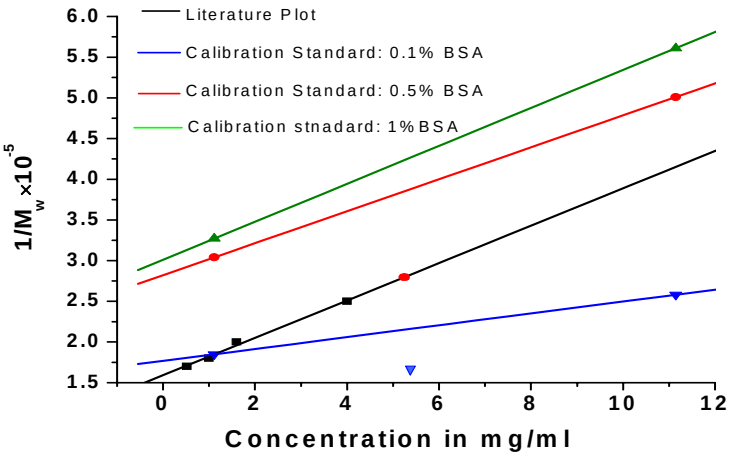

Fig. 37 Plots showing the calculation of molar mass from scattered light intensity, that indicate the dependency of experimental data on selection of the calibration standard for equation (15)

These data show the setup used cannot be correct due to the high dependency on the calibration standard and the slope of the curves being different. An explanation for such a variation can be the irregular background signal with respect to the fiber optics-based scattered light collection. In the earlier setup a photodiode was used for scattered light collection, providing a large area for the detection covering the majority of the illuminated part of the cell sector with respect to the laser, resulting in a constant background signal at the photodiode. This is unlikely to be possible with the use of optical fiber. When manually placing the cell into the path of the optics, the same position can-not be reached as high sensitivity of the PMT will produce a different background signal. Thus, use of a larger area detector is suggested for the future. An alternate test with the use of a biconvex lens, with a beam stop to collect the scattered light, focused on the optical fiber (as in the setup for above experiments) was also carried out (ref. Fig. 38 below).

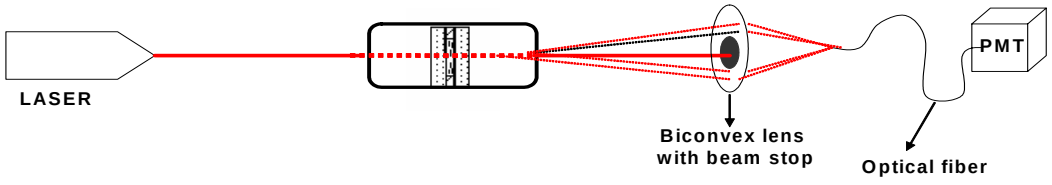

Fig.38 Optics setup with the use of a biconvex lens with beam stop for collection of scattered light

The background signal for this kind of a setup was very high and this led to saturation of the photomultiplier tube. Thus, this setup can not be suggested with a PMT used as the photosensor.

4.2.3Improvement of reproducible detection limit

In the next step of development, involved improvement of sensitivity of the detector system by working with shorter wavelength laser (green laser instead of red laser), as scattering intensity is inversely proportional to the fourth power of this wavelength. Thus, in the setup mentioned in the Fig. 36, the same green laser was applied as for the Raman detector Chapter 3). Tests were carried out on commercial Poly(ethylene oxide) (PEO) and polystyrene (PS) of varying stated molar mass, and solution concentration. These results are shown in Table 2. The molar calculated molar mass was not in concurrence with the supplier stated molar mass, and again showed dependency on the calibration standard.

Table 1 (Calibration standard used: PS 300,000 in toluene)

Sample (with supplier sated molar mass in g/mol)	Concentration in percentage wt/volume	Calculated Molar mass (in g/mol)
PEO (100,000)	0.18%	226796
PEO 100,000	0.9%	64751
PS 90,000	1.8%	112696

Table 2(Calibration standard: PEG 40,000 in water)

Sample (with label claim molar mass in g/mol)	Concentration in percentage wt/volume	Calculated molar mass (in g/mol)
PEO 100,000	0.18%	219928
PEO 100,000	0.9%	154315
PS 90000	1.8%	37984

Discussion: The above results indicate that there was very poor conformity to the measured values of the label claim for the samples. The setup was changed by replacing the photodiode with a PMT, and scattered light was collected from particular positions via optical fibers. This kind of a setup can carry the error of placing the fiber at a position with larger background reflections. From our earlier observations, it was also clear that the

background signal generation from reflections of the cell housing was not homogeneous at every point. Thus, unlike the photodiode setup, a good background signal subtraction was not possible with the PMT setup. The inhomogeneous background signal may be attributed to the fact that while placing the cell manually in the path of the optics; a different background signal may result due to the sensitivity of the PMT. Thus, for working in the front scattering mode, collection of light with a broader area detector is suggested. As a quick check, a biconvex lens with a beam stop was used to collect the scattered light, which always showed saturation of the photodiode signal. Therefore, for measuring scattered light from an AUC cell, the front scattering mode cannot be the mode of choice.

4.3 Photographic Detection

As another option, photographic detection was used. However, it was found that to use this type of detection, a major mechanical device design would be necessary. Alternately, the interference optics path in the centrifuge can be utilized for such a study with little modification, and the CCD based camera can also give satisfactory sensitivity. As an initial attempt, photographs were recorded for an empty cell. The XL-I monochromator was used with the 675nm (30mW) laser fixed in it (ref. fig. 32, photograph with the pulsable diode laser fitted to the XL-I monochromator). The following photograph, Fig.39, was obtained in the fringe display window.

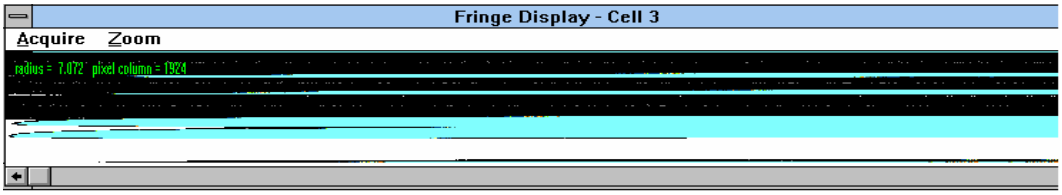

Fig. 39 Photograph of an empty cell with the use of the interference optics path.

In order to search for variation due to the presence of scattered light, the cell was filled with sample (PS latex, Molar mass label claim: 300,000 g/mol). However, no change in the photographic pattern was observed. In the next trial, the cylindrical lenses and the condenser lens were removed from the optics (ref. fig.5). However, no significant improvement could be observed (Fig. 40). The presence of the single white strips in Fig. 40 with the condenser lens removed was not reproducible.

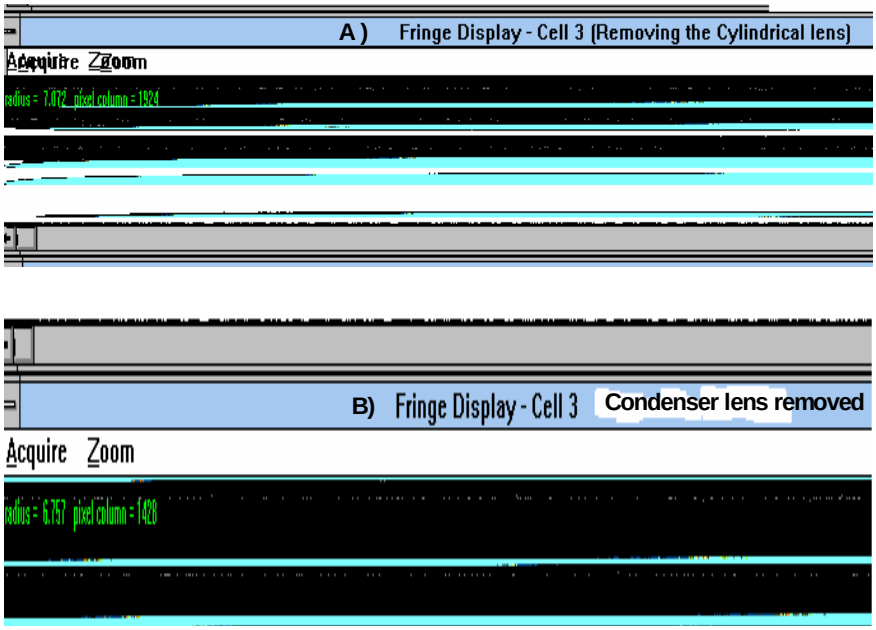

Fig. 40. Photographs obtained for cell with sample(PS 300,000 in toluene 1% wt/volume).The above figure (Fig.A) shows the photograph observed with removal of the cylindrical lens. The figure below (Fig. B) shows the photograph observed with removal of the condenser lens.

With the above data, it can be clearly observed that the interference optics path can not be used for studying light scattering with photographic detection. This may be possible with major modification in the interference optics setup or by using a new mechanical design where the scattered light can be collected in a mirror with a beam stop. This can be followed by devising imaging optics to feed the scattered light to a sensitive camera (as shown in Fig. 41 below).

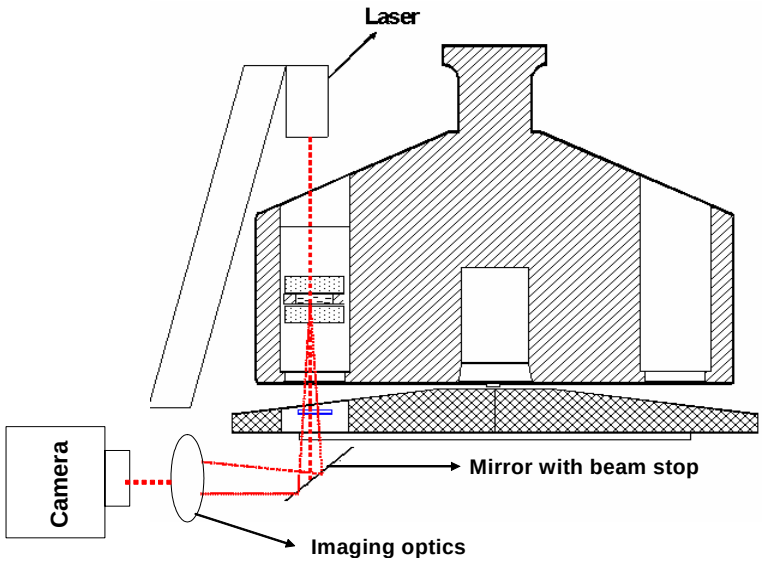

Fig.41 A suggested optics setup for photographic detection

4.4 Conclusion and Outlook

The experiments performed indicate that reliable measurement of scattered light from an AUC cell is possible. However, for such a detection system to work, it is necessary to devise a setup with satisfactory sensitivity and reproducibility. The presence of large background signal, currently ~80% of the total signal for photodiode measurements, must be minimized. In future efforts for a functional small angle light scattering detector, the following points are suggested.

i) Use of a laser with better beam profile: This can contribute to a reduced reducing background signal. In the above mentioned experiments, a diode laser was used, which has an elliptical beam shape and significant stray light. For a better beam profile one may choose a gas laser. The use of a space filter in the incident beam path could also sufficiently reduce the stray light which in turn will reduce the reflections from the cell sector window.

ii) Use of larger area detector: It was observed in the above experiments that the reflections from the cell sector are not the same in all directions. Thus, it is necessary to average the background intensity of the light from the primary beam. This can be achieved by the use of a larger area diode. Since more sensitivity is also highly desired, commercially available Avalanche photodiodes (APD) can be used. This was was by placing the APD in a housing so that it can be exchanged with the condenser lens in interference optics. However, the construction of an adaptable circuit to the AUC could not be completed.

iii) Back-scattering mode: In all the above experiments, the backscattering mode was not attempted due to the necessity of major mechanical modification to the illumination optics. This mode would diminish the background intensity greatly, and therefore, is suggested for future developments.

Chapter. 5

Fast Fiber Optics Based Multiwavelength Detector for Analytical Ultracentrifugation

Multiple wavelength study during an ultracentrifugation experiment has proven to be advantageous, in particular to study interacting macromolecular systems such as proteins[129-131]. A multiwavelength study will generate the possibility to exploit a new source of information: the absorption spectra of the solution at different positions in the centrifugal field. A combination of absorption spectra, scanned at multiple radii, and radial profiles scanned at multiple wavelengths, forms a two-dimensional data surface in radius-wavelength-absorption space, and so contains a lot more information than single radial profiles. The analysis consists of decomposition in terms of products of extinction profiles and exponentials, a problem that is generally much better conditioned than fitting exclusively. Also, the detection of the wavelength dependency of turbidity opens up the possibility to obtain independent information on the particle size in addition to the usual sedimentation coefficient distribution for colloidal systems[132-134]. In the history of AUC, it has been clear that significant effort from many workers towards the development in the field of UV/Vis detection system. The contribution from Flossdorf[135] significantly enhance the detected UV/Vis intensity as did the introduction of a photomultiplier detection system in commercial Beckman instruments[49]. In his attempt to enhance the UV intensity Flossdorf[136] used a parabolic mirror based collimator illumination system, and cylinder optics, to optimize the illumination band in the rotor so that only the two sectors in a cell are illuminated. However, the demand of AUC has become higher and higher with the advent of cheap and powerful computer based resources. This became clear with the introduction of the commercial Beckman Optima XL-A AUC, which far exceeds the experimental possibilities a few decades ago, resulting in increasing demands for data quality and accuracy. Despite this, development in the field of data evaluation has remained much faster than the development in the optical detection systems.

Application for a Multiwavelength detector include determination of extinction coefficients[137] for complicated mixtures, and sedimentation velocity[12] and sedimentation equilibrium[138] experiments for biopolymers, although in the later two cases results reported were for only three scanning wavelengths in the XL-I AUC. However, they illustrate the potential of working simultaneously with hundreds of wavelengths, allowing the user to generate a wavelength scan to every radial position thereby discriminating solutes in a more practical way to visualize. One can foresee the information available from such an experiment for an interacting, complex polymeric mixture. Also the wavelength dependence of the turbidity of colloidal samples is useful to detect as this contains information about their particle size according to the MIE scattering theory[139-142]. With the advent of global analysis approaches for AUC data, Multiwavelength analysis will become an especially important technique for all light-absorbing samples of a colloidal or polymeric nature. With the possibility of fast data collection, another dimension can be added to AUC experiments as speed profile experiments become possible, whereby data is collected simultaneously during acceleration of the centrifuge from 0-60000 rpm. If the detector can collect data with a data acquisition rate on the order of ms, a sedimentation velocity experiment can be designed that with the centrifuge being accelerated from 0-60000 rpm, experimental data can be collected with a minimal diffusion broadening. Parallel to the development of these AUC methodologies, there has also been advances in the UV/Vis technology. Modern UV/Vis spectrometers use CCD line arrays for simultaneous detection of a large number of wavelengths, which is essentially only limited by the CCD array pixel number as well as the quality of the applied diffraction grating for the dispersion of the incoming white light. These spectrometers not only do allow for simultaneous detection of the entire UV-Vis wavelength range, they are furthermore very fast and cheap. Commonly available spectrometers like the USB2000 by Ocean Optics allow for scanning times of down to 3 ms for an entire UV-Vis spectrum [143]. More recent instruments like the Ocean Optics HR4000[144] or the series of CCD and ICCD based spectrometers available from LOT-Oriel[145] are orders of magnitude faster and can scan UV-Vis spectra as fast as 10 μs. The cooled spectrometers give a quite broad linear dynamic range with the advantage of

working with low dark current due to cooling[145]. However, although these fast and powerful UV-Vis detectors are available, they have not yet been applied as detectors for AUC's. One of the reasons could be that these spectrometers are based on fiber optics and also operate with incoming white light. White light with wavelength-dependent refractive indices makes the precise use of refractive optics impossible, at least in the UV range where the conventional achromatic lenses cannot be applied, and the same is true in the visible range if an expensive UV achromat lens system is applied. This obstacle has no parallel in previous AUC optics, that always operates with monochromatic light – or in case of the XL-A AUC with a torroidally curved diffraction grating producing monochromatic light. It is only for this reason that the challenge of a Multiwavelength AUC optics has not previously been undertaken despite the potential benefits. Thus with this motivation, it was decided to start the effort to construct a multiwavelength detector for AUC. The work was carried out in collaboration with the Polymer Physics department of BASF-AG, Ludwigshafen, Germany.

This work was carried on the basis of previous development and experiences of a former PhD student in our group, Patrycia Maciejewska. The work will be divided into generation: The first generation comprises implementation of the previous work with removal problems that were associated with it. The second generation describes development for the data evaluation software and use of partial mirror based optics. In the third generation attempt will be made to design optics and instrument hardware with removal of experienced errors and instrument problem (heat sink modification from preparative to XL-I).

5.1 Development of a Fast Fiber Optics-based Multiwavelength detector for AUC (Generation 1)

5.1.1 The work so far

Work for developing a fast fiber optics-based Multiwavelength VU/Vis detector was in progress. The following conclusions were drawn from the previous work:

i) Construction of a Multiwavelength UV/Vis detector on an preparative XL Ultracentrifuge platform is possible, that can generate Multiwavelength UV/Vis range data.

ii) Reduction of the scan time by a factor > 100 is possible over XL-A, at comparable data quality in time scan mode, however radial scan mode so far remains as slow as XL-A.

iii) Two operation modes could be achieved: Constant velocity – radial scanning and time mode scan – time scanning at constant radius and movement of detector towards meniscus for fast detection could be achieved.

The following problems were highlighted from the initial experience from this work:

i) Very low light intensity through the optics. The loss of light intensity was especially severe in the UV region with almost no intensity at wavelengths below 300nm. Fiber bending also contributes to the loss of intensity.

ii) Lower than expected data quality.

5.1.2 Bench observations to optimize light intensity

Careful observation was performed for the alignment of each optical component used in the experimental setup. A scheme of the previous optical setup is shown in Fig. 82 below:

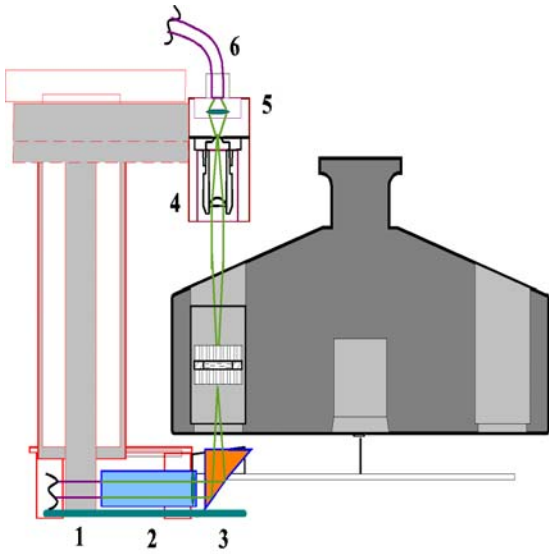

Fig.42 Experimental optics setup used by the previous worker. 1-600 micron patch fiber, UV-Vis (Ocean Optics). 2- The collimating lens system (self built) f = 20.6 mm biconvex. 3-90 °Quartz prism. 4-Slit-lens assembly (from the XL-A) only one lens f = 10 mm biconvex. 5- Focuser (OZ Optics) two lenses f = 10 & 15 mm. 6-1000 micron patch fiber, UV-Vis (Ocean Optics).

A simulation of the setup was constructed on an optical bench using microbench mechanical components from Linos, Göttingen, Germany. It was found that due to inaccurate design of the mechanical housing in the setup, optimal movement of the slit was not possible for it to be in the aligned position. The 25um slit (used from original Beckman XL-A slit-lens assembly, position 4 in Fig. 42) was glued in a cylindrical housing in a previously aligned position. It was decided to replace this part in the mechanical arm with a new design as follows. The design of the detection optics was altered to allow housing of a 20mm biconvex lens o collect transmitted light, followed by a 25 μm precision slit (MellesGriot, Bensheim, Germany) to define the spatial resolution and a 10mm biconvex lens to focuss of light emerging from precision slit back to the fiber. The schematic of this new setup is shown in the Fig.43.

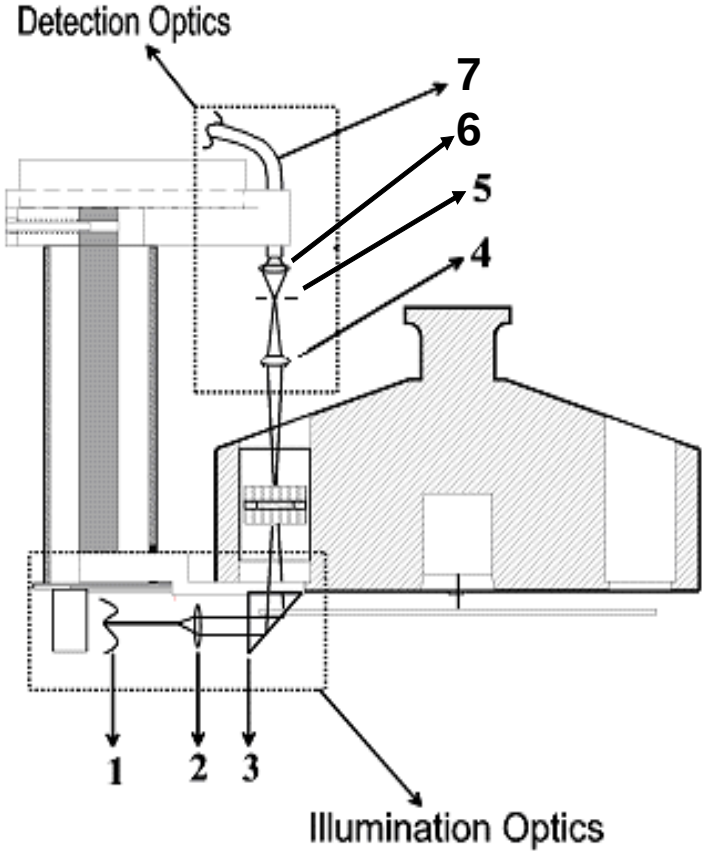

Fig. 43. Modified detector arm. The detector arm. 1, 2 and 3 are same as in the earlier setup. (4) Biconves lens f = 20mm (5) Slit of dimension 25 μm, (6) Biconvex lens f =10mm (7) 600μm patch fiber (Ocean optics). The light path is also shown schematically.

Fig. 44 shows the lamp spectra from both the optics and it can be observed that the new setup displays improved light intensity in the UV range.

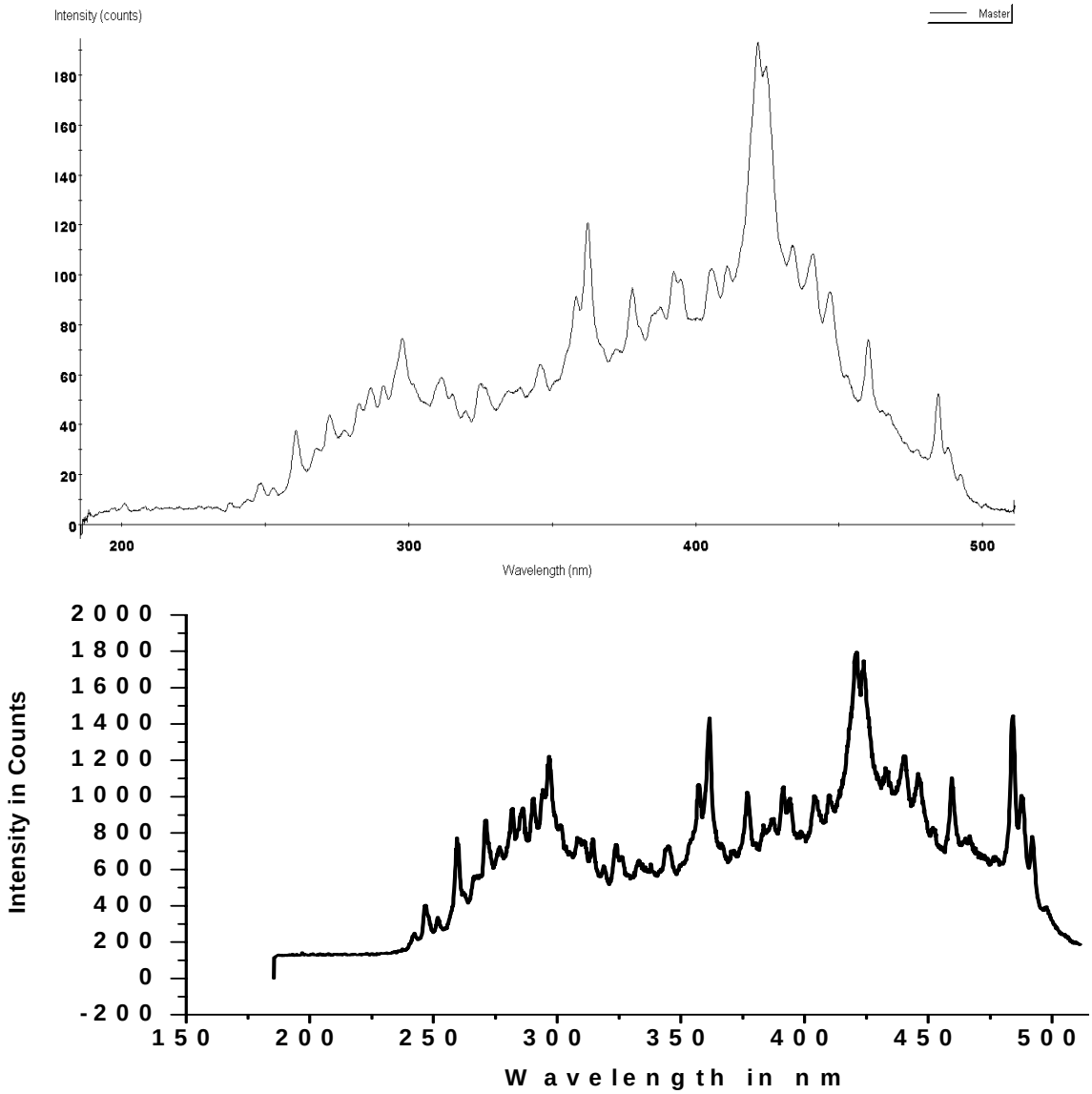

Fig. 44 Lamp spectra at the detection end (position 7 in the above figure) of the optics. The above figure shows lamp spectra from an earlier user setup. The figure below shows the spectra with the modified setup.

5.1.3 Construction of Hardware

For performing the measurements to show the applicability of the detector, the hardware was constructed with the following components (components with a * are newly used one and the others are as in the case of previous worker):

i) **Illumination system:** For illumination, a Hamamatsu L4633-01[146] flash lamp was used.

ii) **Modified Heatsink:** An XL preparative Ultracentrifuge heat sink was modified at BASF-AG. Six holes were drawn to allow for fiber feedthroughs and electrical feedthroughs to be fitted.

iii) **Optical Fibers:** 600 micron patch fiber with SMA 905 connector, UV-Vis and 1000 micron patch fiber from Oceanoptics, Duiven The Netherlands.

iv) **Spectrometer**: USB 2000 Fiber Optics Spectrometer (UV/Vis, SMA 905 connector), Ocean Optics BV, Duiven, the Netherlands.

v) **Electrical feedthrough:** 18 pin electrical feedthrough for electrical connection of the linear actuator, from Electronik GmbH, Munich, Germany

vi) **Optical Bench:** From Owis GmbH, Göttingen, Germany with x, y, z and angular adjustment for coupling the light from the flash lamp and the fiber.

vii) **Optical stage:** From OWIS GmbH, Staufen, Germany with fine-adjustment screws in the x and y directions, for the precise adjustment of the detection optics part of the detector arm.

viii) **Reflection light gate:** This system was developed at BASF, Ludwigshafen, Germany. In this system, a photoelectric reflection light gate is fixed to the bottom of the vacuum chamber which consists of a continuously light-emitting LED and a fast photodiode. A mirror (a polished small strip at the rotor bottom) fitted on the base of the analytical rotor reflects the light of the LED. This alignment provides a TTL pulse for each revolution of the rotor.

ix) ***Precision Slit:** 25 μm precision slit from MellesGriot, Bensheim, Germany

x) ***Lens Holder with x-, y- adjustment:** From OWIS GmbH, Staufen, Germany.

Apart from the above mentioned components, the commercially available parts as described in figure 43 were used. The photographs of the detector arm and the arm placed inside the AUC chamber are shown in the Fig. 45.

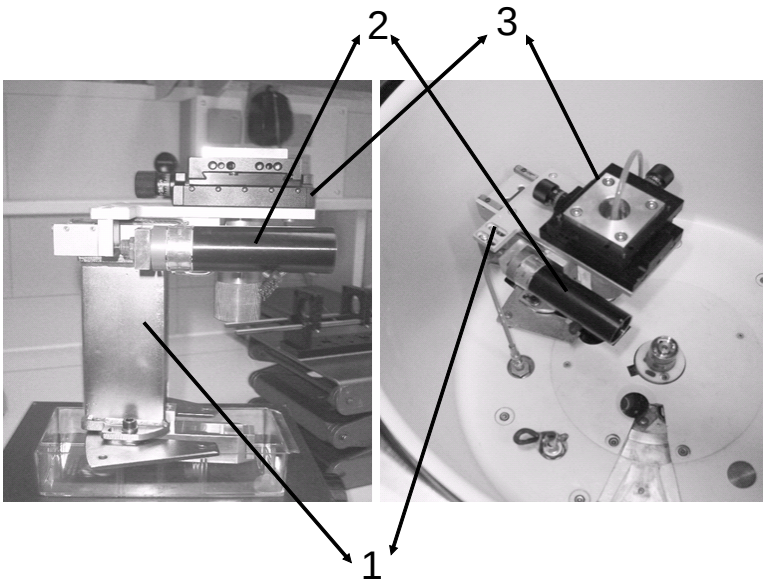

Fig. 45 Left. Photograph of the arm, (1) Detector arm, (2) Stepping motor (0.1 μm resolution at up to 4 mm/s), (3) Detection unit with X-Y positioning screws. Right: Mounted arm in the AUC chamber.

5.1.4 Software development

The software for controlling the multiplexer and the step motor was written using LabVIEW 7.1 (National Instrument, Texas, USA) programming environment. The software was written by Akif Mehmet Gülsün, Department of Electrical and Electronics Engineering, Bilkent University, Ankara, Turkey. The multiplexer software had the feature to define the flashing position for a particular cell. For the data collection from the spectrometer, Oceanoptics commercial software OOIBase32 was used.

5.1.4.1 Fast Mode with speed profiling:

In this mode the detector had to be placed at a fixed point at the cell sectors and data collected as function of time. Data collection needed to be started as the centrifuge starts accelerating from 0-60000. This mode should enable useful information about the sample, especially for colloidal systems with high polydispersity as data collection of even the largest aggregates can be detected. For the fast mode to work in the present system, a multiplexer software was written with the LabVIEW 7.1 environment, which changes the flashing angle position with speed. It was observed that with the speed variation, the angle position for a respective cell sector varies as shown in Fig. 46.

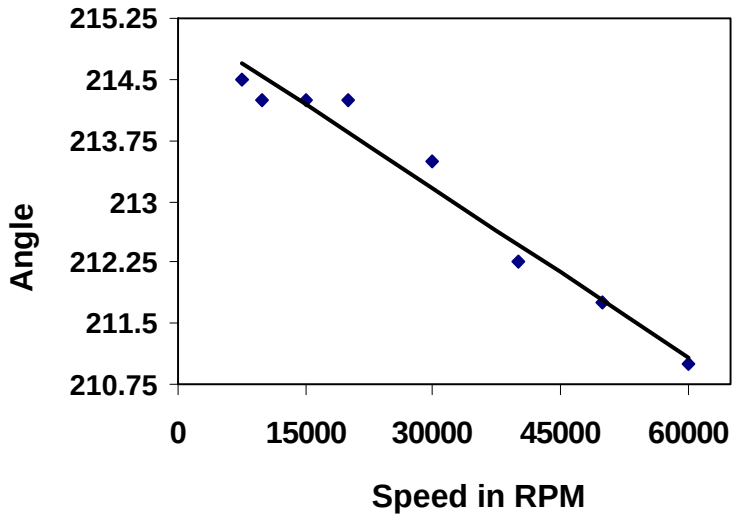

Fig. 46 Variation of flashing angle for the light source to illuminate a particular cell as a function of speed

A correction factor for the flash position for the flash lamp in dependence of rotor speed was introduced in the multiplexer software and as the multiplexer can read the rotor speed, the speed correction of the flashing angle can be performed online by using the regression line in the above figure.

5.2 Alignment of the Optics

An alignment protocol for the optics was constructed as follows. The first step involved with focusing the divergent beam after the right angled prism to the centre of the cell. This was performed by holding a piece of paper at this position glued in a lens holder. The lens holder could be fixed on rails accommodating the lenses at positions 4 and 6 in fig. 43. This was followed by adjusting the position of the lens at position 4 for maximum intensity for a particular wavelength. The position of the slit was adjusted in the same way with an additional adjustment in its x-, y- position, with the help of additional screws in the holder, so that the slit allowed maximum passage of light (as measured by the spectrometer for one wavelength). The position of the lens at position 6 was optimized in the same fashion.

5.3 Results

5.3.1 Time Domain Data: As was realized in the previous work, this mode allows a faster sedimentation velocity experiment to be designed with generation of huge amount of data points. Fig. 47 shows results obtained from a BSA sample (1mg/mL prepared in 0.1N NaCl) for this mode of operation.

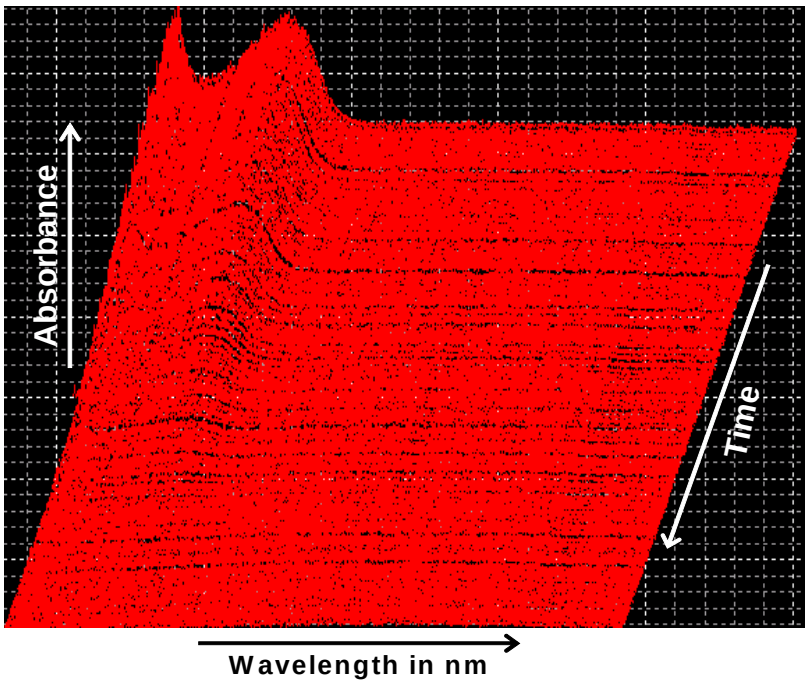

Fig.47 Sedimentation velocity experiment of BSA. 3D view of time mode scan (showed detection up to 240nm). Speed: 50000 rpm, detector position: 6.3cm, Data integration time: 100ms, 1 average. Sample: BSA 1mg/mL in 0.1M NaCl prepared by dilution.

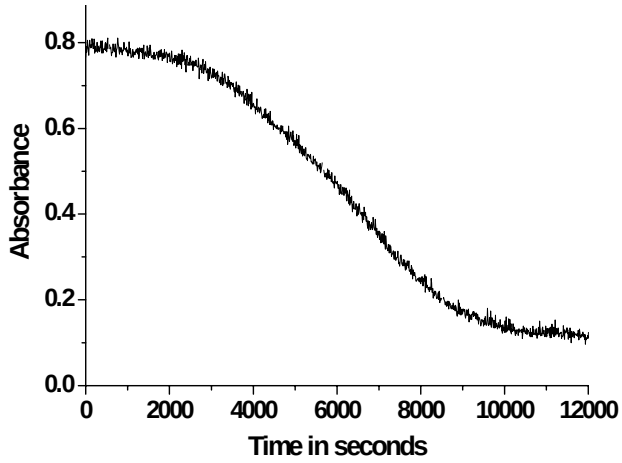

Fig. 48 Absorbance vs time plot for BSA 1 g/L at 280nm. (Experimental conditions; Rotor speed: 50000 rpm, Slit position: 6.1 cm. Data recorded with 100ms integration time and 1 average). The data were not corrected for the reference solvent.

5.3.2 Radial mode data: For this mode to be demonstrated, the step motor was moved with the help of a control program, and data were collected with the help of Ocean Optics commercial software. For plotting the data in 3-D, software written by Prof. Borries Demeler, Univ. Texas, St. Antonio, was used. A 3-D radial plot is shown in the following Fig. 49.

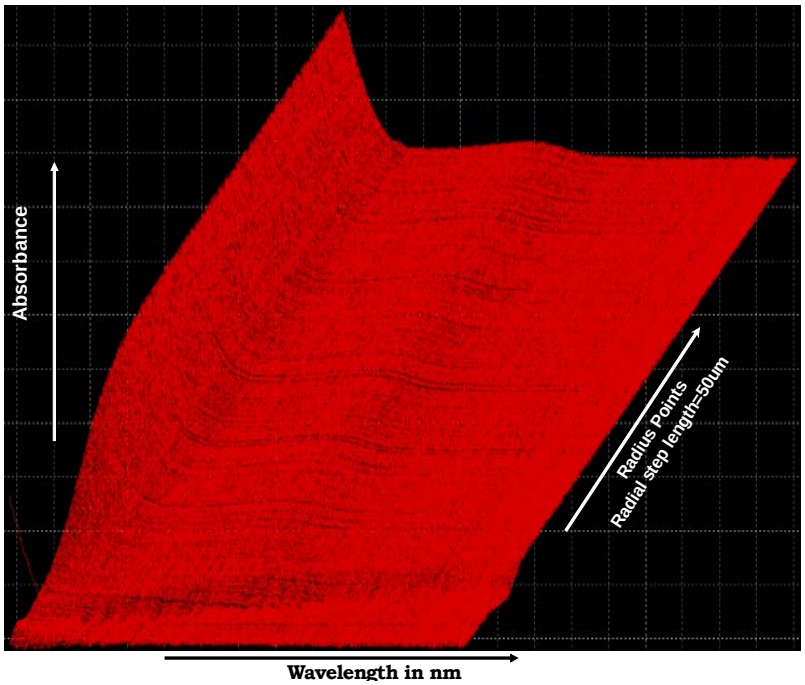

Fig. 49. BSA radial scan. Sample: 0.3ml/mL BSA prepared in 0.1N NaCl. 50,000 rotor speed, radial step: 50µm, scan interval 10s, data acquisition: 100ms integration time and 1 average. The shift in meniscus position with the variation in wavelength may be because of the wavelength dependence of radial resolution.

5.3.3 Speed profile data: To demonstrate the fast data collection and capability of making a speed profile experiment with the detector, a mixture of three Polystyrene Latex particles was allowed to sediment while the centrifuge accelerates from 0 rpm to maximum speed. The results clearly indicate that such an experiment could be possible with the current approach of software development. The experiment was complete in less than 3 minutes time. However, the data collection below 1000 rpm was not possible, due to the Beckman instruments' minimum possible set speed of 1000rpm. As the multiplexer needed the speed value for it to determine the position of flash, generation of correct data was not possible.

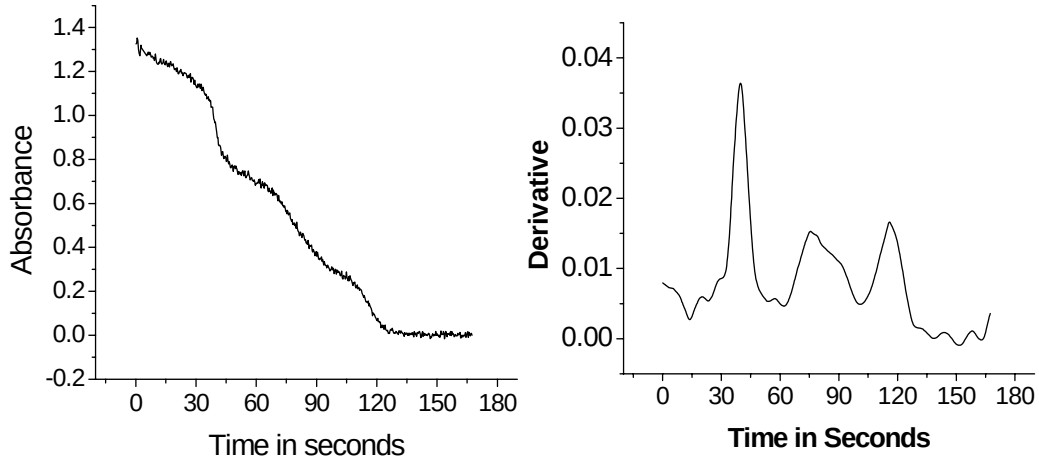

Fig. 50. Fast sedimentation velocity experiment with a Polystyrene Latex mixture of sizes 190nm, 305nm and 605nm in 1:2:2 mixing ratio by wt.; data collected at wavelength 350nm. Left: Experimental raw data. Right: The derivative curve was generated performing differentiation after 5 point FFT smoothing. Slit position: 6.4 cm.

5.4 Discussion

With the available preliminary results, it was clear that the setup should be suitable for constructing a Multiwavelength UV/Vis detector with a much improved data collection speed, as compared to the existing detector with the need to use fibers as the light guide. This setup would allow the option of "plug and play" for different components to work on further developments. However, following problems would have to be circumvented for such a detector:

i) **Use of optical elements free of chromatic aberration:** Lens based optics give rise to the problem of wavelength dependency of radial resolution. This problem may become severe with the use of more and more refracting components. Also, while aligning one can only work with one wavelength for fine adjustments, which would make data inferior for other wavelengths. Thus the error introduced in the data will depend upon two factors: data quality limited by optics resolution and by alignment. However, it may be mentioned that this effect is also present in the commercial Beckmann XL-instruments' as they use lens based scanning systems. Fig. 51 shows the wavelength dependence of radial resolution, as observed with the present optics with that in XL-A optic.

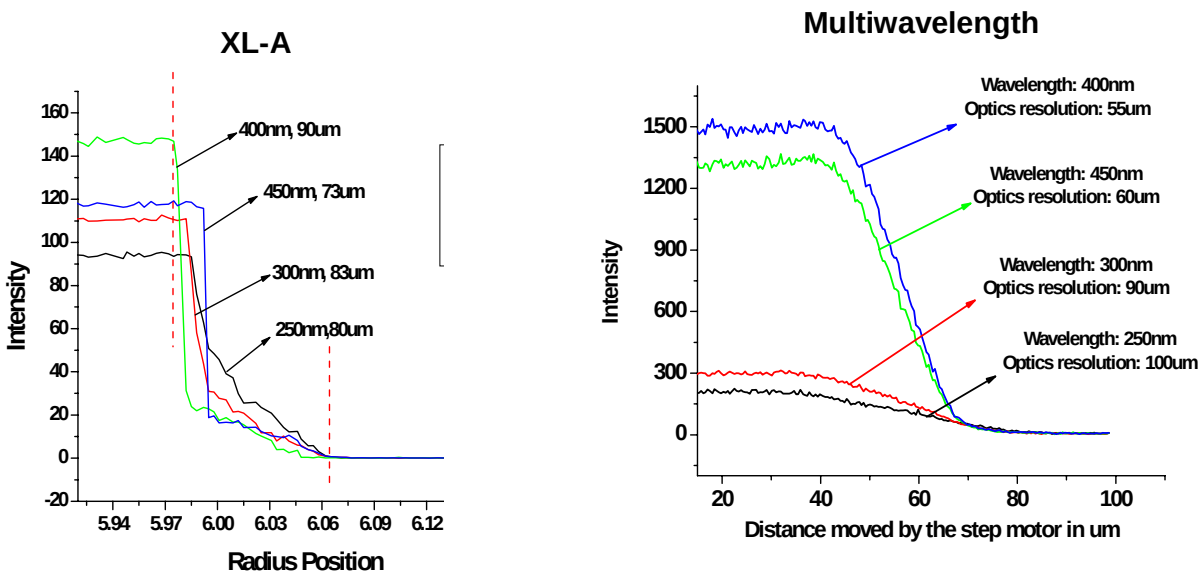

Fig. 51 Optical resolution dependence on wavelength. A counterbalance cell hole was scanned with the movement of the step motor. Experimental condition for Multiwavelength detector: step motor movement:3um/step, data acquisition:100μs integration time, 1averaging. For XL-A, intensity scan is performed on the counter balance holes as the detector scans the counter balance cell radially. As expected, the effect is more severe in case of Multiwavelength detector due to the use of larger focal length lenses.

ii) Use of Parallel light for the illumination optics: The use of parallel light for the detection optics is highly desirable, since with a divergent optics, achieving satisfactory alignment will be very difficult. One problem may be cited that of difficulty while fine adjusting the optics for making coincidence of the optical axis of illumination and detection optics. During alignment of the optics, this was achieved by moving the x, y screws at the detection optics to the maximum intensity in the lamp spectrum for a particular wavelength. However, it is possible that the whole light may not be entering the collecting lens. Also, there is the problem of inefficient focusing by the outer part, compared with the central part of the lens. Also, the use of larger diameter lenses can not be suggested because of the space constraint, as for using a bigger diameter lens one will have to select lenses with higher focal length and consequently a longer detector arm as shown in Fig. 52.

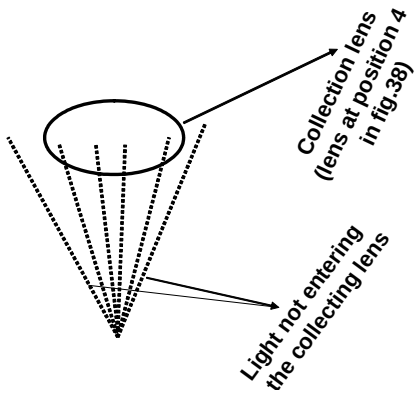

Fig. 52: Inefficient collection of the transmitted light by the collection lens

iii) Design of the optics arm without fiber bending: During the measurements, we investigated the amount of light intensity loss because of fiber bending as this is a well known phenomenon. Also, the design of the illumination optics had a fiber bending point of ~90°. The light loss was quite prominent (Fig. 53) in the UV range compared to the visible range and the peak at the lowest possible wavelength (~228nm) in the lamp spectra vanished with the detector arm transferred to the centrifuge.

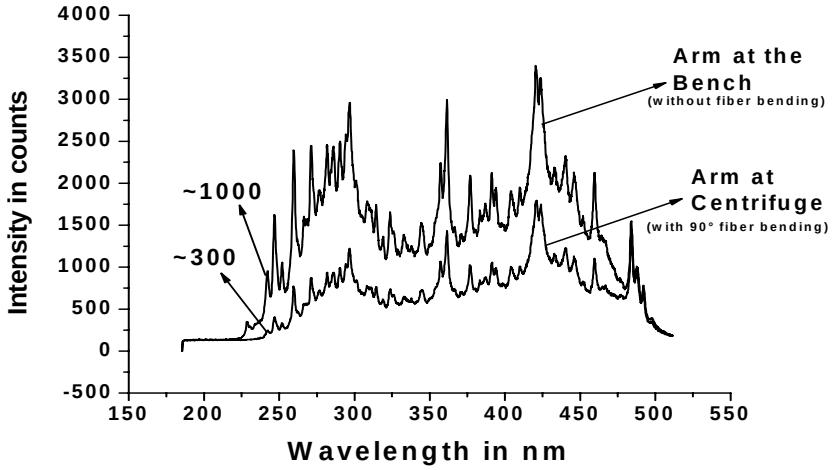

Fig. 53 Loss of light due to fiber bending. The detector was aligned and the lamp spectrum was recorded at the bench (Arm at the bench). Lamp spectra recorded after the detector was transferred to the centrifuge (Arm at the centrifuge), showed about 70% light loss in the UV region.

Thus for the next generation, it was postulated to work on a design to minimize fiber bending, using mirror based optics with maximum achievable collimation.

Chapter 6

Fast Fiber Optics Based Multiwavelength Detector for AUC Generation-II

To this point it can be said empirically that a Multiwavelength detection system can be constructed on a preparative Ultracentrifuge platform with the possibility to generate 3-D radial scans and much faster data acquisition. A further improvement can be made with the introduction of sophisticated software with improved optics that can generate data that are free of optical errors. This chapter covers software development for the detector, with possible developments and replacements of optical parts on the basis of the first generation development.

6.1 Hardware Development

It was envisaged during the first generation development that working with a collimated light beam should allow for higher intensity in the optics, and this was therefore used for the illumination optics. However, since collimation optics constructed by the use of lenses will always be accompanied by the chromatic aberration error replacing these optics with a mirror-based setup was expected to be free of this error as mirrors do not show chromatic aberration. An off axis parabolic (OAP) mirror could serve for such a purpose. Also an OAP can result in enhanced UV intensity[136,137]. Introduction of such a system can result in quite encouraging data generation as this kind of an illumination system will diminish the error due to alignment and chromatic aberration. A representative sketch of the mirror setup for the illumination optics is shown in the fig 54.

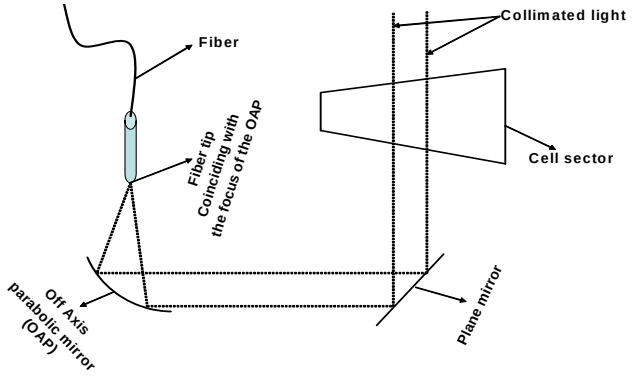

Fig.54 Setup for collimated white light in the illumination optics.

For the requirements of the system, it was envisioned that the Off Axis Parabolic (OAP) mirror would have to be custom built, while the other parts could be obtained commercially. To achieve the desired spot size (~2mm diameter), a mirror of dimensions smaller than those available commercially would be required. Due to the long time required for custom manufacturing of the mirror, the software programming for the data collection was completed with possible improvements in the optics for more light intensity at the detection end. In order to achieve this, a setup was chosen whereby the spectrometer could be coupled directly to the arm. Coupling the spectrometer to the arm allowed us to make use of the spectrometer slit for defining the spatial resolution, and thus also gave us the opportunity to remove the extra slit in the optics path that was responsible for largest loss of intensity. Indeed, this optical setup provided us with such a high light intensity that the spectrometer was saturated at all wavelengths. This was a result of its limited 12 bit technology resulting in a maximum number of 4096 counts, and so to avoid this situation, (an iris diaphragm was employed at the beginning of the detection optics) to bring down the intensity reaching the spectrometer to measurable values. The same components were used in the optics design, except for the two lenses (f = 60mm and 12.5mm) and the Iris Diaphragm in the detection optics from LINOS Photonics GmbH & Co. KG, Göttingen, Germany). A schematic depiction of the designed setup is shown in Fig. 55 along with its photographic representation in Fig. 56.

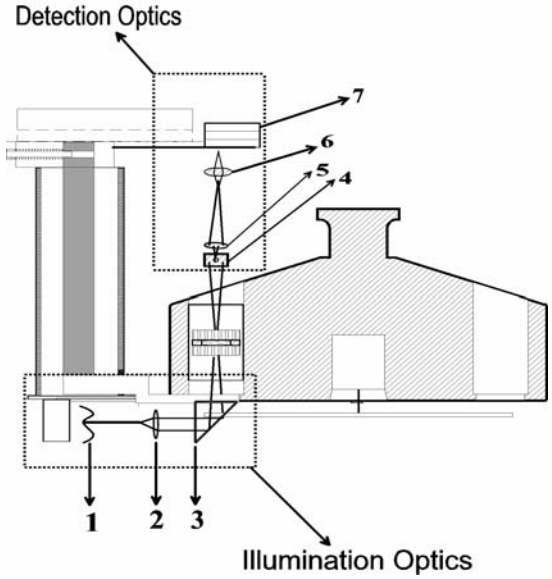

Fig 55. The detector arm. (1) 600 micron patch fiber UV/Vis (Ocean optics), (2) The collimating lens system (self built), f= 20.6mm biconvex, (3) 90° Quartz Prism, (4)Iris Diaphragm for reducing the high light intensity (5) Focusing biconvex lens (60mm), (6) Focusing biconvex lens (12.5mm), (7) Spectrometer. The light path is also shown schematically.

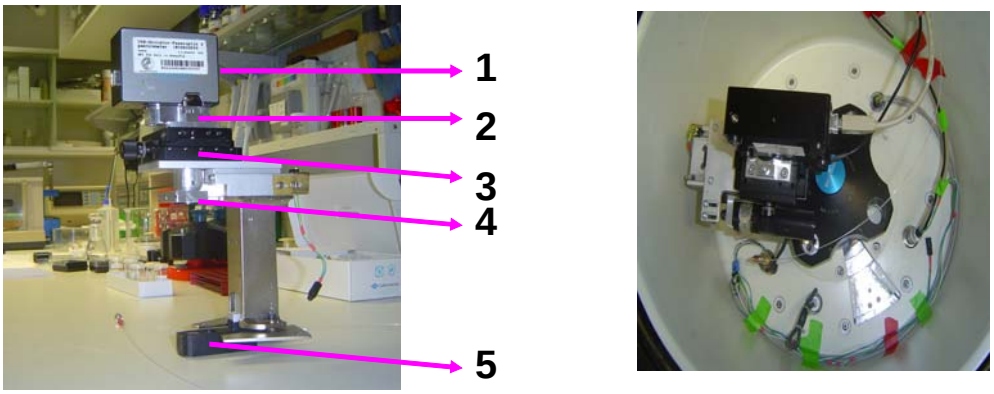

Fig 56. Left: Photograph of the arm: 1.Spectrometer; 2.Lens, f= 12.5mm biconvex; 3.Table with the possibility of x, y movement, 4.Lens: 60mm biconvex, 5.Position for fitting the self built collimation optics system and the 90° quartz prism. Right: The arm fitted in the centrifuge.

6.2 Software Development

Software for total control of the Ultracentrifuge and the data collection of the detector was written under the LabVIEW 7.1 environment (by Akif Mehmet Gülsün, Department of Electrical and Electronics Engineering, Bilkent University, Ankara, Turkey). It could precisely control the movement of the step motor, via a serial port, data collection from the spectrometer through the USB port, and the firing of the lamp (with the multiplexer). Also, full instrument control was possible. The general software design was kept similar to that of the Beckman XL-A user interface for the sake of user convenience. The software had the following features:

1) General Options

Before starting an experiment, some important parameters of the experiment could be adjusted:

Rotor Adjustment: 4 hole or 8 hole rotor

XL Settings Adjustment: Speed, temperature and time setting of ultracentrifuge

Scan Mode*(as discussed in Chapter 5 for first generation)*

Time Mode Scan: This mode was designed with the need in mind for samples which sediment too fast to perform a radial calibration before the experiment.

Radial Mode Scan : as discussed in Chapter 5.

Scan Options *Adjustment*

Acquire intensity data instead of absorbance: Default is absorbance data

Filter scan intensities below a certain level: Only in radial mode scan

Stop XL after last scan

Make radial calibration after experiment

Method Scan Options *Adjustment*

Delayed Start: Time delay before the first scan

Time between Scans: In Radial Mode only

Number of Scans: In Radial Mode only

Experiment Directory: To define data saving path.

2) Cell Options

For both, time mode and radial mode scans, after enabling desired cells, their experimental parameters should be adjusted, which differ in the two modes

Common Options

Here one can select up to four wavelengths for online radial scan observations, also these radial scans are saved in separate files. The feature of saving the full spectra with the selected wavelength range is implemented.

Time Mode Options

Radius: Detector position in the cell

Acquisition/Averaging time for one data point

Radial Mode Options

Rmin and Rmax: minimum and maximum radial distance

Radial Step: radial step size between two detector readings (settings possible from 0.1- 100 micrometer)

Replicates: number of data points collected at each wavelength

Set All Settings Identical to Cell 1: set the parameters of cell 1 for each cell

The operational front panel of the software is shown in Fig. 57.

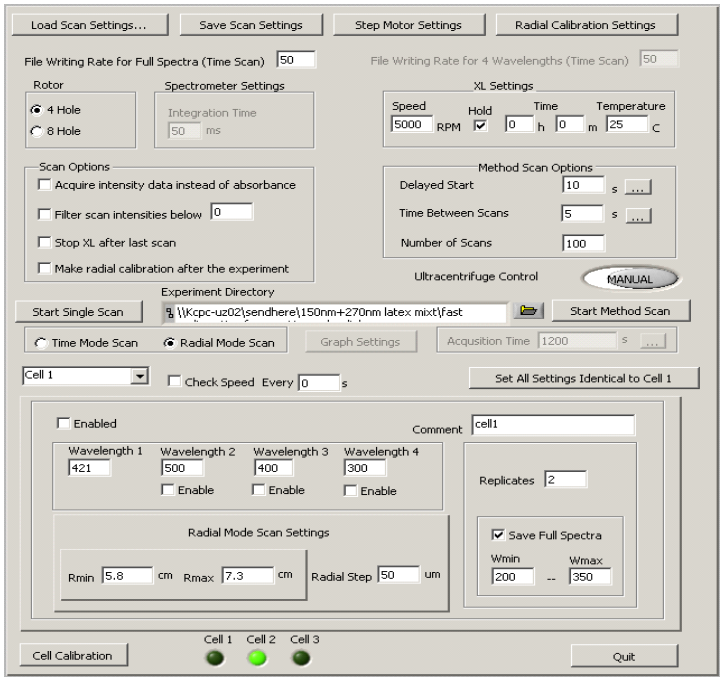

Fig. 57 Front panel of the instrument control and data acquisition software.

While writing the software for the data acquisition, a constant reference signal value was used for the calculation of absorbance from the sample intensity value. This was done in order to achieve faster data acquisition by not performing the reference sector scan. The fixed integration time of 50ms for the spectrometer was thus the rate limiting step and data acquisition became slow: 4 mins for scanning a 1.1 cm column of the cell sector with spectra saving option, 1 replicate, 50um step size, or 3 mins with the same parameters without spectra saving.

3) Calibration Settings

***Cell Calibration*:** used to set the angular cell positions with respect to the triggering pulse.

***Position*:** Angle from the trigger pulse to the cell. A predefinition of this to the program for every experiment is necessary as the cell position is dependent upon the rotor speed. For effective working with the program, the cell angle position at every rotor speed is determined and saved as a file for later use. The position determination is carried out at a fixed radial position of the detector (usually the middle position for normal experiment and for radial calibration experiments at the very top position). A cell calibration window is depicted in Fig. 58.

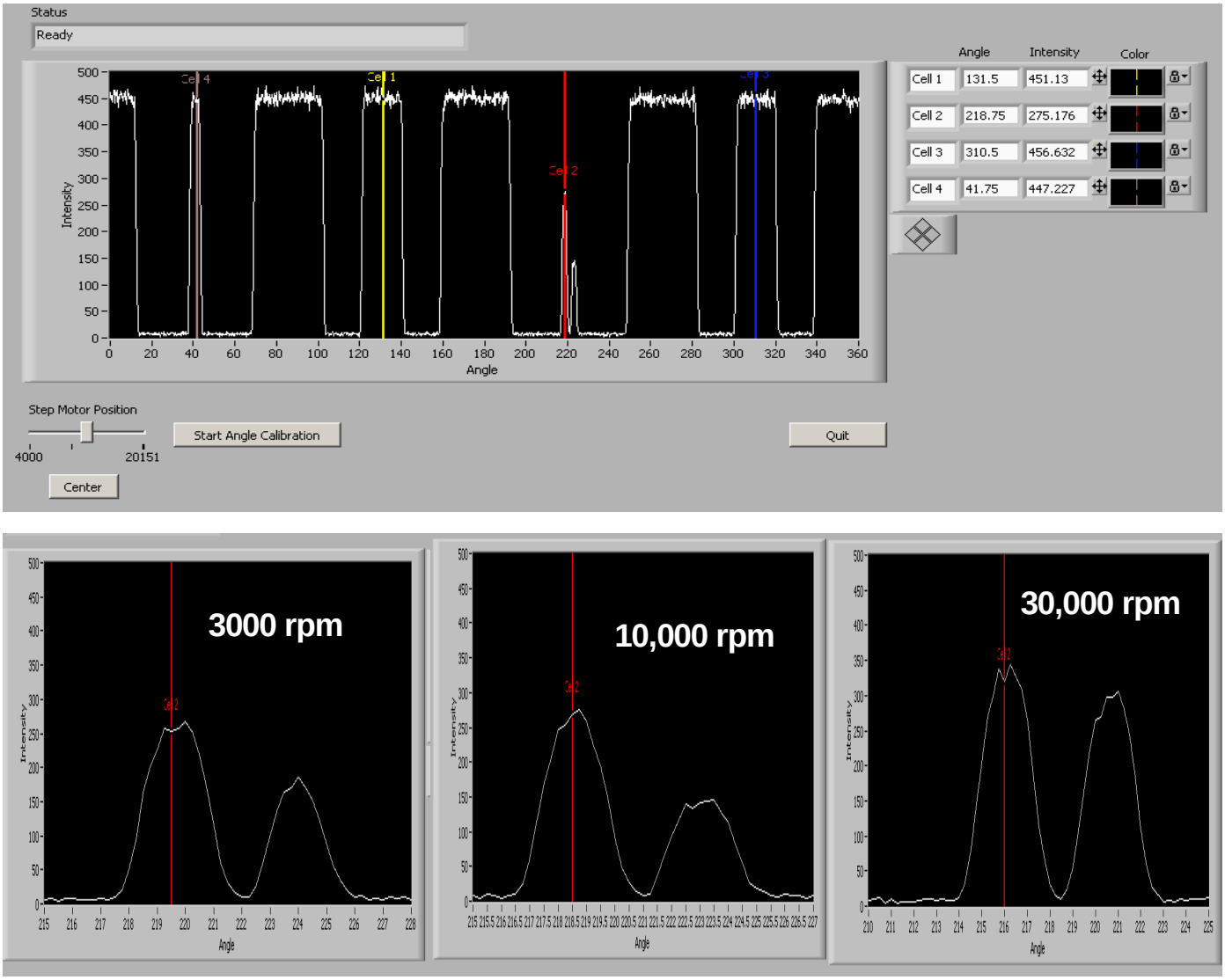

Fig. 58 The cell calibration determination window (this was performed for 'Cell 2' in a 4-hole rotor). The other cell positions were empty. Top: The whole window: first inflexion position from left indicates the zero position of the rotor. This follows the counter balance (in this case the counter balance used had a hole in the middle so that inflexion can be seen), the scallop position, cell-1, scallop, cell-2 (in this case, this slot had a double sector cell with sample as is seen with the variation in intensity for both the sectors), scallop, cell-3, scallop respectively. The lower part shows zoomed cell calibration window for cell-2 at different speed. The variation of cell position with speed is clearly visible.

This cell calibration needs to be introduced into the program and only needs to be performed once for each rotor. Thus in the general program (ref. fig 57) once the slot for cell calibration at the bottom left is clicked the following menu appears where the cell position can be introduced. This pull down menu looks like as shown in Fig. 59.

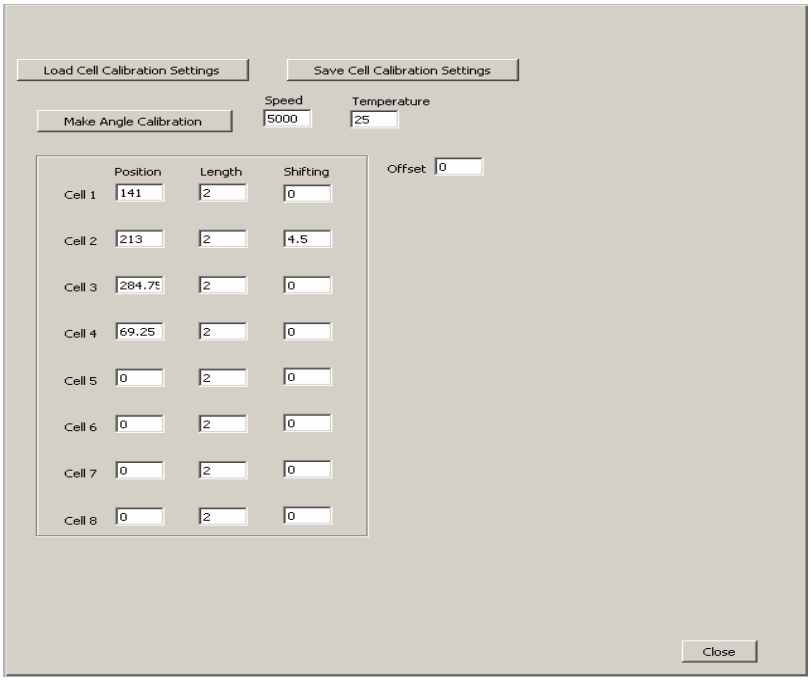

Fig.59 Cell calibration value introduction window.

Length: sector angle

Shifting: To provide access to different position in the cell, e.g. reference and sample sector to allow correction of the sample for the reference solvent (for the middle position it is always 4.5°)

Angle Calibration**:** For cell position.

> ***Radial Calibration*****:** For inner and outer radii of the cell. This can also be predetermined for later use. This evaluation is performed at 3000 rpm rotor speed. An angle calibration is performed at this speed of the rotor and the angle calibration is set at this position. In the general program (ref. fig 57), while selecting the radial calibration, optional selection is made to perform a new radial calibration. The file generated has two inflections first from the inner hole of the counter balance and second from the outer hole as shown in Fig. 60. This file can be saved and used until the detector is physically removed from the chamber, or a different counter balance cell is used.

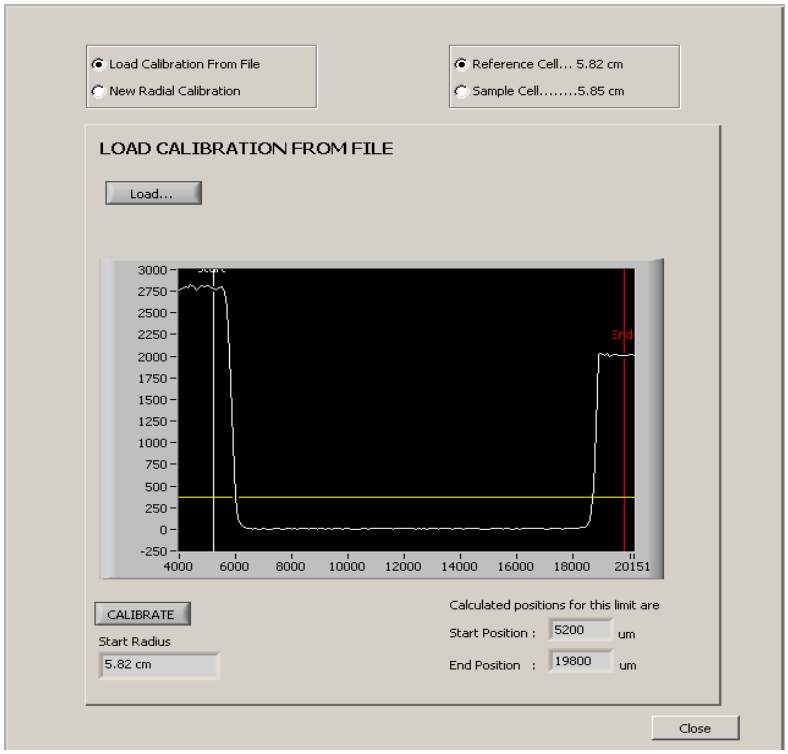

Fig. 60. A radial calibration window

Step Motor Settings: Adjustment of Port, Minimum and Maximum positions of motor

Graph Settings: Determination of Scale Settings for the online data viewing window.

4) Fast velocity profile mode

It was clear that the cell angle position varies to a great extent with the rotor speed so that the lamp flash needs continuous correction with a 2° sector angle, the cell would already be lost when the centrifuge speed reaches 10000 rpm. For the general program this speed correction has been implemented, as this program was written for operation with a single rotor speed. However, the effect can be exploited for writing the software for the fast velocity profile mode. Thus, a separate program was written with a small modification in the multiplexer logic such that with change in the speed of the centrifuge, the detector angular flash position would change. The change in angle position can be read from a previously saved file with a plot of angle vs speed and it appears as in the figure 62. The program has the following features:

General scan parameters:

Acquisition time: This is user definable. The centrifuge can be stopped before the final speed is reached or may be left at highest speed for longer time.

Final speed: User can select the final speed.

Radial scan parameters: User can define the radial positions for inner and outer hole in counter balance from the radial calibration file (fig 60).

Wavelengths: The user can define the wavelengths for online data viewing with the option to save the full spectra.

Radius: User needs define the radius position of the detector.

The general program has the following look (Fig. 61):

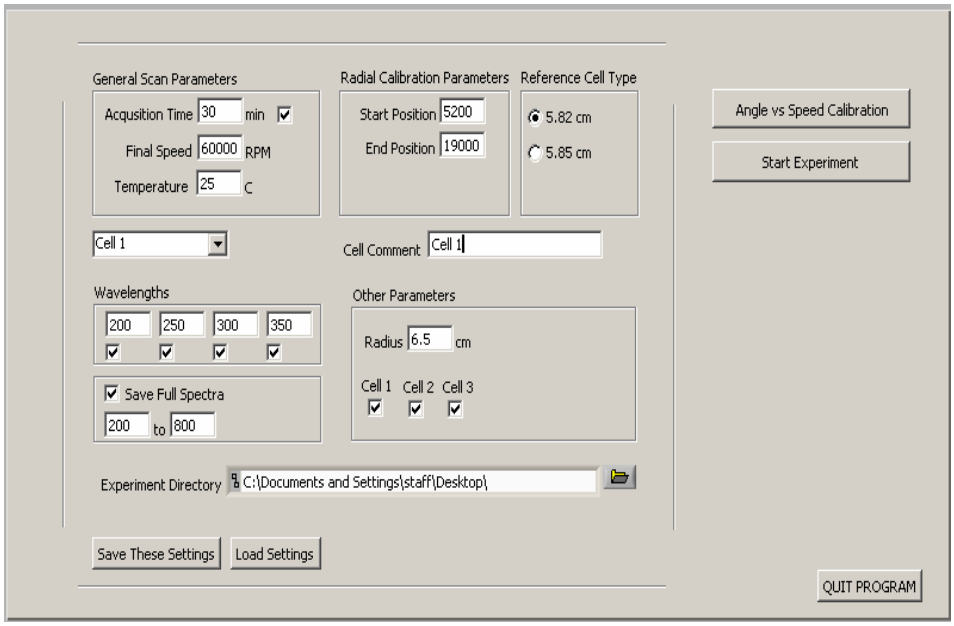

Fig.61 Front panel for fast velocity profiling program

Angle vs Speed Calibration: This will have to be read from a previously stored file that can be created while the detector is installed in the first instance. For this to be performed, the user needs to define the wavelength and angle range to avoid undue experiment time, while covering the desired variation limit, speed range (minimum 1000 rpm, as this is the lowest possible speed in commercial instruments) and angle increment. An angle vs speed plot is shown in Fig. 62.

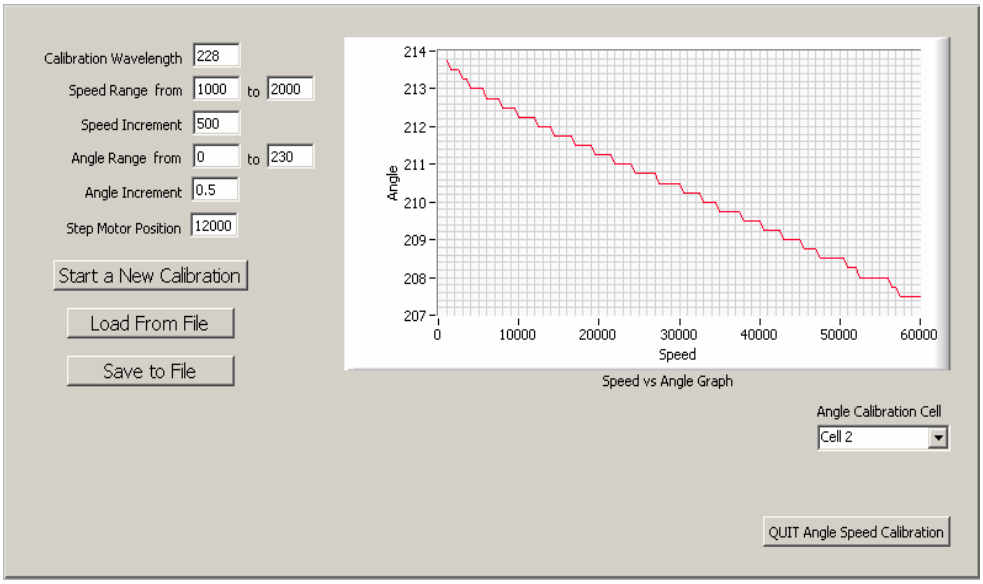

Fig. 62. Angle vs speed plot for cell 2.

Until now the work for the option with other cell positions has not been implemented. The software with complete data acquisition from all the four cells is yet to be completed.

6.3 Alignment of the optics

An alignment procedure was worked out for this optical setup, beginning with the same procedure as described for the generation-1 detector. Thus after focusing the light at the middle of the cell sector, the 60mm lens was placed. Adjustment with the x-, y- screws were performed to get the beam at the optical axis of the arm. This can be performed by placing a pin hole at the position of the final focusing lens (12.5mm lens, Position -2 in fig. 56). This was followed by the adjustment of the position of the lens at position-2 in fig. 56 so as to get maximum intensity for the lowest possible wavelength in the lamp spectrum (in this case, 228.44nm) to optimize the system performance in the UV.

6.4 Optics performance test

For checking the basic system performance, one of the holes in the counter balance was scanned with movement of the step motor and recording the intensity variation with the Oceanoptics, commercial software for the USB spectrometer. First the cell position of the inner hole of the counterbalance cell was determined with the help of the cell

calibration option in the general program. The multiplexer program was started for defining the cell calibration position for the flash. For movement of the step motor, the program was started and the initial and the final positions of the stepmotor were defined along with the time/step. The following observations were obtained (Fig. 63).

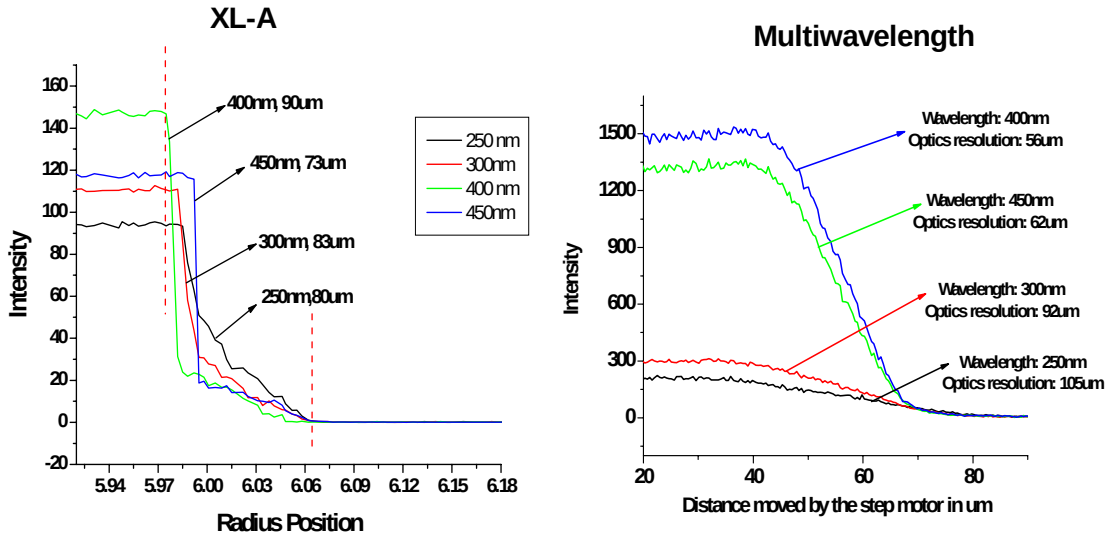

Fig 63. Optics resolution test for the detector. The wavelength dependency of optics resolution is clearly observed, as is the effect present in XL-A optics. For data collection, the intensity data were generated as the detector scans a counterbalance cell hole while the rotor spins at 3,000 rpm.

6.5. Measurement results to check the detector reliability

With the completion of the basic software design and an aligned hardware design, it was necessary to perform representative measurements and compare them to measurement results from the commercial instrument or to literature data.

i) Three colloid mixture: As a check of all three modes, a sample with mixtures of colloidal particles of three different sizes was prepared. The data looked comparable on the basis of their evaluation to determine the sedimentation coefficient "s" value.

The sample was a mixture of three Polystyrene latex particles with label claim sizes 270nm, 203nm and 150nm. It was prepared by mixing, followed by dilution with water until optimum UV intensity from the AUC cell was observed. Measurements were performed on this sample for all three possible modes with the Multiwavelength detector: Fast velocity profiling, Radial mode and Time mode. These were compared with parallel measurements from the commercial Beckman XL-A AUC. Evaluation of the radial scans was performed with the Sedfit program. For evaluation of fast velocity mode data, the mid

point of the step is considered. First order differentiation can be performed on the data set in order to accurately determine the midpoint of this step. The corresponding $\omega^2 t$ value is noted for this point. A radial scan of the sedimented sample is performed to determine the meniscus position of the sample in the cell, and all the data are substituted into the equation $s = \ln (r/r_m) / \omega^2 t$. The evaluation of the time mode data can also be performed in the same way. The results obtained are summarized in table 3:

Table 3

Sample	**s from XL-A Radial scan (5000 rpm) (in S)**	**Multiwavelength Detector data**		
		s from Radial scan (5000rpm) (in S)	**s from fast scan mode (using $s=\ln(r/r_m)/\omega^2 t$) (in S)**	**s from Time mode scan (using $s=\ln(r/r_m)/\omega^2 t$) (in S)**
270nm	1639	1624	1698	1699
203nm	935	914	1019	935
150nm	515	495	562	495

The raw data with their evaluation are shown in Fig. 64. The additional advantage of data averaging is also possible, due to the availability of large dataset.

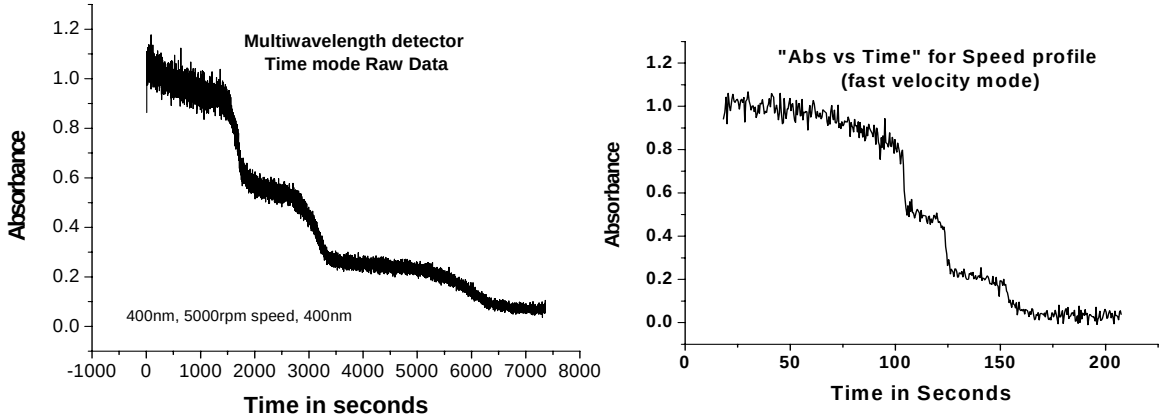

Fig.64 Three colloid mixture data in time mode and fast velocity profiling mode. (The detection wavelength in both cased was: 400nm)

Fig. 65 shows the comparison of evaluation of the data collected with the multiwavelength detector and from reference XL-A experiment where data were collected for the same sample with identical scan conditions. The evaluations show good concordance for both evaluations. Fig. 66 shows the raw data from multiwavelength and XL-A. The presence of

three steps corresponding the three component latex particles show the desired performance of the detector.

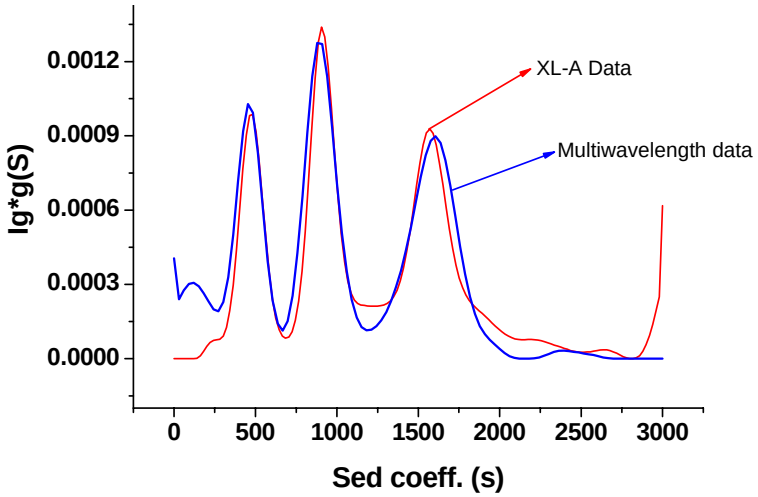

Fig 65. Comparison of Sedfit evaluation of raw data from Multiwavelength detector and XL-A.

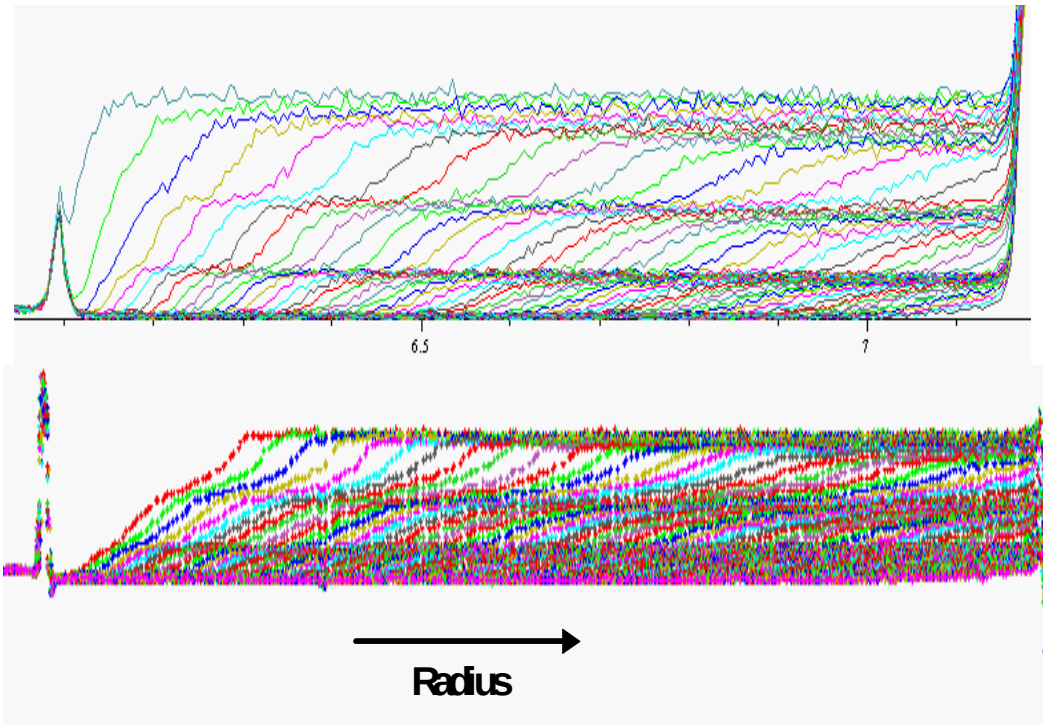

Fig.: 66 Snapshot of raw data loaded in sedfit. Above: Multiwavelength data. Below: XL-I Data.

ii) BSA sample: BSA sample (1mg/mL in 0.1N NaCl) was measured with the Multiwavelength detector optics, which led to a good agreement with the literature value: 64000D. These data are shown in Fig. 67.

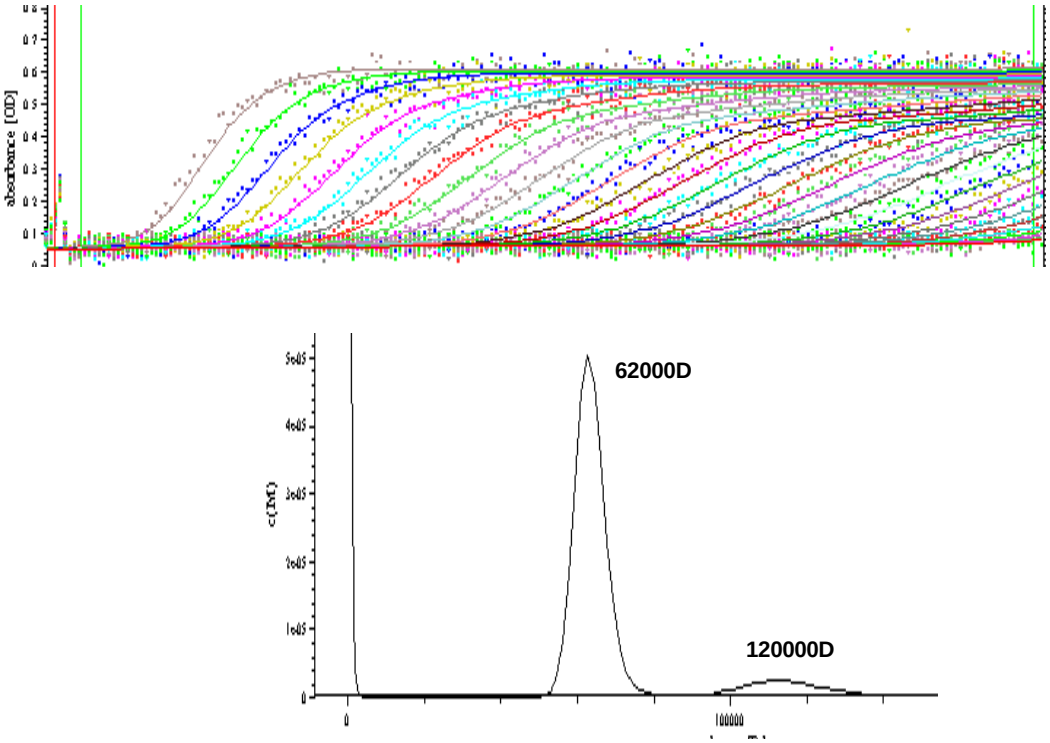

Fig.67: BSA raw data and evaluation with sedfit (Multiwavelength data). Sample: BSA 1mg/mL in 0.1 N NaCl, 50,000 rpm, 10s scan interval, detection wavelength: 275nm. (both of the presentations are sedfit snapshots). (literature value of BSA Molecular weight:64 kD).

6.6 Conclusion of the first phase work for 2nd generation Multiwavelength detector

From the available results in our hand, it could be concluded that with the present hardware construction and software development, Multiwavelength data generation is possible which shows reasonable accuracy after their evaluation. The fast velocity profiling data were also valid. However, decreasing the effect of chromatic aberration would enhance the data quality. Thus work for the development with mirror based optics was the next priority.

6.7 Further Improvements of the 2nd generation Multiwavelength detector

The available results showed that the designed hardware and software can generate data that show satisfactory concordance with the reported data. Thus, it was concluded that with the present software we can proceed with the necessary optical improvements, to get rid of the previously stated errors found in the first generation detector. As a next step for

development, the possibility of working with mirror optics in the illumination part was considered. The completed custom built mirror-based collimation optics construction was found to produce almost collimated light with tolerable divergence (the exact value was not measured). Also, it has been stated in the literature that if one works with divergent light, prisms can show aberration effects. Therefore a new optical setup was designed that fits to our existing hardware. For constructing the arm, the following components were used:

i) Mirror based collimation optics: This part was custom built by LFM Laboratory for Precision Machining, University of Bremen, Germany. It was supplied as a pre-aligned unit with a 50 micron fiber (OZ Optics, Canada, part no. QMMJ-55-UVVIS-50/125-1-0.5) with its tip positioned at the focal point of an Off Axis Parabolic (OAP) mirror of focal length 2.5mm.

The focal length of the mirror was chosen on the basis of the fact that the emerging beam from the mirror will be ~3mm in diameter and the cladding diameter of the fiber was fixed at 50microns so that one can use commercially available parts with tolerable divergence of the beam. For the design of the mirror unit, two points needed to be considered. First there was the necessity of a off axis parabolic mirror with very small focal length, and consequently a very small dimension. The use of a small focal length mirror was unavoidable as this was the determining factor for the spot size of the emerging beam. Secondly, a very small point light source was required, due to the fact that with a smaller focal length, the divergence of the outgoing parallel beam will be decided by the dimension of the source. Thus the source must be placed in the focus of the mirror with highest possible precision, however diminishing the fiber diameter also decreases the intensity of light. Keeping in mind the above two factors, as a compromise the fiber diameter was fixed at 50 microns.

ii) High Poser Xe-Flash lamp: Hamamatsu Photonics GmbH, Germany (part no. L9456-12. This lamp enables direct fiber coupling with an SMA connection. This had the advantage of avoiding alignment of the fiber to lamp distance (unlike in the earlier lamp, L4633-01 from the same manufacturer). The new lamp also has a higher flash life and

higher output stability (light output intensity variation 1.5% for this module and 5% for the earlier one), compact modular size and a high light emission repetition rate (up to 530 Hz)[147]

iii)Plane mirror: 45° elliptical flat mirror coated with UV-enhanced Aluminium from Edmund Optics Inc., Germany (part no. NT43-573).

iv)Biconvex lens: Biconvex lenses of focal length 60mm and 12.5mm were obtained from LINOS Photonics GmbH & Co. KG, Göttingen, Germany.

v) Iris Diaphragm: From LINOS Photonics GmbH & Co. KG, Göttingen, Germany.

The other parts were equal to those described for the first generation detector: Oceanoptics spectrometer of the USB series, Step motor for precision movement of the detector arm, vacuum feed through for guiding the light into the vacuum chamber, x-y stage for fine adjustment of the detection optics, and an electrical feed through for supplying power to the step motor and connecting the computer data cable.

A schematic diagram of the optics is shown in Fig. 68:

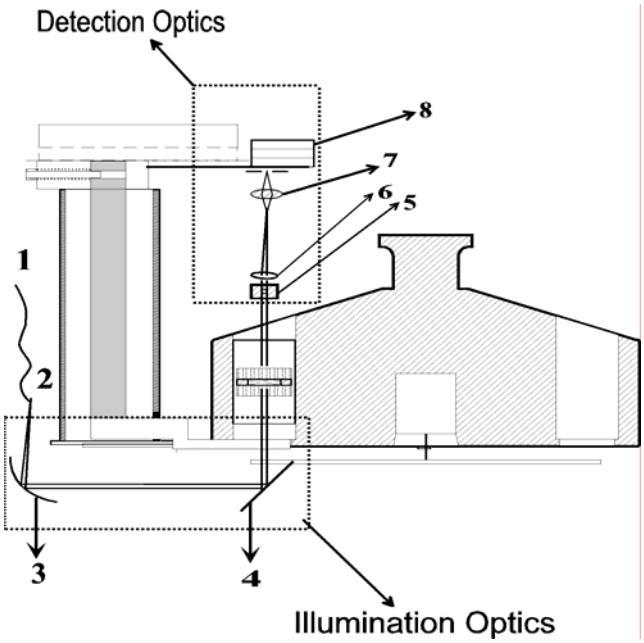

Fig.68 The optics arm. (1) 50 micron fiber UV/Vis (OZ optics), (2) Tip of the 50micron fiber and focus of the Off axis parabolic mirror, (3) Off axis parabolic mirror (from LFM Bremen) (4) Plane mirror (Edmunds optics) (5)Iris Diaphragm for reducing the high light intensity (6) Focusing biconvex lens (60mm), (7) Focusing biconvex lens (12.5mm), (8) Spectrometer fitted in a x-,y- stage. The light path is also shown schematically.

6.7.1 Alignment of the optics: With the above setup ready for work, there was the necessity to work out an alignment procedure for the optics. The internal alignment of the Off Axis Parabolic (OAP) mirror was performed by the manufacturer. It needed alignment only in the vertical position after fixing the fiber to the unit.

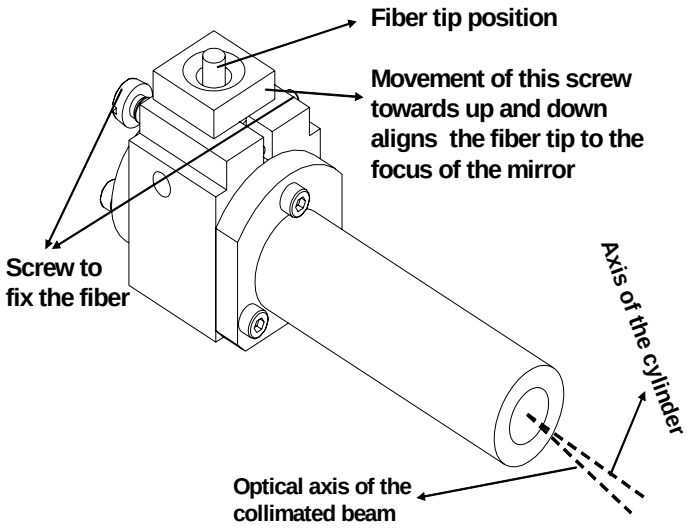

Fig.69. OAP unit housing. The alignment required movement in the vertical position of the fiber tip, as well as aligning the axis of the cylinder and the optical axis of the beam.

It was observed that the collimated beam emerging from the Off Axis Parabolic Mirror (OAP) housing did not exactly match the optical axis of the beam path and working with such a beam could not give a properly aligned optics. In order to circumvent this problem, three small screws were fitted at the bottom part of the plane mirror holder, allowing movement of the beam with the tilting of the plane mirror and turning of the mirror holder finally so that the collimated beam was in the right place. This workaround is quite important as the fiber tip must be placed precisely at the focus of the tiny mirror. Adjusting the position of the plane mirror to its optimal position was performed with the help of a laser, and replacing this with the beam for the final adjustment with respect to rotation of the mirror holder. After alignment of the collimated beam, the optical axis of this beam and the detection optics needed to be aligned. This was achieved by moving the x-, y- stage where the spectrometer was fixed. Fig. 70 can lead to a better understanding of this alignment.

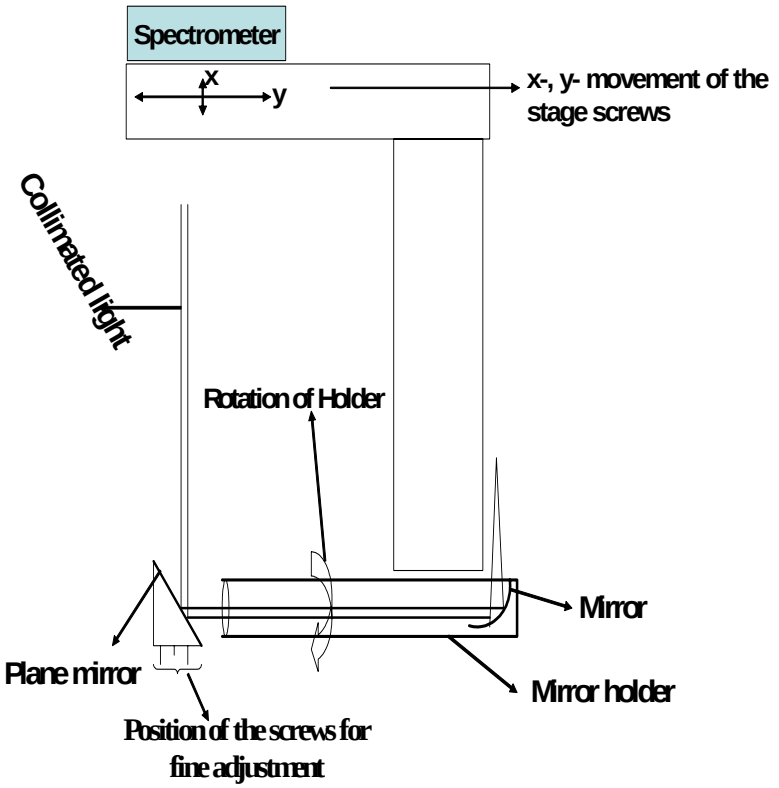

Fig.70 Schematic description of the alignment of different optical elements.

To achieve the optimum aligned position of the two lenses in the detection optics, the lens positions were fixed at the position of highest intensity in the spectrometer. The optical resolution was then maximized by adjusting with the variation of the lens position in front of the spectrometer, and finally a fine adjustment of the detection optics with respect to its x-y movement completed the alignment.

6.7.2 Optics Performance Test

i) Optics Resolution: A normal optics resolution test was performed as with the earlier detector generation at 3000 rpm by scanning the inner hole of the counterbalance cell. The results, shown in Fig. 71 still show that effects of chromatic aberration due to two remaining lenses , although it is reduced significantly in comparison to the second generation optics.

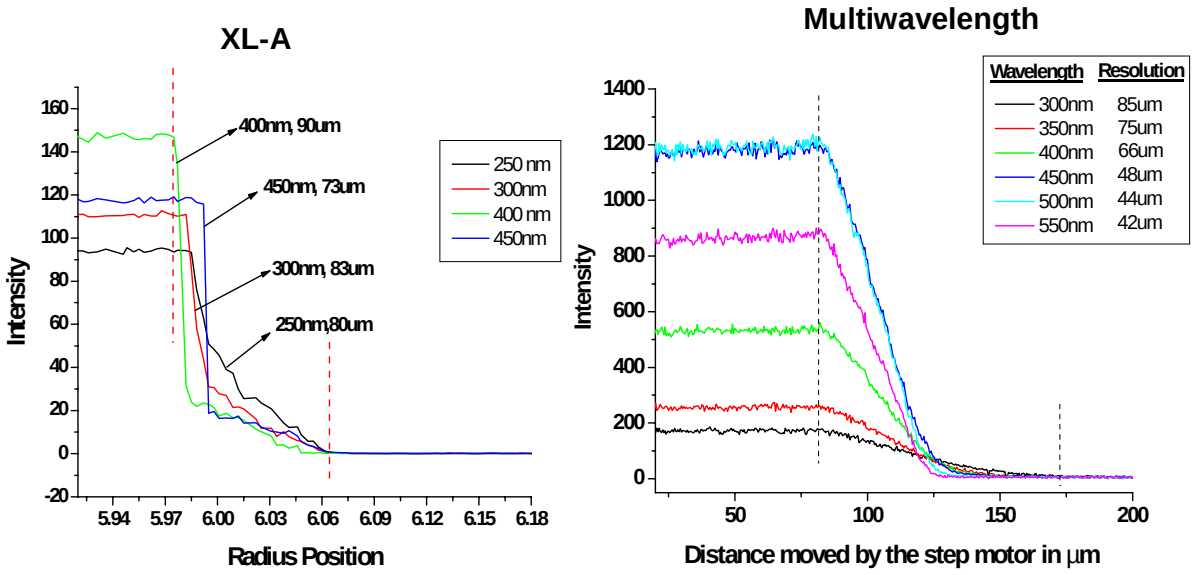

Fig. 71 Optics resolution as a test for the performance of the optics. The dependence of radial resolution on wavelength is persistent as there were two lenses in the detection optics (however decreased as compared to Generation-2). For Multiwavelength data: rotor speed 3000rpm, step size: 1um, time/step: 100us. For XL-A data, intensity scan was performed on a counter balance cell hole as the rotor spins at a speed of 3,000 rpm.

ii) Test for signal to noise: The existence of intensity variation from flash to flash. A correction for this flash variation had been corrected in the commercial single wavelength optics. Effort was made in the current setup to perform corrections by recording reference intensity in a photodiode. However, this was not successful as the photodiode response to the whole wavelength range was not the same as that from the spectrometer. The photodiode has fixed spectral characteristics that would never be comparable to the CCD chip detection in the spectrometer where every pixel in the CCD chip corresponds to a particular wavelength. A rational solution would be to use a dual channel spectrometer where a portion of the incident light to the detector may be diverted and measured as identical signal to the spectrometer collecting the data. However, since this was evident to us already, it was decided to perform a test in order to see the effect on the data with this flash variation. For performing this test, the detector was moved along the sample sector at a step size of 10μm with wait time of 100μs at rotor speed of 3000 rpm. A constant value from the mid position of the reference sector was subtracted. The plot was generated as 'abs.' vs time (which in turn corresponds to the step motor position). A standard deviation of 0.04695 (for flash intensity variation along the cell sector Fig. 72) and 0.10641 (for

flash intensity variation at a fixed detector position Fig.73) was recorded for the whole set of values which can be regarded as acceptable.

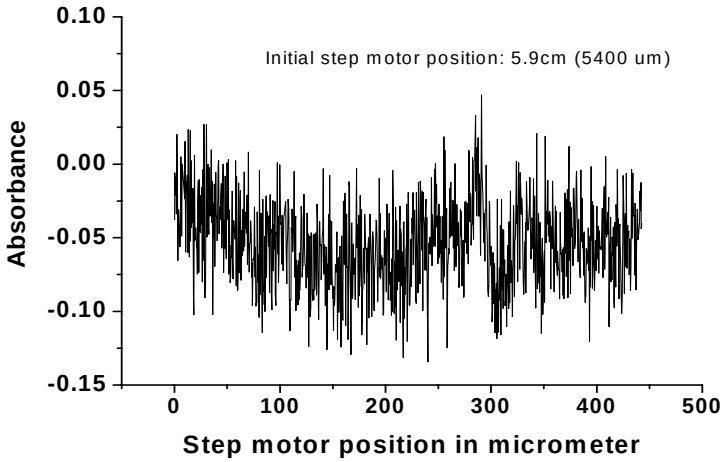

Fig 72. Variation of flash intensity along the cell sector. The test was performed by recording the absorbance value at different positions of the cell sample sector and taking the mid point of the ref. Sector as the ref. signal intensity value. Standard deviation: 0.04695. Working wavelength: 229nm.

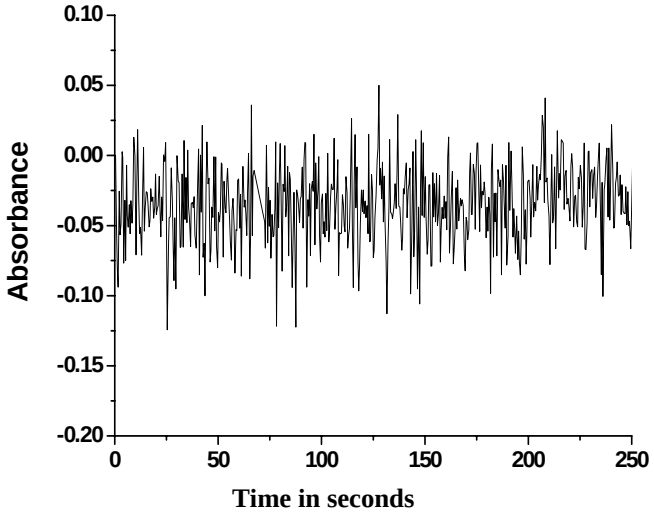

Fig. 73 Flash variation at a fixed detector position with time. Detector Position: 6.4cm, 3000rpm, Data collection: 50us, 1av. Working wavelength: 229 nm. Standard deviation: 0.10641.

6.7.3 Experimental results

For demonstrating the applicability of the detector, some representative measurements were carried out. However, the available data evaluation software can not read the multiwavelength data set to be displayed in three dimensions. The Ultrascan software by Prof. Borries Demeler, Univ. Texas, San Antonio has been modified so that the data can be viewed in three dimensional space. However, this software is yet to be

implemented at MPI and therefore only data sets with the three dimensional display obtained from Prof. Demeler are displayed here in the desired 3-D mode.

i) Sample-BSA: A BSA sample was prepared (concentration 0.5mg/mL in 0.1N NaCl) The evaluation of data from the multiwavelength detector and reference experiment carried out in the commercial instrument showed the conformity.

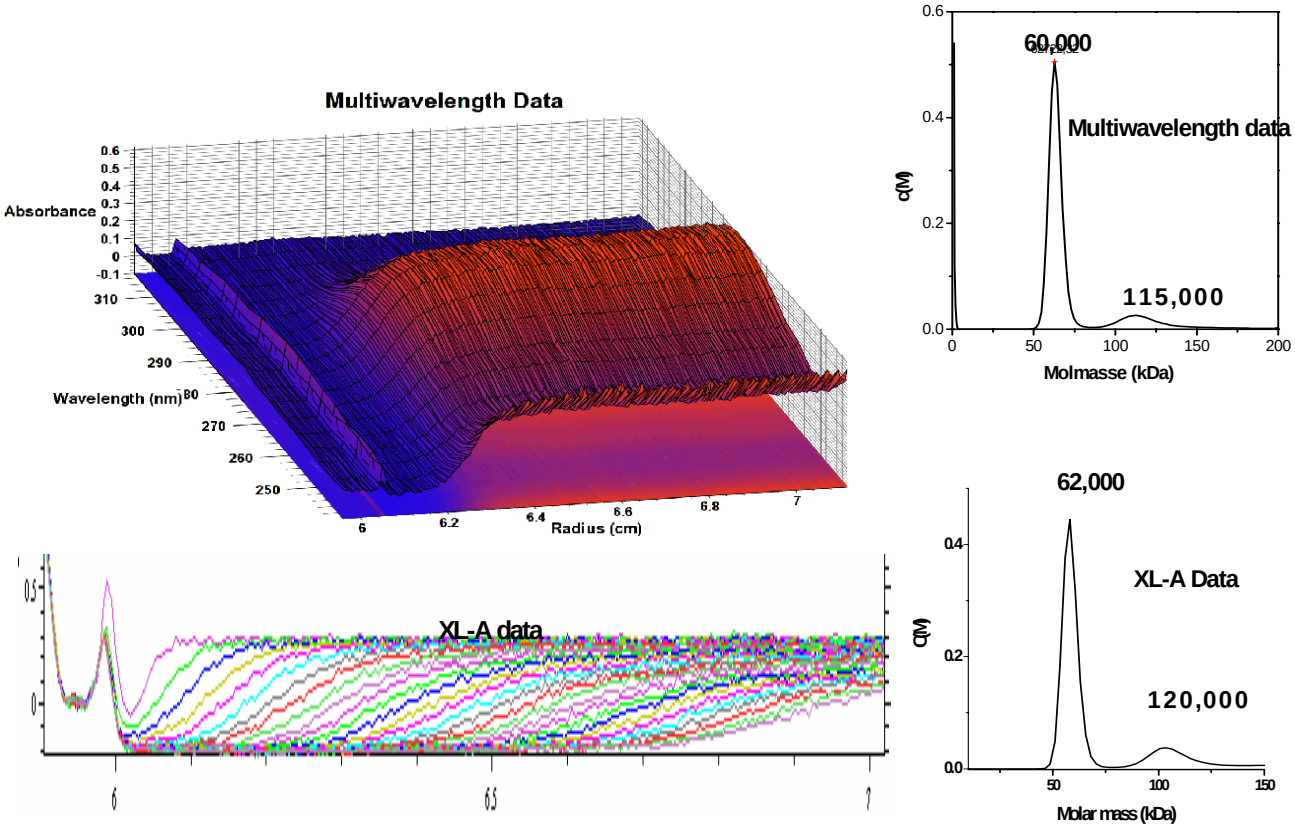

Fig 74. Raw data from 0.5mg/mL BSA sample in 0.1N Nacl with evaluation The figure on top is one scan in 3-D from a multiwavelength file (figure obtained from Prof. Demeler and reproduced with permission), experimental conditions; Speed:50,000 rpm. Scan intv.: 10s. radial step 50µm. The figure at the bottom is the view of a complete experiment with its radial scans (experimental conditions: 60,000 rpm, 1min scan interval, 50um radial step). The evaluations are shown in right. The molar mass calculated with the values $\bar{v}$ =0.730, ρ=1g/mL, viscosity:0.01g/cm (literature value for BSA molecular weight: 64 kD)

ii) Four component protein mixture (Hemoglobin, Myoglobin, Catalase and Cytochrome C): A four protein mixture solution (of Hemoglobin, Myoglobin, Catalase and Cytochrome C) was prepared by mixing equal quantity of 0.1mg/mL solution (in phosphate buffer at pH7) of each protein. The results obtained are shown below:

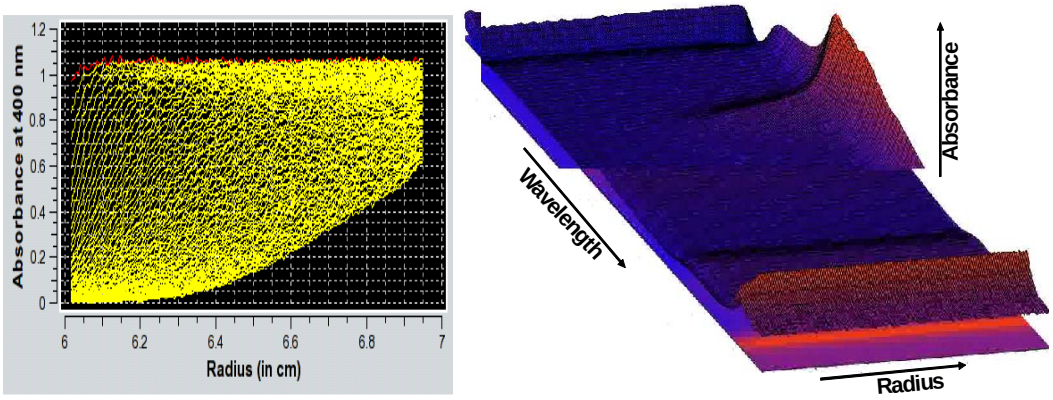

Fig.75 2-D and 3-D display of the radial scan for the four component protein mixture. The plot was created from 3-D movie display of the data viewer of Ultrascan software.(with permission from Prof. Demeler). Experimental conditions: speed: 50,000 rpm, scan interval:10s, temp:25°C. Better separation is displayed in the 3-D plot.

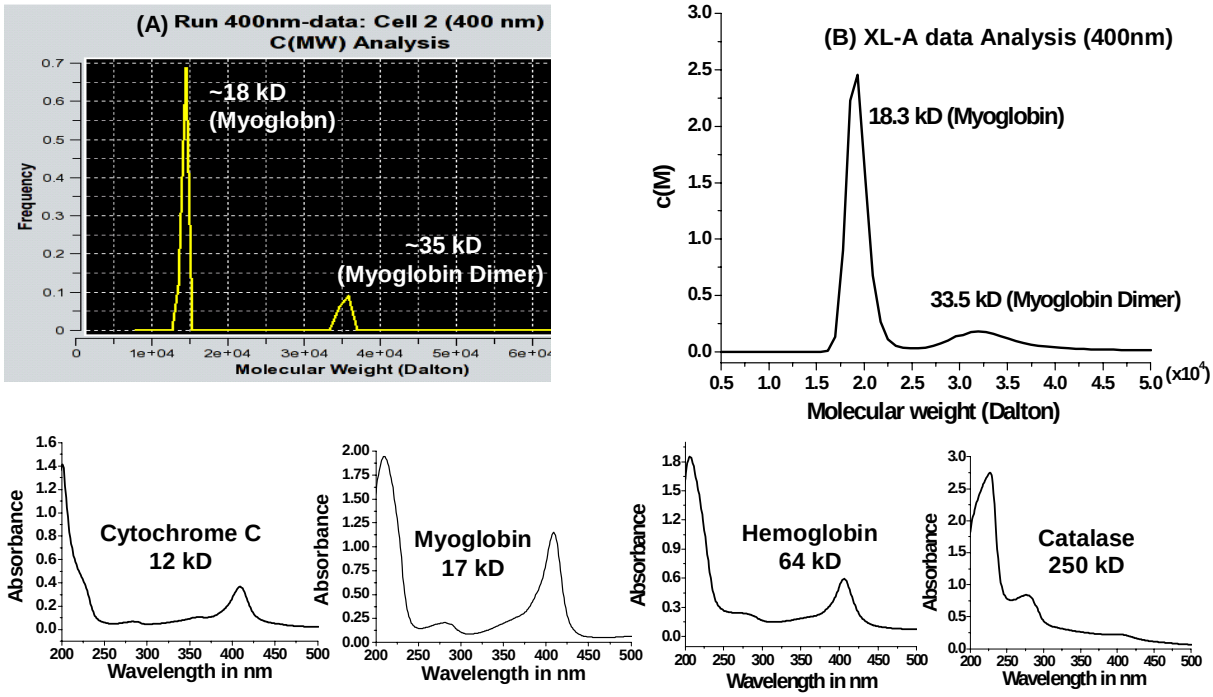

Fig.76.Comparison of evaluation of four protein mixture data and test for sensitivity of the detection system. Above: (A) Evaluation with Ultrascan for the multiwavelength data (with permission from Prof Demeler). This plot is a screen shot of the evaluation results sent by Pof. Demeler. The molecular weight values are entered afterwards as read from the visual look at the plot. Experimental conditions: 50,000 rpm, 10s scan interval, 25°C, radial step: 50µm. (B) Evaluation of XL-A data for the same sample with sedfit. Experimental condition; speed: 50,000 rpm, 3 min scan interval, 25°C, radial step: 50µm. One of the four proteins Myoglobin (17 kD) and its dimer could be detected at the wavelength 400nm. Other three proteins (Cytochrome C, Hemoglobin and Catalase) show low extinction values at that wavelength and could not be detected. Below: Wavelength scans for individual proteins with solution concentration before mixing (0.1 mg/mL). The spectra reveal that the proteins Cytochrome C, Hemoglobin and Catalase show very low absorption at 400 nm and thus could not be detected. The experiment also indicates that sensitivity of the detection system is 0.025mg/mL for Myoglobin with detection at 400nm.

The results presented above clearly show that better separation of components can be visualized with a 3-D data display. Also, the user can select any wavelength in the range of 200-800nm for separate evaluation. These are clear advantages over existing commercial instruments as the user can see the raw data in 3-D space so as to select the wavelength for evaluation. Also, the presence of data sets for the whole wavelength range allows the user to perform the evaluation at the selected wavelength. For working wavelength of 400nm, one of the four proteins Myoglobin (and its dimer) could be detected as other three show low extinction at that wavelength. The experiment can also give information about the sensitivity of the detection system, a 0.025mg/mL Myoglobin solution in phosphate buffer at pH: 7 is satisfactorily detectable at 400nm. The other three proteins could not be detected for the same solution concentration at 400nm.

ii) Quantum size effect study for TiO_2 particles: It is a well known fact that TiO_2 particles show the Q-size effect. In the past the particle size characterization of TiO_2 or other samples showing these effects, involved time consuming experimental work. Determining the relation between band gap and particle size involved synthesis of monodisperse particles of defined size, their particle size determination (usually by TEM) and then UV/Vis characterization. This time consuming analysis work can be done by a single experiment in Multiwavelength detection AUC. The radial scans can be used for establishing this because as the particles are fractionated in the centrifugal field, a shift in the wavelength maxima for different particles can be simultaneously observed, as shown in Fig. 77. In commercially available instruments, in order to demonstrate the same effect one needs to carry out wavelength scan at different radial positions (Fig. 78), which is also a time consuming experiment and risks a loss of information as data enrichment is rather slow.

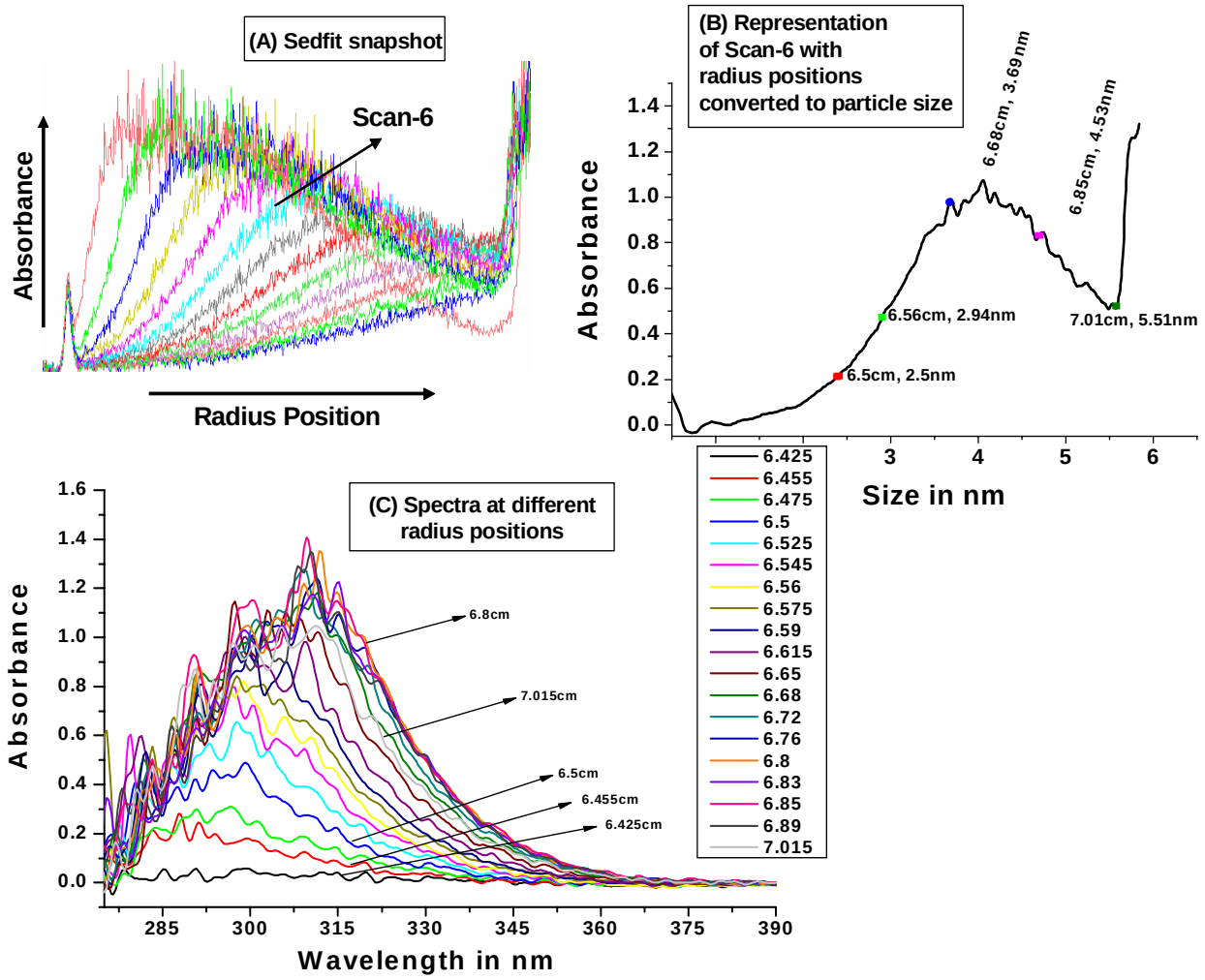

Fig.77 Synthetic boundary experiment for the TiO_2 sample (Experimental conditions: 30,000rpm, 320detection wavelength. 30µm radial step, 10s scan interval). (A) Sedfit snapshot of the synthetic boundary radial scans. (B) Scan 6 [marked in (A)] with radius position converted to particle size (radius to size distribution is performed by first conversion of radius to s and then s to d distribution using the equation $s=\ln(r/r_m)/\omega^2 t$ followed by $d_i = \sqrt{\frac{18\eta s_i}{\rho_2 - \rho}}$). All the plots are generated with raw data from the same Multiwavelength experiment (scan 6 in this case). (C) Spectra of TiO_2 particles of different sizes occurring at different radius positions for the same radial scan (here scan-6). The spectra are generated with 15 points FFT smoothing as they appear to be noisy [ref. point (ii) in section 6.8]. The plots clearly indicate that the same experimental results can be used for extracting informations of relationship between band gap position and the particle size (Spectra for each particle size and radius position can obtained from the same experiment) unlike commercial XL-A instrument, where for every radial position a time consuming wavelength scan needs to be performed.

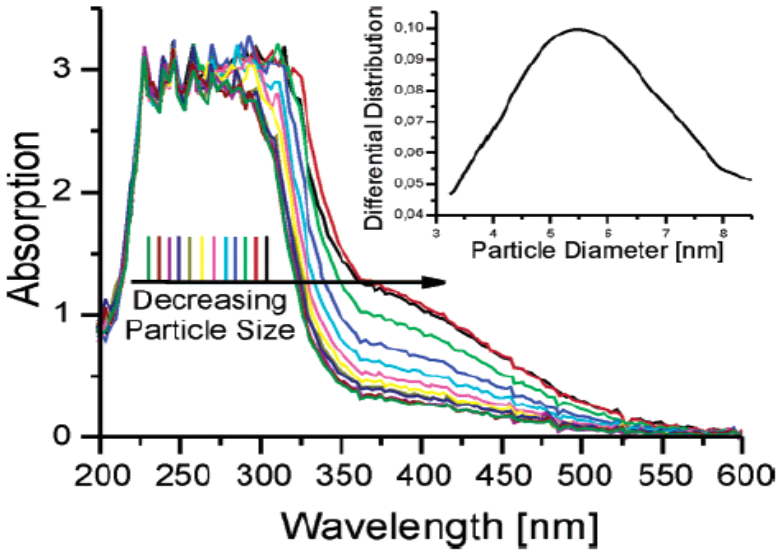

Fig 78 Analytical Ultracentrifugation data to show the shift in wavelength maxima with particle size (for similar sample, dopamine functionalized titania nanoparticle) to show the shift in wavelength maxima with particle size. Inset: particle size distribution curve. In order to show the same effect as in fig. 77, wavelength scans at different radial positions are needed, which is also a time consuming experiment and risks a loss of information as data enrichment is rather slow (reproduced with permission[148]). In this case, the spectra get red-shift with decreasing particle size as a result of interaction of dopamine with TiO_2.

6.8 Discussion -2nd Generation Multiwavelength Detector

i) Better alignment could be achieved: The experimental results available from the 2nd generation Multiwavelength detector demonstrated data generation that is concordant with that of reference experiments with the commercial instrument or literature values. This was already evident in the earlier development of the 2nd generation setup with divergent optics. However, the further development with mirror based collimation optics showed improved intensity in the UV region of the lamp spectra. This can be attributed to the fact that while aligning the optics, chromatic aberration was reduced, so that less and optimization in the visible region (which was the only wavelength range available for alignment) did not invoke much error in the UV region. A comparison of signal intensity in the various optical setups is shown in Fig. 79.

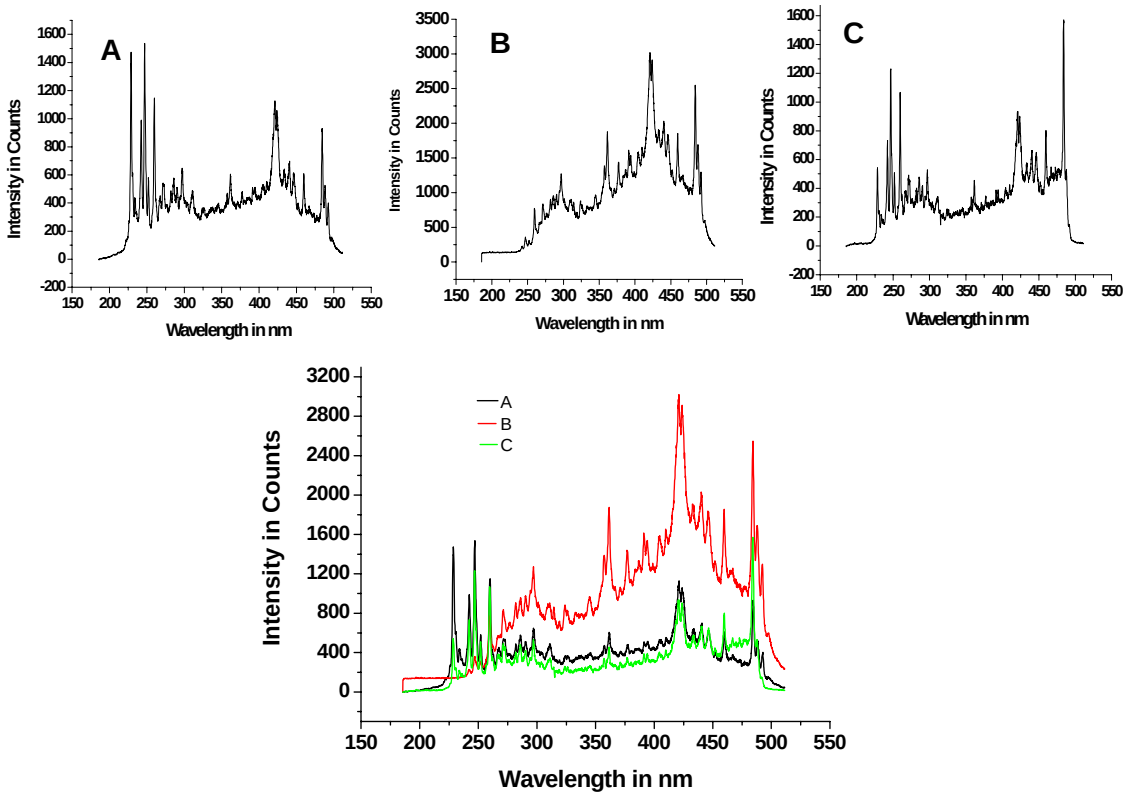

Fig.79 The lamp spectra in different optical setups. This can be considered as an indication that better alignment in the UV region could be achieved with the introduction of mirror based collimation optics. Top: (A) Lamp spectra by direct coupling of the spectrometer to the lamp with a 10 micron fiber. (B) Lamp spectra of the divergent 2nd generation optics (ref. fig. 55, here a biconvex lens of focal length 20.6 mm was used for focusing the light into the cell sector). (C) Lamp spectra with the use of mirror based collimation optics. The enhanced intensity in the visible region in fig B is due to the fact that while aligning the optics, the UV region could not be taken into account (lenses were used in the whole optics component) and also there was overall gain in intensity as a larger cladding diameter fiber (600 micron compared to 50 micron in the case of (C) was used for illumination. Bottom: overlay of lamp spectra recorded in each optical setup.

The above figure clearly indicates that the use of a reflective, instead of refractive element for construction of the optics is desirable, as it diminishes the error in the alignment due to the chromatic aberration, improving the data quality. Also, the introduction of the Off Axis Parabolic mirror reduces the loss of light intensity due to fiber bending. This 90° mirror replaces directly the fiber bend in the detector arm.

ii) Possibility of data averaging could improve the signal to noise ratio: Unlike the commercial instrument, the data generated in our Multiwavelength setup, has a huge volume. The user can select a combination of data sets to generate new data with better signal to noise ratio and to work with an enhanced sensitivity. This is possible because

multiple wavelength data sets are acquired for each radial scan of the sedimenting species. This is even possible for peak wavelengths in a spectrum. An example is shown in figure 80.

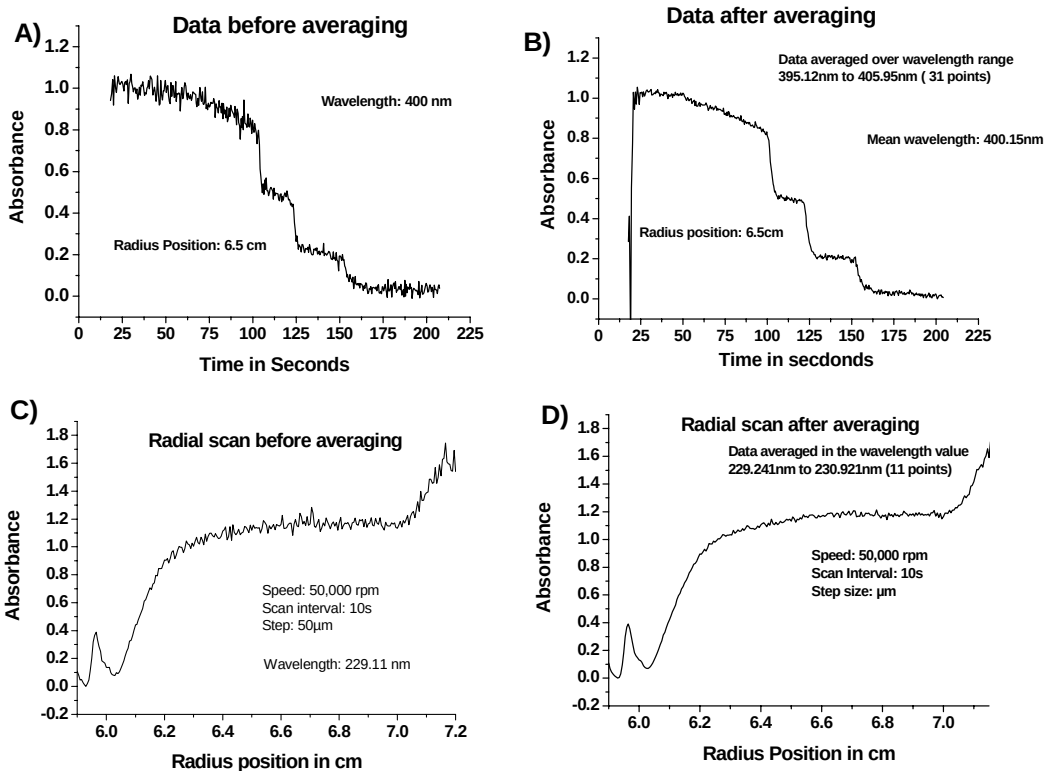

Fig. 80. Improvement in data quality with averaging. This feature can be implemented for data generated with Multiwavelength detector as the data set contains whole UV/Vis range of wavelength. The upper half of the figure shows averaging of a fast mode velocity profile data set for a sample with three latexes mixed and diluted to give optimum UV intensity. A) Raw data for single wavelength B) Data averaged over 31 wavelength points. The lower half of the data shows the same effect for a radial scan. The scan was taken from the sample of a four protein mixture. C) Radial scan for a single wavelength from the multiwavelength data set (229.11nm). D) Data averaged over 11 wavelength points.

iii) Necessary improvement of the data acquisition software: As shown in Fig. 81, the Multiwavelength data generated with our multiplexer and step motor control program showed significant noise compared with data generated from our written program, and those generated with the use of commercial software.

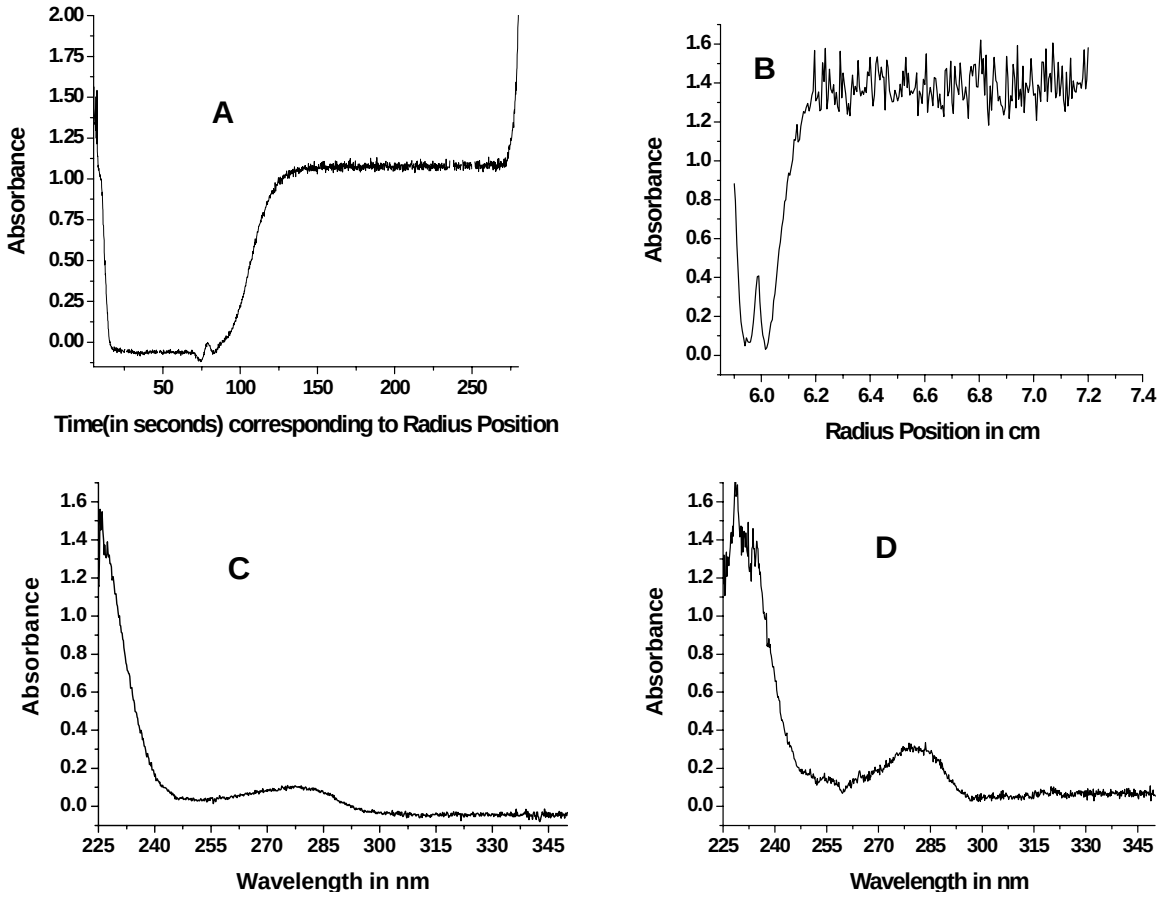

Fig.81. Observation of noisy data from the data generated with our software and its comparison to that with commercial Ocean Optics data collection software for the USB series of spectrometers. The upper part of the figure corresponds to a comparison for radial scans. (Experimental conditions: 50,000 rpm, step size: 25 um, sample: 0.5mg/mL BSA in 0.1N NaCl, wavelength: 232nm. Fig.A: Radial scan generated with the commercial Ocean optics software. For the data collection, multiplexer software was used to define the position of the flash, the step motor program was used to control the movement of the step motor for radial scanning and data was collected with the commercial Ocean Optics software with integration time of 50ms and 1 average. Fig B: Radial scan with the data from the software developed at MPI, under the same experimental conditions. Fig.C &D : Spectra from a position in the radial scan. Note that the absorbance value varies as the corresponding scans and the radial positions are not similar. Experimental data with software developed at MPI corresponds to automatic data generation, while for the data in Fig. A and C, the scanning needs manual control to start the software.

iv) Difference in spectral response for XL-A data and the Multiwavelength data at lower wavelength: There is also a difference in the data for XL-A and Multiwavelength with respect to their spectral response at lower wavelength. This can be attributed to the difference in lamp spectra for both the setup (for our setup, the minimum detection limit is 229nm) and thus a direct comparison of XL-A generated wavelength scan and a spectra from our setup only up to 229nm.

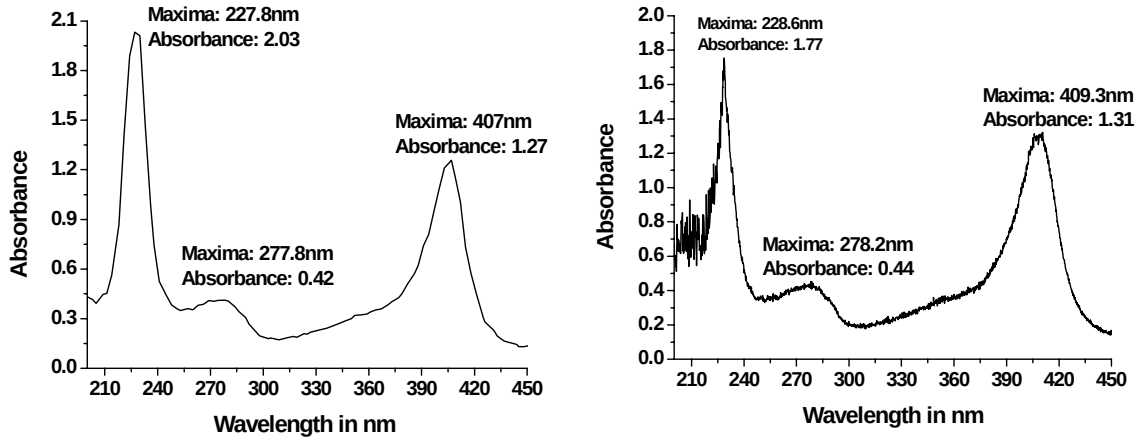

Fig. 82: Difference in spectral response for commercial XL-A and Multiwavelength data at lower wavelength (below 229nm). The spectra were generated for the sample, an equimolar mixture of four proteins, Hemoglobin, Myoglobin, Catalase, and cytochrome in phosphate buffer at pH 7 (the sample used for fig 70 and 71) left: data generated from the XL-A (a wavelength scan with step size of 5nm and 2 replicates and rotor speed 3000 rpm), right: data from Multiwavelength detector (50ms integration time, 1 average). The multiwavelength data is selected from the first scan (to ensure no sedimentation) of the experiment and at the same radial position of 6.5 cm (experimental conditions: 50,000 rpm, 10s scan interval, 50μm radial step). A direct comparison of the two systems is valid for wavelengths greater than 229nm.

It can be concluded that designed optics system can generate 3-D data with optimum accuracy (the data presented in the experimental result section). Improvement in optics is necessary for precise alignment in the UV region with less chromatic aberration. Also, the data collection software should be improved so that the resulting experimental data are less noisy. This could be achieved with better programming of the spectrometer readout and triggering routines (as in the commercial Ocean Optics software).

6.9 Third Generation Multiwavelength Detector

The second generation data clearly indicate that the construction of a Multiwavelength UV/Vis detector is possible which can generate fast and rich data set. The effect of chromatic aberration that was present in the data so far may be eliminated by the use of mirror-based optics. Such an optical system has been developed at the MPI and is in its final construction stage. However, due to lack of time, experimental data could not be generated anymore to prove the detector performance and reliability.

A new heat sink modification was performed keeping in mind the fact that the Beckman warranty is lost with the drilling of holes into the heat sink, which was a disadvantage of the first and second generation detector set-up. Also, repair of feed-throughs is difficult with the existing design as this needs removal of the can from the vacuum chamber, which often gives rise to the problem of breaking of the Peltier elements below the can. In order to circumvent this, a new design modification was developed for the heat sink using the Analytical XL-I platform. To draw in the fibers and the electrical cables, a hole in the socket for fitting the monochromator in the XL-I was utilized (In the commercial XL-I Ultracentrifuge, light from the Xe flash lamp emerges through this hole towards the toroidal mirror). A cut on the can was performed with the possibility to accommodate the detector arm and its movement for radial scanning. The new heat sink modification allows for working with the lens based arm as in the second generation, as well as the newly designed mirror-based detector optics arm. It is a modular system, which maintains the Beckman warranty and allows modifications without intrusion into the instrument.

The third generation detector arm can be constructed using some commercially available components in addition to some components already used in the second generation detector. For the final construction of the detector arm, the collimation optics, plane mirror for deflecting the collimated beam at·90° angle and guiding it through the cell sector, the spectrometer and precision slit for defining the spatial resolution of the detector were used as in the second generation optics. In addition, the following commercially available components were used for complete construction of the optics arm in conjunction with the above mentioned parts:

i) **Four fiber vacuum feed through**: This feed through is equipped with two fibers of cladding diameter 50 microns and two fibers of cladding diameter 1000 microns. The 50 micron fibers are to be used for the collimation optics as this cladding diameter is pre-requisite for the construction of this optics (as discussed earlier). The 1000 micron fibers can be used for the detection optics as the light emerging from the optics has a diminished intensity compared to the incoming light. This vacuum

feed through was obtained from OZ Optics, Canada (part no.: VAC-04-N-QMMJ-55-UVVIS-50/125,940/1000-1,1.4-1,2.5)

ii) **Off Axis Parabolic Mirror:** Obtained from Melles Griot, Bensheim, Germany (part no. 02 POA 011/028, coated with UV-enhanced Aluminum). This mirror focuses the transmitted light from the cell sector to the fiber, which is directly coupled to the UV/Vis spectrometer.

For drawing the fiber and electrical cables into the centrifuge, a vacuum tight box was designed which can accommodate all the components in a base plate so as to give them a housing space with their respective vacuum feed throughs away from the small hole in the monochromator socket. A schematic drawing of this modification is shown in the figure 83. The overall 3rd generation setup is shown schematically in Fig. 84, and photographically in Fig. 85 and 86.

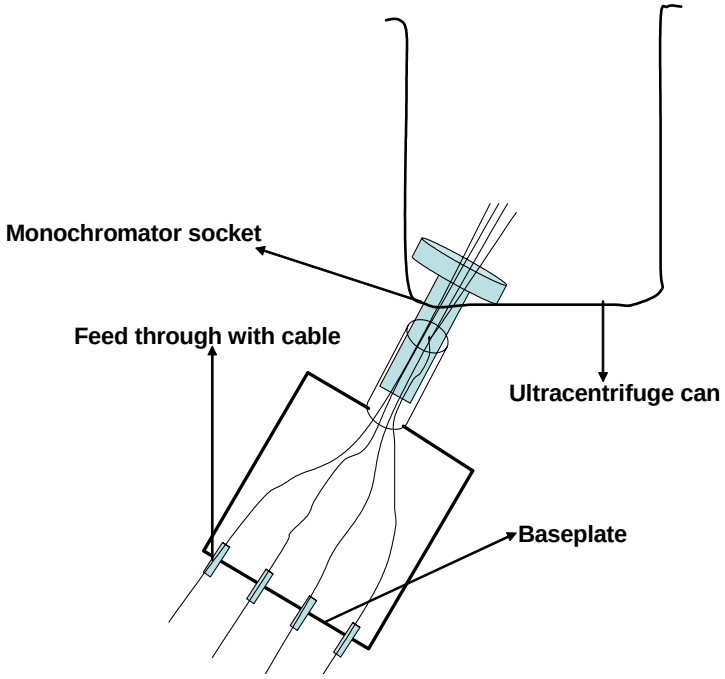

Fig. 83 Schematic drawing describing the modification for drawing the cables and fibers into the vacuum chamber.

Scheme of optics setup and photographs showing its mounting (3rd generation)

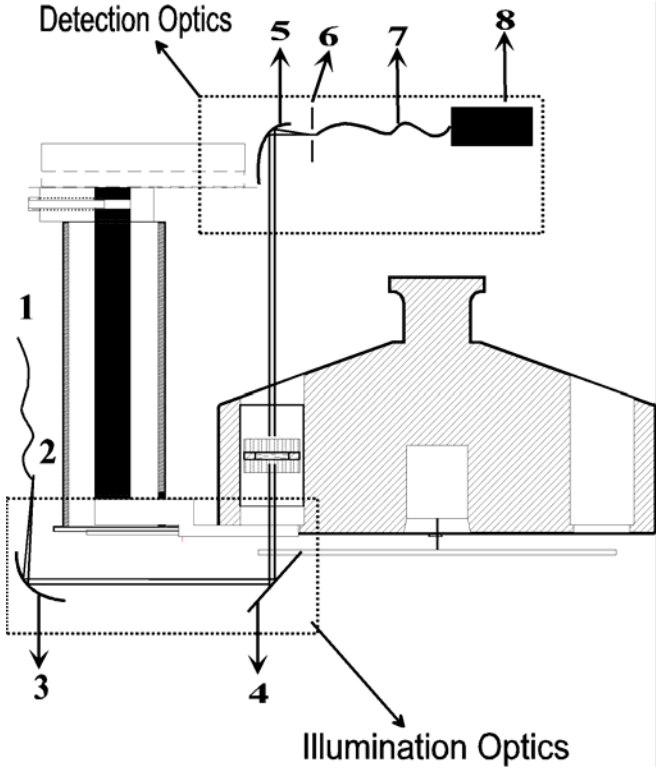

Fig. 84 The third generation optics arm. (1) 50 micron fiber (UV/Vis from the vacuum feed through), (2) Tip of the 50micron fiber and focus of the OAP, (3) Off axis parabolic mirror (from LFM Bremen) (4) Plane mirror (Edmunds optics) (5)Focusing OAP (6) 25µm Precision slit (7) 1000 micron UV/Vis fiber (from the vacuum feed through), (8) Spectrometer. The light path is also shown schematically.

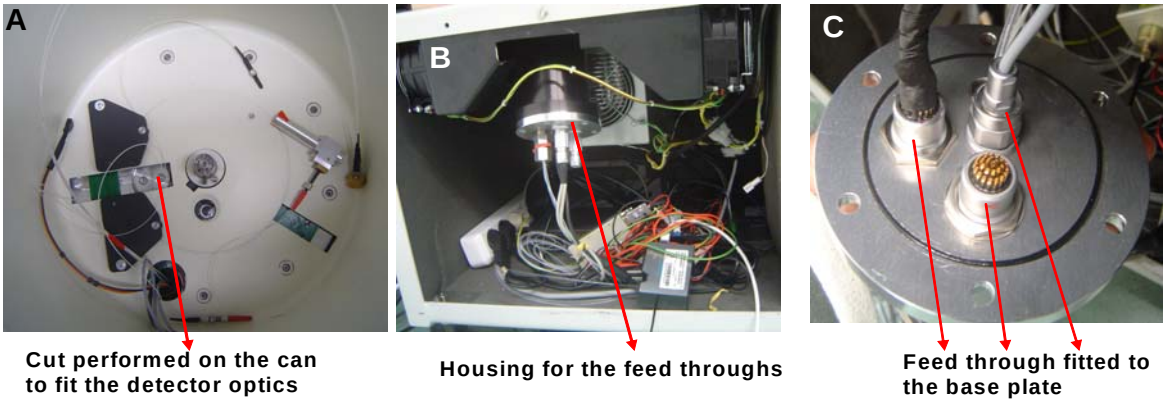

Fig. 85 Photographs showing the modification of the can for fitting the detector arm and modification for drawing the cables into the vacuum chamber. Fig A shows the view of the can from the top. Fig B and C show the housing constructed to be fitted for drawing cables inside the vacuum chamber.

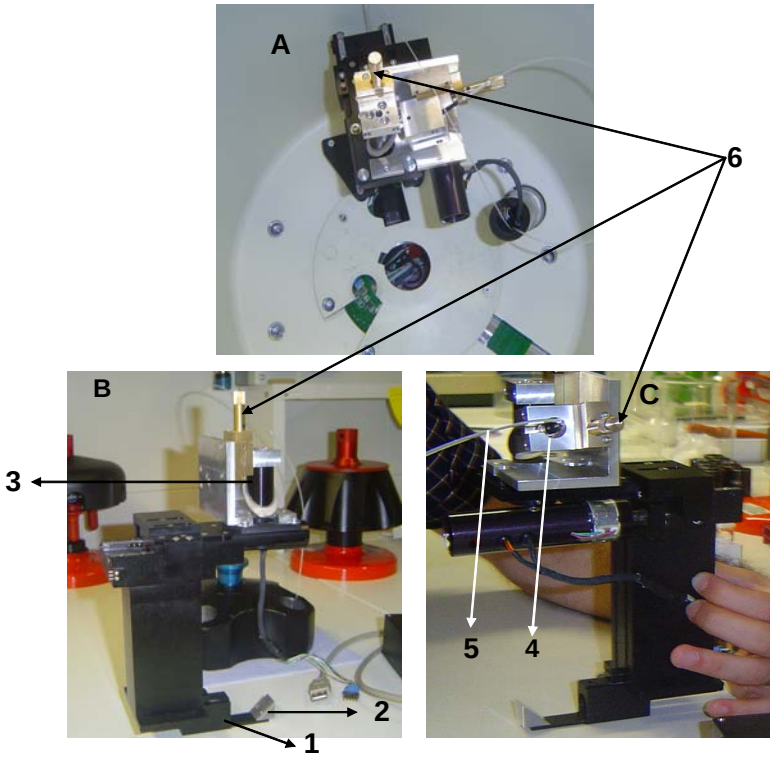

Fig. 86. A) The third generation detector arm mounted in the AUC vacuum chamber. B and C) Lateral views of the detector arm. In the figures, 1-the position for fitting the mirror based collimation optics housing. 2-the position of the plane mirror used for deflecting the collimated beam and guiding it through the cell sector. 3-parabolic mirror (OAP) for focusing the collimated light emerging from the cell sector. 4- housing for the precision slit for defining the spatial resolution . This part also accommodates the SMA connector of the fiber collecting the light after the slit. 5-fiber with emerging transmitted light to be connected to the spectrometer. 6-precision screws for fine adjusting the position of the mirror in position 3 and the position of the slit with the fiber (position 4) necessary while aligning the optics.

The construction of the third generation detector arm was completed with the implementation of the heat sink modification. The final adaptation of the whole setup could not be carried out as more fine adjustment of the arm with mechanical modification was necessary. For the same reason, data generation to test the detector performance could not be carried out. Nevertheless, with the third generation optics, a chromatic aberration free setup is expected that can be more precisely aligned for the whole wavelength range.

Chapter-7

7.1 Conclusion

In this work approaches for development of a new detection system for the Analytical Ultracentrifuge (AUC) were explored. Unlike its counterpart in chromatography fractionation techniques, Multidetection system for AUC has not yet been fully implemented. However, many applications can be foreseen for such Multidetection capability. In this study we tried to couple existing fundamental spectroscopic and scattering techniques, that are used in day to day science as tools for extracting analyte information, into such an AUC detector. Trials were performed to employ Raman, small angle laser light scattering and an improved UV/Vis detection incorporating the possibility to work with the whole range of wavelengths, to study analyte behaviour during ultracentrifugation experiments. Conclusions were drawn for the applicability of Raman detector for AUC, that for such a detection system to work one needs to employ very high power laser. It was also realized that for a Small Angle Laser Light Scattering detector, sensitive photosensors with large active area like APD should be incorporated. The development for a fast fiber optics based multiwavelength detector was completed.

It became obvious that with the generation of data in 3-D space in a UV/Vis detection system, the user can select the wavelength for evaluation after completion of an experiment. This allows evaluation of results that supplies more information, an application which can be cited, e.g. for studying protein interactions where the individual protein before interaction absorbs at one wavelength, that changes to another value after their association (This applicability was proven with successful Multiwavelength detection of a four component protein mixture). In current commercial instruments the user can work with only three selected wavelengths. Users' software (Sedvel), however, offers the option to evaluate data with many wavelengths, which is not available in a data set from XL-A. For this experimental demand, a Multiwavelength detector can satisfy a requirement of the AUC user community as the data set contains information from all wavelengths in the range 230-800nm. The detector construction was completed with a lens-based modular design. Software programming and a proper alignment procedure for

this optical system were also performed. The data generated with this system was evaluated with normal evaluation software used by the AUC community (Sedfit and Ultrascan) which showed their concordance with reference measurements and literature values. Also, the capability of much faster data generation unlike that possible with commercial instruments was demonstrated, by collecting data for a sedimentation velocity experiment using a mixture of three latexes. The results shown were similar to those of a commercial instrument, whereas the experiment time for our designed optics was ~3 minutes, while the same experiment took ~2hours in the commercial instrument. This fast mode of data generation can be used for detection of aggregates which sediment in the early phase of an experiment and with maximum diffusion suppression (this experiment needs a longer time and much more careful measurement in commercial XL-A). Unlike the XL-A, data generation with wavelength resolution allows a wavelength scan at every radial position. This is useful e.g. for demonstrating the Q-size effect for a sample. In the present XL-A setup, in order to demonstrate this effect, a time consuming wavelength scan is necessary at various radial positions, which in our setup is automatically generated while performing a normal radial scan. Thus such an experiment does not require any extra effort from the user, and a complete set of spectra for different particle sizes are available from a single radial scan, which contains a number of spectra many times higher than can be generated from an XL-A wavelength scan. Also, the introduction of the time mode scan makes the detection system more versatile. This mode can be used for aggregate determination as they tend to sediment at the beginning of an experiment. The data averaging option can lead to better raw data visualization and also better fitting for global analysis.

7.2 Detector development in Analytical Ultracentrifuge-A future outlook

Although the AUC user community is quite small, for some areas of research and industrial applications, such as for determination of particle size distribution of polymers and dispersions or for interaction studies of proteins, the technique remains unequivocal However, the lack of appropriate detectors is often a disadvantage of present analytical ultracentrifugation. The existing detection systems are not very precise, not fast enough,

and data acquisition is often not really “online”. Though the existing interference system is fast, it lacks precision. Thus to meet the experimental expectations for AUC, it is necessary to design and develop new detection systems. The need for new detection systems has been well documented[82, 83, 84].

There have been few efforts for developing new detection systems in AUC. Improvements in existing detector systems can be accomplished by enhancing data acquisition speed or data precision by application of sensitive and high resolution devices (PMT, Avalanche photodiode, High resolution CCD cameras), or reduction of noise by signal averaging. However, this would only increase the data quality and not the amount of complimentary data, which could be used for the full description of a system under investigation in a global analysis approach.

A rationale for new detection systems can be put forward with reference to Svedberg equation:

$$M = sRT / D(1 - \bar{v}\,\rho_0)$$

Ideally, introduction of a Multidetection system in AUC should allow that all the quantities in the Svedberg equation can be simultaneously determined from a single experiment. The experimental setup available allows determination of s and other quantities need to be determined by using different techniques. However introduction of a Laser Doppler Anemometry (LDA) detector in AUC can enable determination of s without any knowledge of cell dimensions (e.g. the meniscus position, radius and bottom position) and also for a single particle. A Small Angle Laser Light scattering (SLS) detection system can be used for the determination of M in the above equation. With the introduction of a Dynamic Light Scattering (DLS) detector, D can be measured. A preliminary test with a pulsed laser already showed that the determination of the particle size is possible with short illumination times. All of these quantities would be available as distributions. The solution of the Svedberg equation with the three quantities available so far can yield the density (VBAR) distribution of the sample. Also, invoking a Raman detection system to AUC, can serve as the vital step for supplying information about the chemistry of the components in a complex mixture. In addition, development of fast data generation capability for the detection system shortens experiment time and enriches experimental

data with more valuable information, as with such a system the process of sedimentation can be followed in more detail. Our experiment with the fast Multiwavelength detector has already proven that such a system is possible and as many as seven samples can be characterized in less than three minutes time.

It may be mentioned that adaptation of recent commercial products can enhance the detector performance manifold, as has also been proven in our study to adopt a CCD-based spectrometer for the Multiwavelength detector. Another example may be the design of a plug and play system for SLS and LDA. Implementation of an LDA system to AUC will be quite valuable as it can allow online measurement of the sedimentation coefficient. LDA works on the principle that, when a particle passes through intersection volume formed by the two coherent laser beams, the scattered light, received by a detector, has components from both beams which interfere on the surface of the detector. Due to changes in the difference between the optical path lengths of the two components, this interference produces pulsating light intensity, as the particle moves through the measurement volume, which is related to the velocity of the particle. Measurement of this velocity can enable determination of s (using the equation $u/\ \omega^2 r \equiv s$), which in turn can be related to the particle size. As the equation does not contain any term for cell dimension, s can be determined without the knowledge of these. Also, since the determination of the particle velocity (u) is online, the s can also be determined online. The design could use a commercially available modular LDA probe[149] that can be easily fitted to a detector arm as was used in our Multiwavelength study. A scheme of the envisaged design is shown in Fig. 87:

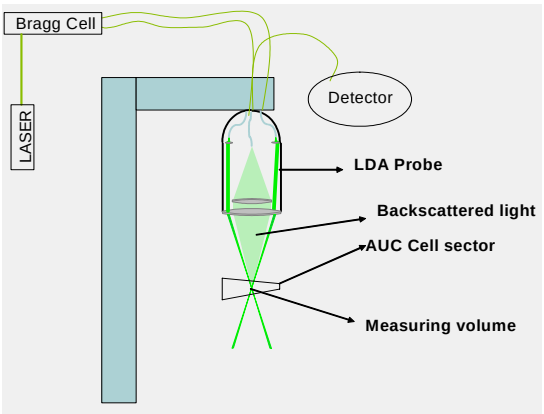

Fig.87. LDA set up for AUC in backscattering mode.

The necessary fibers (after the Bragg cell) can be drawn into the vacuum chamber with the use of feed throughs as in the Multiwavelength detector setup, and the whole assembly can be fitted to the detector arm. (The use of a Bragg cell can be omitted for SLS experiments). A promising setup may be the front scattering setup using an Avalanche Photodiode (APD) with the application of beam stops at the proper place. This setup gives the advantage of working with a strong scattered light signal.

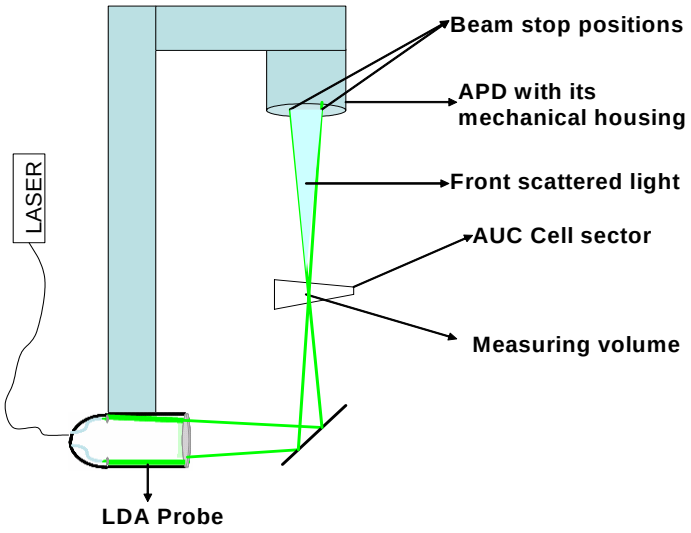

Fig.88. LDA setup for front scattering mode

Both of the above setups can be exchangeable with an SLS detector but it would need to be investigated how far the detected scattered light can be simultaneously used to detect the particle size or the molar mass. Commercially available LDA systems are not highly sensitive as they are not designed for performing measurements on very small objects. However, custom made systems with the use of a high power (and shorter wavelength) laser can be suggested.

Development of a Raman system as an exchangeable detector with Fluorescence detection system can also be tried as both can be designed on the basis of confocal optics. A schematic with adaptation of all the detection system for AUC is shown in the figure 89.

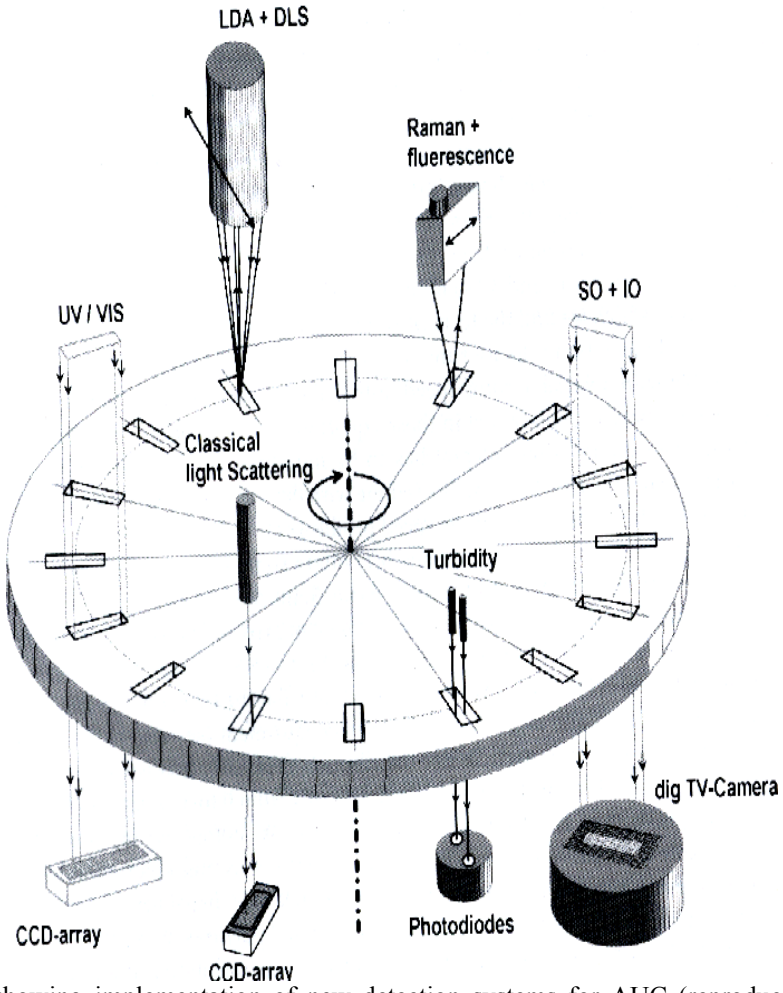

Fig 89.Schematics showing implementation of new detection systems for AUC (reproduced with permission from ref. 83)

Thus it can be concluded that for AUC new detection systems can be developed which can give experimental data for a complete characterization of polymers and colloids. Also, the same setup can yield valuable information for biological macromolecular systems. It has been also been proven during the Multiwavelength detector studies that fast detectors and fast mode experiments are possible for AUC. The Multiwavelength detector development can be taken with the aim to augment existing detection systems with respect to making them faster, more informative and designing a complete new detection system. A first step towards this was achieved in our studies with the development of a fast Multiwavelength detector and establishing the requirements for Raman and Small Angle Light Scattering detector.

Appendix-I **Mechanical Drawing of different parts used for construction of the optics. The measurement units are according to German system (in mm)**

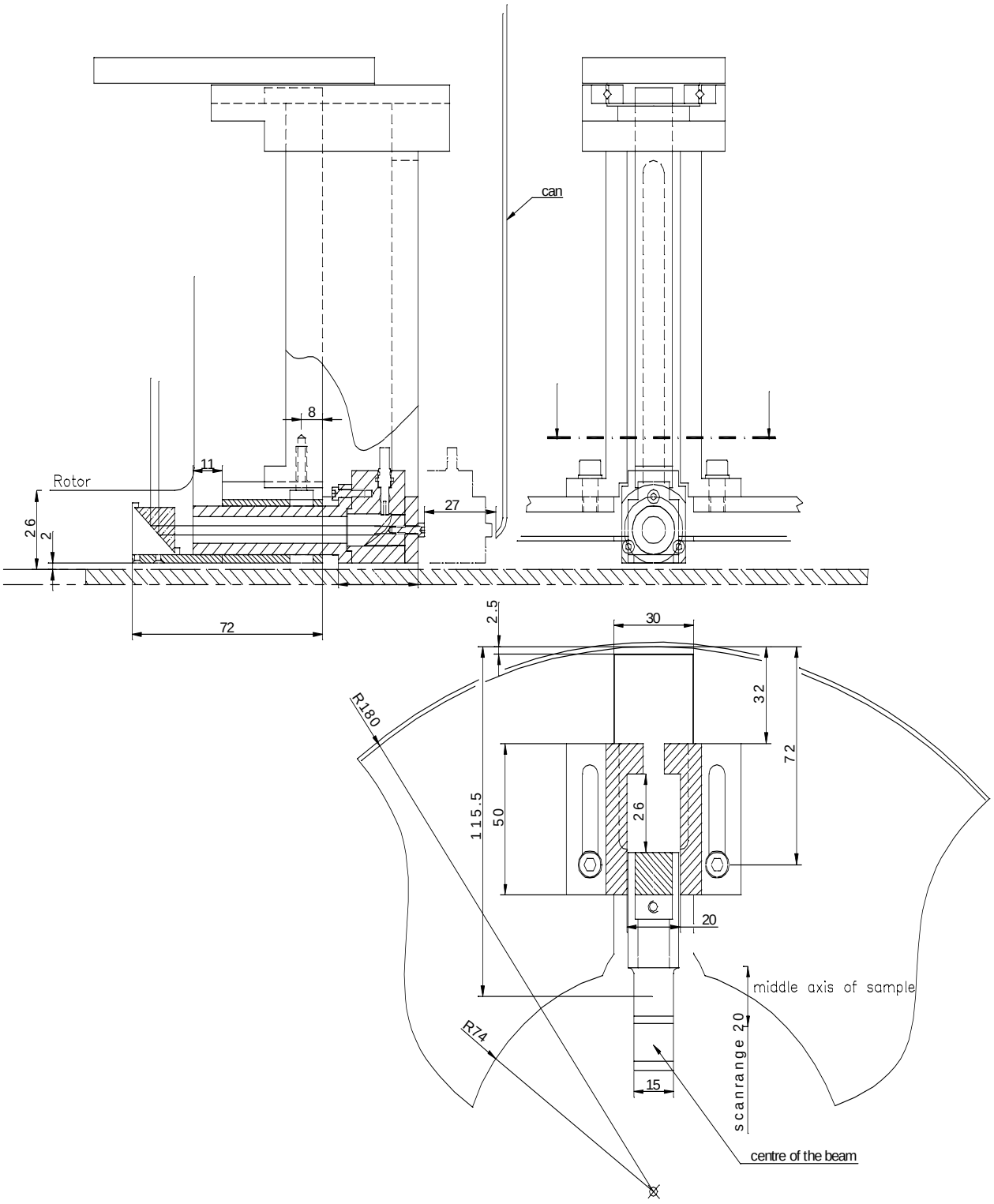

Fig.90 Mechanical drawing of the detector arm.

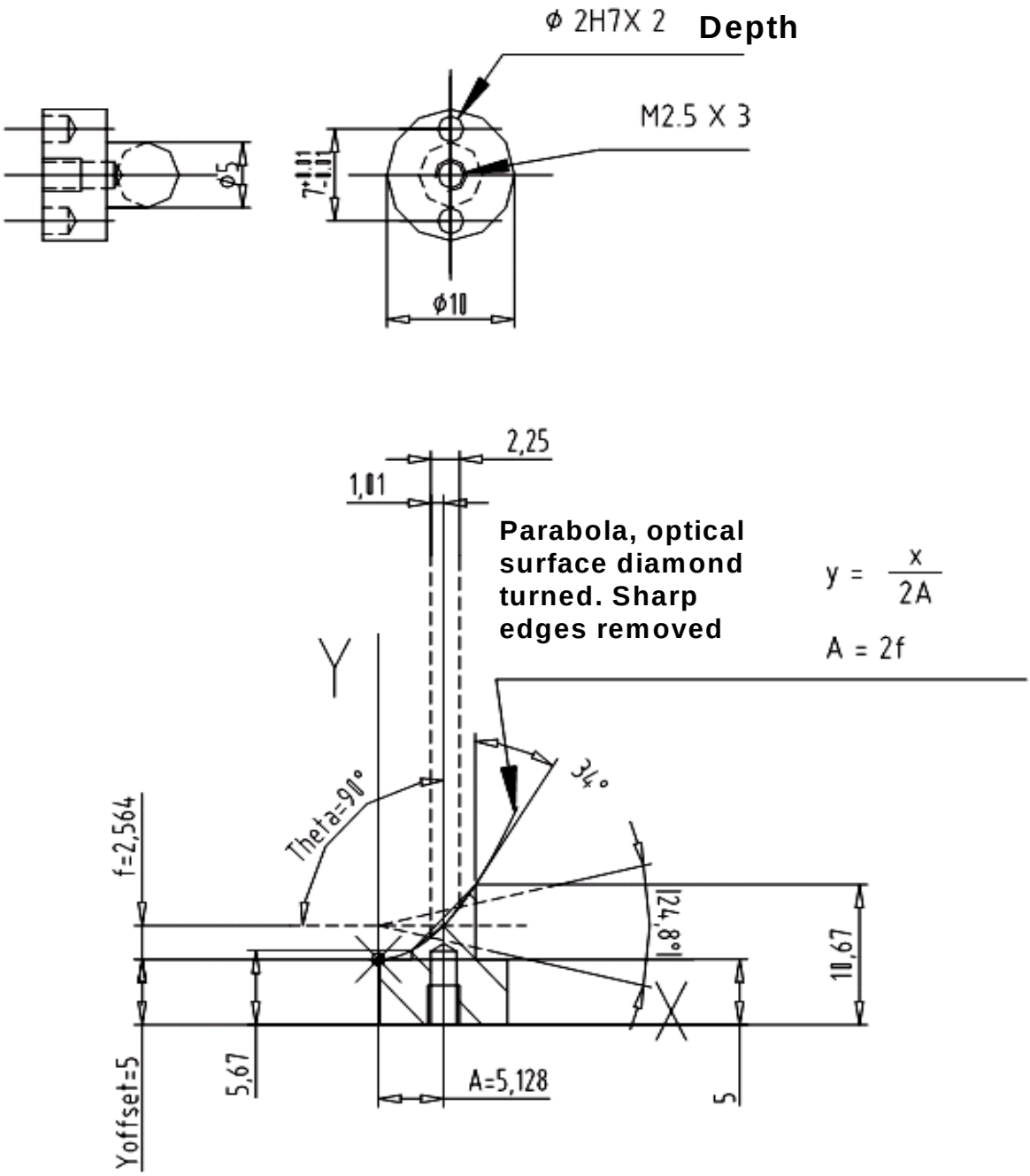

Fig. 91: Mechanical drawing of the Off Axis Parabolic Mirror (focal length: 2.564mm)

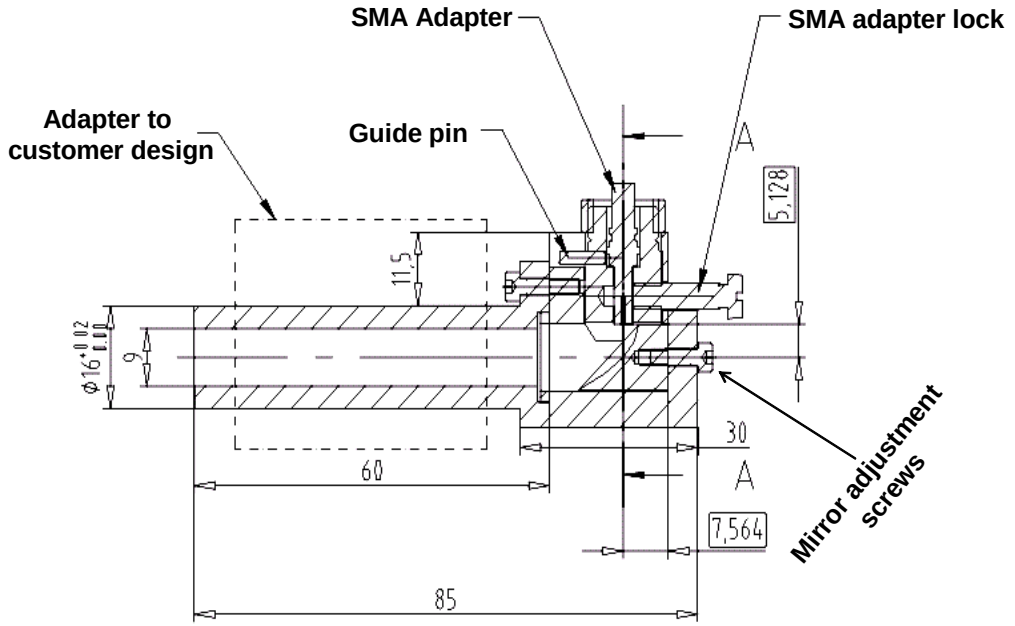

Fig. 92: Drawing of the Off Axis Parabolic Mirror housing used for collimation optics.

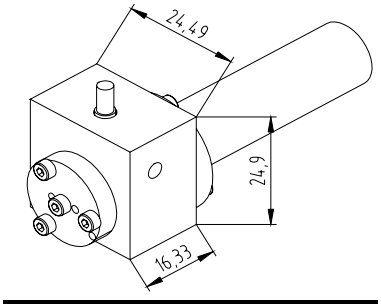

Fig. 93: Off Axis Parabolic Mirror housing (top view)

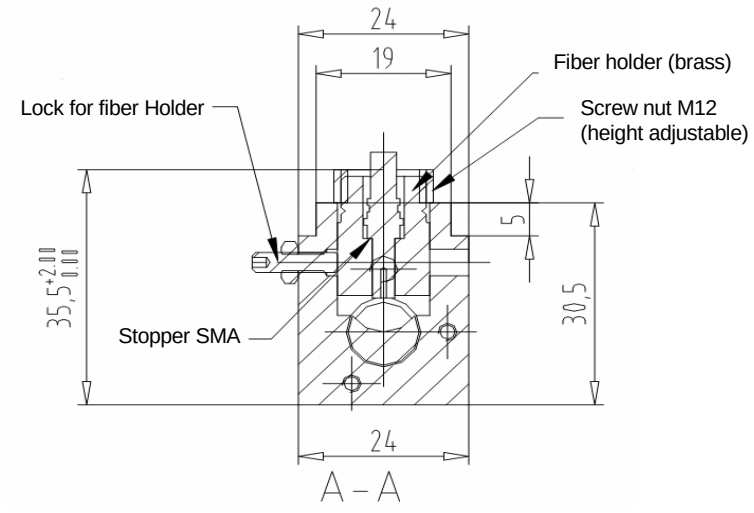

Fig. 94: Front view of the Off Axis Parabolic Mirror housing

Appendix-II E*stimation of construction cost for the 2nd generation Multiwavelength Detector*

Sl No.	Item Description	Part No.	Supplier	Cost
1	Mirror based Collimation Optics with housing	Not Applicable (a custom made item)	LFM Laboratory for Precision Machining, University of Bremen, Germany.	2600 €
2	Four channel Fiber feed through (UV/Vis)	VAC-04-N-QMMJ-55-UVVIS-50/125,940/1000-1,1.4-1,2.5	OZ Optics Limited, Ottawa, Canada	1375 €
3	*USB series UV/Vis Spectrometer with accessories (including software)	USB 2G 558 USB 2E 3390	Ocean Optics BV, Duiven, the Netherlands	2500 € (each)
4	Linear actuator (with accessories: Power supply)	T-LA-28-SV	Zaber Technologies Inc. Columbia, Canada	700 €
5	Biconvex Quatrz lenses (focal length: 12.5mm & 60mm)	G311-210-000 (f-60mm) G311-204-000(f=12.5mm)	LINOS Photonics GmbH & Co. KG, Goettingen, Germany	80 € 115€
6	High Power Xe- Flash lamp	L-9456-12	Hamamatsu Photonics K K., Electron Tube Division, Japan	865 €
7	Power supply for the lamp	51672755	Conrad Electronic, Hirschau, Germany	35 €
8	Electrical feed through	HGP 3S 318 CLL SV FFA 3S 318 CLAC 11	LEMO Elektronik GmbH, München, Germany	35 € 35 €
9	LabView 7.1 Software development environment	850670R-03	National Instruments Corporation, Austin, Texas, USA	1100 €
10	Heat sink modification (preparative to a XL-I heat sink)	Heat sink assembly, XLA2: 363404 Can Assembly, XLA: 363348	Beckman Coulter GmbH, Krefeld, Germany	8000 €
11	Cost of the mechanical components necessary		Leibniz-Institut für Molekulare Pharmakologie, 13125 Berlin.	10800€
			Total Cost	**28240 €**

Note: The above construction cost is on the basis of the detector adaptation to a preparative XL ultracentrifuge (cost: ~50,000€). The cost for manufacturing the detector arm with the necessary modification in the XL-I is just an estimate. The cost for constructing the reflection light gate is not included here as this was done at BASF, Ludwigshafen. USB 2000 series spectrometers have been discontinued by the supplier, however, UB4000 (cost: 2,500€) can be used instead (from the same supplier)

Appendix-III Alignment procedure for 2nd Generation optics

The alignment procedure consists of alignment of the mirror based collimator optics and then that of other optical components as described below:

1. Place a pinhole at the position of the 60mm biconvex lens (see fig. A, the position 6).
2. Fix a laser pointer at the slot where the collimation optics can be fitted (see fig. C).
3. Adjust the position of the three screws at the bottom of the plane mirror slot so that the emerging laser beam from the pointer hits the mid point in the pinhole (fig. C). These positions of the screws should be kept intact.
4. Remove the laser pointer from the collimator optics slot.
5. Place the mirror-based collimator optics in its slot.
6. Turn the cylindrical holder so that the white light beam hits the mid point in the pin hole (ref. fig. C)
7. Place the 60mm biconvex lens at its position (see fig. A)
8. Adjust the position of the 12.5mm biconvex lens (at position 7, in fig. A) in vertical direction to its highest intensity in the lamp spectra.
9. Make an optical resolution test (see sec. 6.4) and check if the position of the lens at position-7 is at optimum aligned position (compare with fig. B). The position of this lens should be adjusted in order to achieve the optimum optical resolution.

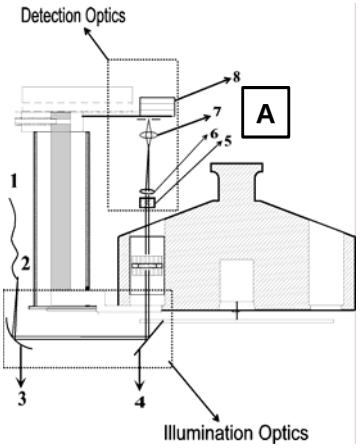

Fig.A (1) 50 micron fiber UV/Vis, (2) Tip of the 50micron fiber, (3) Off axis parabolic mirror (4) Plane mirror (5)Iris Diaphragm(6) Focusing biconvex lens (60mm), (7) Focusing biconvex lens (12.5mm), (8) Spectrometer fitted in a x-,y- stage.

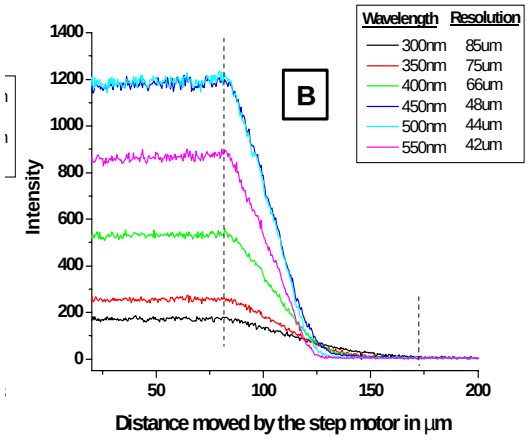

Fig. B Optics resolution test. Intensity scan to be performed on a counter balance cell hole as the rotor spins at a speed of 3,000 rpm. Experimental conditions: step size: 1um, time/step: 100us.

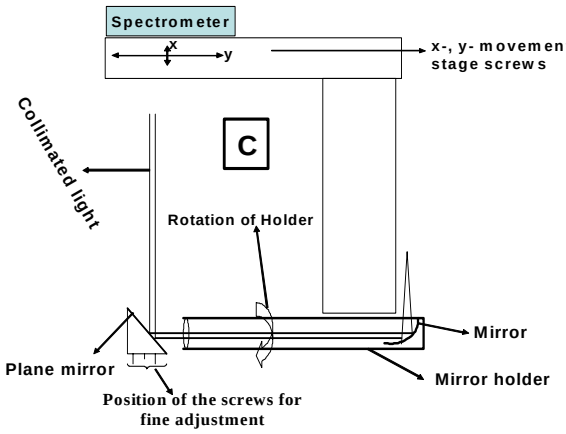

Fig.C Schematic description of the alignment of different optical elements in the arm

Zusammenfassung

In der vorliegenden Arbeit wurde die Entwicklung neuer Detektoren für die Analytische Ultrazentrifugation (AUZ) untersucht und vorangetrieben. Im Gegensatz zu chromatgraphischen. Fraktionierungsmethoden werden Multidetektionssysteme bis heute nicht in der AUZ eingesetzt.

Hier wird die Möglichkeit geprüft, bekannte spektroskopische sowie Streumethoden simultan zur Probenanalyse in der AUZ einzusetzen mit dem Ziel, simultan komplimentäre Informationen über die Probe zu erhalten. So wurde versucht, Raman- und UV/VIS-Spektroskopie (letztere mit der Möglichkeit, das gesamte Wellenlängenspektrum auszunutzen) und statische Lichtstreuung zu kombinieren, um das Analytverhalten während des Ultrazentrifugationsexperimentes zu untersuchen. Es wurden zum einen die Ramanspektroskopie als Detektionssystem für chemische Funktionalität in der AUZ geprüft und zum anderen gezeigt, daß die statische Kleinwinkel Lichtstreuung als direkter Molmassendetektor für den Einsatz in der AUZ geeignet erscheint. Zum anderen wurde die Entwicklung eines Multi-Wellenlängen-UV/VIS-Detektors abgeschlossen, um seine Eignung für den Einsatz in der AUZ und die damit verbundene Möglichkeiten der schnelleren und umfassenderen Datenerzeugung gegenüber kommerziellen Geräten zu zeigen.

Dieser Multiwellendetektor liefert anstelle eines Absorptionswertes für jede radiale Position in der Messzelle direkt ein ganzes UV-Vis Spektrum und erzeugt eine zusaetzliche Dimension der Messdaten, was die Möglichkeiten der Analyse von komplexen Systemen mit multiplen Chromophoren, Teilchengrößenbestimmung über Wellenlängenabhängigkeit der Trübung oder auch der Datenmittelung enorm vergrößert. Desweiteren erlaubt der Detektor die Anwendung von Geschwindigkeitsprofilen zur Analyse extrem polydisperser Systeme. Die Entwicklung des Detektors beruht auf einem auf Linsen basierenden System mit modularem Aufbau. Dabei war die sorgfältige Ausrichtung des optischen Systems ein essentieller Punkt, um seine Eignung zu überprüfen zu können.

An einer Mischung von drei Kolloiden, Halbleiternanopartikeln sowie Proteinen und deren Mischungen ist es hier gelungen, die erfolgreiche Entwicklung des UV/VIS-Detektors zu demonstrieren: Die Daten konnten schneller und mit wesentlich mehr Informationsgehalt, als auf allen kommerziellen Geräten generiert werden. Die Sedimentationskoeffizientenverteilungen stimmen dabei mit denen aus herkömmlichen Sedimentationsgeschwindigkeitsexperimenten überein, unterliegen jedoch nicht einer signifikanten diffusionsbedingten Verbreiterung.

Es ist in dieser Arbeit somit gelungen, zum einen die Lichtstreuung als aussichtsreiche Methode für ein Detektorsystem in der AUZ aufzuzeigen, und zum anderen einen Multi-Wellenlängen-UV/VIS-Detektor zu entwickeln, der eine Datenerzeugung von bislang noch nicht erreichter Schnelligkeit im dreidimensionalen Raum ermöglicht.

Popular abstract

In this work approaches for new detection system development for an Analytical Ultracentrifuge (AUC) were explored. Unlike its counterpart in chromatography fractionation techniques, the use of a Multidetection system for AUC has not yet been implemented to full extent despite its potential benefit. In this study we tried to couple existing fundamental spectroscopic and scattering techniques that are used in day to day science as tool for extracting analyte information. Trials were performed for adapting Raman, Light scattering and UV/Vis (with possibility to work with the whole range of wavelengths) to AUC. Conclusions were drawn for Raman and Light scattering to be a possible detection system for AUC, while the development for a fast fiber optics based multiwavelength detector was completed. The multiwavelength detector demonstrated the capability of data generation matching the literature and reference measurement data and faster data collection than that of the commercial instrument.

It became obvious that with the generation of data in 3-D space in the UV/Vis detection system, the user can select the wavelength for the evaluation of experimental results as the data set contains the whole range of information from UV/Vis wavelength. The detector showed the data generation with much faster speed unlike the commercial instruments. The advantage of fast data generation was exemplified with the evaluation of data for a mixture of three colloids. These data were in conformity with measurement results from normal radial experiments and without significant diffusion broadening. Thus conclusions were drawn that with our designed Multiwavelength detector, meaningful data in 3-D space can be collected with much faster speed of data generation.

Symbols

d_i: particle diamtere

D: Diffusion coefficient

f: frictional coefficient

F_b: buoyant force

F_f: frictional force

F_s: gravitational force on a sedimenting particle

I: intensity of transmitted light

I_0: intensity of incident light

m: mass of a particle

m_0: mass of fluid that can be displaced by a particle

ω: angular velocity

r: distance of a particle from the axis of rotation

M: molar mass in g/mol

M_w: weight average molar mass

N: Avogadro's number

$\bar{v}$: partial specific volume

ρ_0: density of the solvent

ρ_2: density of sedimenting particle

η: solvent viscosity

R: gas constant

s: sedimentation coefficient

T: absolute temperature

λ: wavelength (e.g. for light)

Abbreviations

APD:	Avalanche Photodiode
AUC:	Analytical Ultracentrifugation
BSA:	Bovine Serum Albumin
BASF:	Badische Anilin-und-Soda-Fabrik
CCD:	Charge Coupled Device
DNA:	DeoxyRibonucleic Acid
FTIR:	Fourier Transform Infra Red spectroscopy
GC:	Gas Chromatography
HTS:	High Throughput Sampling
HPTLC:	High Performance Thin Layer Chromatography
MS:	Mass Spectrometry
NA:	Numerical Aperture
Nd:YAG:	Neodymium-Yttrium Aluminium garnet
OAP:	Off Axis Parabolic Mirror.
PMT:	Photo Multiplier Tube
RPM:	Revolutions per Minute
RNA:	Ribo Nucleic Acid
SDS:	Sodium Dodecyl Sulphate
SMA:	Sub Miniature version A
TLC:	Thin Layer Chromatography
TTL:	Transistor Transistor logic
TEM:	Transmission Electron Microscopy
USB:	Universal Serial Bus
UV:	Ultraviolet

Acknowledgements

I would like to take this opportunity to thank all the people who contributed to this work.

I am indebted to Prof. Dr. Markus Antonietti for financial support and allowing me to carry out my doctoral work at MPI-KGF.

I am grateful to Dr. Helmut Cölfen for his never ending eagerness to help me at every front to his maximum whenever it was necessary. Once again my special thanks to him for bearing extra pain to read my thesis with valuable suggestions even from his hospital bed.

Many thanks to Andreas Kretzschmar for various mechanical design and construction of mechanical parts.

Thanks to Henryk Pitas and Monika Scholz for the electronics work while building up the instrumental setup

Special thanks to Akif Mehmeet Gülsun, Bilkent University, Ankara, Turkey for writing the software for instrument control and data collection.

Thanks to Prof. Borries Demeler, University of Texas, San Antonio, Texas, USA for the data viewer software.

Thanks to Frau Barth and Antje for their helpful assistance in the lab.

Thanks to Dr. Lars Börger, Dr. Wendel Wohlleben, Mr. Manfred Stadler, Mr. Thomas Meier, BASF-AG, Ludwigshafen for various experimental components during laboratory work.

Thanks to Dr. Cecile Huin, Dr. Holger Strauss, Jong Seto and Dr. Miles Page for finding time to read my thesis.

My deep gratitude to all the members of MPI-KGF who made my life easier. To name a few out of many, I owe my thanks to Nicole and Nadine for their warm friendliness and making our office a memorable one. Also, our funny days with Özlem and Emre to get a relief from the pain of Golm time.

Thanks to my parents and sisters and brother for their constant inspiration and the conversations that I could stay aloof from homesickness.

Finally, I wish to thank Max Planck Society and BASF-AG for financial support.

References

[1] Aurenkollektiv New Trends in Chemistry, Akademie-Verlag. Berlin 1982

[2] Skoog D A, Leary J J; Principles of Instrumental analysis, 4th ed. Saunders: Fort Worth, 1992

[3] Fung, E. N.; Chu, I.; Nomeir, A. A.; Rapid Commun. Mass Spectrom., 18 (2004) 2046

[4] Lopez-Avila V, Hill H H; Anal Chem., 69 (1997) 289R

[5]Workman J. Jr., Koch Mel, Veltkamp D; Anal Chem., 77 (2005) 3789

[6] Johnson K. J., Wright B. W. Jarman, K. H. Synovec, R. E.; J. Chromatogr., A 996 (2003) 141

[7] LaTorre, A; Rigol, A.; Lacorte, S.; Barcelo, D.; J. Chromatogr., A 991 (2003) 205

[8] Roussel, C.; Del Rio, A.; Pierrot-Sanders, J.; Piras, P.; Vanthuyne, N.; J. Chromatogr. A, 2004, 1037 (1-2), 3110328

[9] Barreca, D.; Gasparotto, A; Tondello, E; Bruno, G.; Losurdo, M; J. Appl. Phys. 96 (2004) 1655

[10] Hutter, K. J.; Lange, C.; Brewing Yest Fermentation Performance, 2nd Ed.; Blackwell Publishing Ltd.; Oxford, UK., 2003; pg.169

[11] Gurden, S.P.; Lage, E. M.; de Faria. C. G.; Joekes, I.; Ferreira, M. M. C.; J. Chemom. 17 (2003) 400

[12] Andersson, M.; Svensson, o.; Folestad, S.; Josefson, M.; Wahlund, K.G.; Chemom. Intell. Lab. Syst. 75 (2005)1

[13] Zhang, F,; Brueschweiler, R.; Chem. Phys. Chem. 5 (2004) 794

[14] Ito, K.; Kato, T.; Ona, T.; Vib. Spectrosc 35 (2004) 159

[15] Wildgoose, G. G.; Lawrence, N. S.; Leventis, H. C.; Li. J.; Jones, T. G. J.; Compton, R. G.; J. Mater. Chem. 15 (2005) 953

[16] Kingston, H. Abstracts of the 35th Central Regional Meeting of the American Chemical Society, Pittsburg, PA, Oct.19-22, 2003; p 47.

[17] Hopke, P. K.; Anal Chim Acta 500 (2003) 185

[18] Ertl, P.; Selzer, P.; Muehlabacher, J.; Drg Discovery Today: BIOSILICO 2 (2004) 201

[19] Saundrs, K. C. Drug Discovery Today; Technol. 1(2004) 373

[20] Cadapakam JV, Zelechonok Y; Anal Chem. 75 (2003) 3484

[21] Gilar M, Olivova P, Daly AE, Gebler JC; Anal Chem. 77 (2005) 6426

[22] Roger P, Axelos MAV, Colonna P; Macromolecules, 33 (2000) 2446

[23] Osterloh K, Borchert HH, Kroll C; Detector: ESR for Chrmatography, Encyclopedia of separation science, Vol. 2, Academic Press (2000)

[24] Svedberg T, Rinde H; J. Am. Chem. Soc. 45 (1924) 2

[25] Svedberg T, Pedersen K O; The Ultracentrifuge, Claredon Press, Oxford (1940)

[26] Balbo A, Minor KH, Velikovsky CA, Mariuzza RA, Peterson CB, Schuck P; Proc. Natl Acad Sci USA 102 (2005) 81

[27] http://www.analyticalultracentrifugation.com

[28] http://www.analyticalultracentrifugation.com/sedphat/sedphat.htm

[29] http://www.ultrascan.uthscsa.edu

[30] http://www.bbri.org/faculty/stafford/AUCRL.html

[31] Lloyd P.H. Optical Methods In Ultracentrifugation, Electrophoresis, and Diffusion; Clarendon Press, Oxford 1974.

[32] Lamm O, Ark. Math. Astron. Fysik 21B, Nr. 2, (1929) 1

[33] Ralston G; Introduction to Analytical Ultracentrifugation, Beckman Coulter Inc.Fullerton, US.

[34] Lee J. C., S Rajendran; Studies of macromolecular interaction by sedimentation velocity, in T M Schuster and Laue T M; Modern analytical ultracentrifugation, Birkhäuser, Boston, Basel, Berlin(1994) 138.

[35] Goldberg R J; J. Phys. Chem. 57 (1953) 194

[36] Van Holde KE, Weischet WO; Biopolymers 17 (1978) 1387

[37] Demeler B, Saber H, Hansen JC; Biophys 72 (1997) 397

[38] Muramatsu N, Minton A. P., Anal Biochem. 168 (1988) 345

[39] Stafford W. F., 'Method for obtaining sedimentation coefficient distributions' in Harding S. E., Rowe A. J., Horton J. C., Analytical ultracentrifugation in biochemistry and polymer science, The royal society of chemistry, Cambridge (1992) 359.

[40] Yaphantis D.A., Biophys J 45 (1984) 324a

[41] Stafford W. F., Anal Biochem. 203 (1992) 295

[42] Van Holde K.E., Baldwin R. L., J. Phys. Chem. 62 (1958) 734

[43] Yaphantis D.A., Ann N. Y. Acad Sci. 88 (1960) 586

[44] Mächtle. W, 'Analysis of polymer dispersions with an eight cell AUC multiplexer: High resolution particle size distribution and density gradient tecniques' in Harding SE, Rowe AJ, Horton JC, Analytical Ultracentrifugation in biochemistry and polymer science, The royal society of chemistry, Cambridge (1992) 147.

[45] Budd PM; Progr. Colloid Polym Sci. 94 (1994) 107

[46] Vinograd J, Lebowitz J, Radloff R, Watson R, Laipis P Proc Natl. Acad. Sci, USA 53 (1965) 1104

[47] Lebowitz J, Teale M, Schuck P, Biochem. Soc. Trans. 26 (1998) 745

[48] http://www.analyticalultracentrifugation.com/sedfit_help_analytical_zone_centrifugation.htm

[49] Giebeler R (1992) The Optima XL-A: A New Analytical Ultracentrifuge with a Novel Precision Absorption Optical System, in: Harding SE et al (ed) Analytical Ultracentrifugation in Biochemistry and Polymer Science, Royal Society of Chemistry, Cambridge, 16

[50] Schachman HK, Ultracentrifugation in Biochemistry, Academic Press (1959)

[51] Flossdorf J; Makromol Chem 181 (1980) 715

[52] Laue TM, PhD Dissertation, 1981 University of Connecticut, Storrs CT

[53] Laue TM, On-Line Data Acquisition and Analysis from the Rayleigh Interferometer in Harding SE, Rowe AJ, Horton JC, Analytical Ultracentrifugation in biochemistry and polymer science, The royal society of chemistry, Cambridge (1992) 147

[54] Rowe AJ, Jones SW, Thomas DG, Harding SE; Method for offline analysis of sedimentation velocity and sedimentation equilibrium patterns, in Harding SE, Rowe AJ, Horton JC, Analytical Ultracentrifugation in biochemistry and polymer science, The royal society of chemistry, Cambridge (1992) 147.

[55] Harding SE, Rowe AJ; Optics and Lasers in Engineering; 8 (1988) 83

[56] Flossdorf J, Schilling H, Schindler KP; Makromol Chem 179 (1978) 1617

[57] Scheibling G, J Chim Phys; 47 (1950) 688

[58] Lavrenko P, Lavrenko V, Tsvetkov V, Prog. Colloid Polym Sci. 113 (1999) 14

[59] Lebdev AA; Tr Gos Opt Inst Leningr 5 (1931) 53

[60] "Beobachtungen nach einer neuen optischen Methode", Toeppler. A; Bonn 1864

[61] Tanner CC; Trans. Faraday Soc. 23 (1927) 75

[62] Lamm O; Nova Acta R. Soc. Sci. Upsal. 10, Nt. 6, 1937

[63] Instrument Manual of SPINCO Model E Analytical Ultracentrifuge, Beckman Instruments, Inc. Spinco Division, Palo Alto, California.

[64] Cölfen H, Borchard W; Ultrasensitive Schlieren Optical System Biomedical Diagnostic Instrumentation, Proc. SPIE 2136 (1994)

[65] Mächtle. W, Börger L; Analytical Ultracentrifugation of Polymers and Nanoparticles, Springer Laboratory Manuals in Polymer Science (2006).

[66] Mächtle. W: Progr. Colloid. Inte. Sci. 113 (1999) 1

[67] Börger L, Lechner MD, Stadler M; Prog. Colloid Polym Sci 127 (2004) 19

[68] Klodwig U, Mächtle, Colloid Polym. Sci 267(1989) 1117

[69] Clewlow AC, Errington N, Rowe AJ; Eur. Biophys. J. 25 (1997) 311

[70] Cölfen H, Borchard W; 94 (1994) 90

[71] MacGregor I. K., Anderson A. L., Laue T. M.; Biophysical Chemsitry 108 (2004) 165-185.

[72] Schmidt B, Riesner D, A Fluorescence Detection system for Analytical Ultracentrifuge and its Application to Proteins, Nucleic Acis, Viroids and Viruses in Harding SE, Rowe AJ, Horton JC, Analytical Ultracentrifugation in biochemistry and polymer science, The royal society of chemistry, Cambridge (1992)

[73] Cantow HJ; Makromol Chem 70 (1964)130

[74] Mächtle. W; Makromol Chem 185 (1984) 1025

[75] Scholtan W, Lange H; Kolloid Z Z Polym 250 (1972) 782

[76] Mächtle W, Börger L; Analytical Ultracentrifugation, Instrumentation, in Analytical ultracentrifugation of Polymers and Nanoparticles, Springer (2005)

[77] Svedberg T,Pedersen KO; The Ultracentrifuge, Clarendon Press, Oxford (1940)

[78] Cölfen H, Völkel A.; Progr. Colloid Polym Sci 2004 (127) 31-47

[79] Liu. J, Shire S. J.; J. Pharm Sci. Vol. 88, No. 12.

[80] Shire S. J.; Modern Analytical Ultracentrifugation, Todd M Schuster, Thomas Laue, Birkhäuser

[81] Ralston G.; Introduction to Analytical Ultracentrifugation, Beckman Instruments Inc, California.

[82] Analytical Ultracentrifugation Techniques and Methods, Edited by Scott DJ, Harding SE, Rowe AJ., RSC Publishing (2005)

[83] Analytical Ultracentrifugation of Polymers and Nanoparticles by Mächtle W, Börger L, Springer (2005)

[84] Analytical Ultracentrifugation in biochemistry and polymer science, edited by Harding SE, Rowe AJ, Horton JC, The royal society of chemistry, Cambridge (1992)

[85] Svedberg T, Rinde H, J. Am. Chem Soc. 46 (1924) 2677

[86] Rinde H, The distribution of the sizes of particles in gold sols, PhD thesis Upasala (1928)

[87] Nichols J B, Physics 1 (1931) 254

[88] Nichols J B, Kramer E O, Bailey E D, J. Phys. Chem., 36 (1932) 326

[89] Rapport DH, Vogel W, Cölfen H, Schlögl R; J. Phys. Chem. B 101 (1997) 136

[90] Müller HG, Herrmann F; Progr. Colloid Polym. Sci. 107 (1997) 136

[91] Mächtle. W; Biophys. J. 76 (1999) 1080

[92] Cölfen H, Pauk T, Colloid Polym Sci. 275 (1997) 136

[93] Richards, J. P.; Stickelmeyer, M. P.; Flora, D. B.; Chance, R. E.; Frank, B. H..; Defelippis, M. R.; Pharm. Res. 1998 (15) 1434-1441

[94] Verley, P. G.; Brown, A. J.; Dawkes, H. C.; Burns, N. R.; Eur. Biophys. J. 1997, (25), 437-443

[95] Philo, J. S.; Aoki, K. H.; Arakawa, T.; Narhi, L. O.; Wen, J.; Biochemistry 1996, (35), 1681-1691.

[96] Pennica, D.; Kohr, W. J.; Weber, Fendly B. M.; Shire, S. J.; Raab, H. E.; Borchardt, P. E.; Lweis, M.; Goedel, D. V.; Biochemistry 1992 (31) 1134-1141

[97] Pennica, D.; Lam, V. T.; Weber. R. F.; Kohr, W. J.; Basa, L. J.; Spellman, M. W.; Ashkenazi. A; Shire, S. J.; Goedel, D. V.; Biochemistry 1993 (32) 3131-3138

[98] Cunningham, B. C.; Mulkerrin, M. G.; Wells J. A.; Science, 1991, 253, 545-548.

[99] Liu, J.; Laue, T. M.; Choi, H. U.; Tang, L. H.; Rosenberg, L.; J. Biol. Chem. 1994 (269) 28366-28373.

[100] Winfield, P.; Graber, P.; Moonen, P.; Craig, S.; Pain, R. H.; Eur. J. Biochem. 1988, (173), 65-72

[101] Van Holde, K. E.; Weischet, W.; Biopolymers 1978 (17) 1387-1403

[102] Demeler, B.; Saber, H.; Hansen, J. C.; Biophys. J. 1997 (72) 397-407

[103] Hansen. J. C.; Lebowitz, J.; Demeler, B.; Biochemistry 1994 (33) 13155-13163

[104] Hansen, J. C.; Ausio, J; Stanik, V. H.; van Holde K. E.; Biochemistry 1989 (28) 9129-9136

[105] Gill, S. C.; Yager, T. D.; von Hippel, P. H.; J. Mol. Biol. 1991 (220) 325-333

[106] Stafford, W. F. I.; Curr. Opin Biotechnol. 1997, (8) 14-24

[107] Stafford, W. F.; Anal. Biochem. 1992 (72) 397-407

[108] Liu. J.; Ruppel, J.; Shire, S. J.; Pharm. Res. 1997 (14) 1388-1393

[109] Laue, T. M.; Johnson, A. E.; Esmon, C. T.; Yphantis, D. A.; Biochemistry 1984 (23) 1339-1348

[110] Kim, S. J.; Tsukiyama, T.; Lewis, M. S.; Wu, C.; Protein Sci. 1994 (3) 1040-1051

[111] Behlke J, Eur Biophys. J. 25 (1997) 319

[112] Behlke J, Ristau O; Eur Biophys. J. 25 (1997) 325

[113] Harding SE; Sedimentation Analysis of Polysaccharides, in: Harding SE et al (ed) Analytical Ultracentrifugation in Biochemistry and Polymer Science, Royal Society of Chemistry, Cambridge, 16

[114] Mächtle W; Progr. Colloid Polym. Sci 86 (1991) 111

[115] Malacara D, Malacara Z; Handbook of Optical Design, 2nd Ed. Marcel Dekker, New York, Basel.

[116] Kisters D, Borchard W; Progr. Colloid Polym Sci 1994, 113, 10.

[117] Börger L, Lechner MD, Stadler M; Progr. Colloid Polym Sci 2004, 127, 19

[118] Mächtle W, Progr. Colloid Polym Sci; 1999, 113, 1

[119] Rockholt DL, Royce CR, Richards; Biophys Chem 1976, 5, 55

[120] Kim J E, McCamant D W, Zhu L, Mathies R A; J Phys. Chem B 2001, 105, 1240-1249.

[121] Kochendoerfer G. G., Lin S.W., Sakmar T.P., Mathies R. A.; Trends Biochem. Sci.1999, 24, 300–305.

[122] Wu Y J, Xu Y Z, Zhao Y, Wang D J, Weng S F, Wu J G, Xu D F; SPECTROSCOPY AND SPECTRAL ANALYSIS

25, 9, 1408-1411, SEP 2005

[123] DeGraff. B A, Hennip M, Jones J M, Salter C, Schaertel S A, Chem. Educator 2002, 7, 15-18.

[124] www.chromexinc.com/ (accessed in 2003 Nov.)

[125] http://www.kosi.com/ (accessed in 2003 Nov.)

[126] http://www.jyinc.com/ (accessed in 2003 Nov.)

[127] Liu T, Chu Benjamin; Encyclopedia of Surface and Colloid Science; Marcel Dekker, Inc. 2002.

[128] Chu B. Laser Light-Scattering, 2nd Ed.; Academic Press:New York, 1991.

[129] Schuck P; Prog. Colloid & Polym. Sc. (1994) 94 1

[130] Servillo L, Brewer HB, Osborne JC; Biophys Chem (1981) 13 29

[131] Lakatos S, Minton P; J Biol Chem. (1991) 226 18707

[132] Cantow HJ (1964) Makromol. Chem. 70: 130

[133] Scholtan W, Lange H (1972) Kolloid Z Z Polym. 250: 782

[134] Müller HG (1989) Colloid Polym. Sci. 267: 1113

[135] Flossdorf J (1980) Makromol. Chem. 181: 715

[136] Flossdorf J, Schillig H (1979); Feinwerktechnik Messtechnik 93: 87

[137] Voelker P (1995) Progr Colloid Polym Sci 99: 162

[138] Vistica J, Dam J, Balbo A, Yikilmaz E, Mariuzza RA, Rouault TA, Schuck P (2004) Anal Biochem 326: 234

[139] Gledhill RJ (1962) J Phys Chem 66: 458

[140] Bateman JB, Weneck EJ, Eshler DC (1959) J Colloid Sci 14: 308

[141] Heller W, Bhatnagar HL, Nakagaki M (1962) J Chem Phys 36: 1163

[142] Hosono M, Sugii S, Kusudo O, Tsuji W (1973) Bull Inst Chem Res, Kyoto Univ 51: 104

[143] http://oceanoptics.com/technical/engineering/USB2000%20OEM%20Data%20Sheet.pdf

[144] http://oceanoptics.com/technical/engineering/OEM%20Data%20Sheet%20--%20HR4000.pdf

[145] www.lot-oriel.com/ccd

[146] http://usa.hamamatsu.com/en/products/electron-tube-division/light-sources/xenon-flash-lamps.php.

[147] Instruction Manual for Xe Flash Lamp Module (L-9455, L-9456 series), Hamamatsu PhotonicsK. K., Electron Tube Division, Japan.

[148] Niederberger M, Garnweitner G, Krumeich f; Nesper r, Cölfen H, Antonietti M (2004) *Chem. Mater.*4**,** *16,* 1202.

[149] dantecdynamic.com